RICE UNIVERSITY

A Numerical Resistor Network Model for the Determination of Electrical Properties of Nanocomposites

by

Bradley Ward, 2nd Lt USAF

A THESIS SUBMITTED
IN PARTIAL FULFILLMENT OF THE
REQUIREMENTS FOR THE DEGREE

Master of Science

APPROVED, THESIS COMMITTEE

Dr. Pol D. Spanos, Chair
Lewis B. Ryon Professor in Engineering

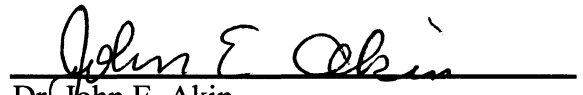

Dr. John E. Akin
Professor of Mechanical Engineering &
Materials Science

Dr. Ilinca Stanciulescu
Assistant Professor of Civil Engineering

HOUSTON, TEXAS
April 2011

Abstract

A Numerical Resistor Network Model for the Determination of Electrical Properties of Nanocomposites

by

Bradley Ward

This thesis introduces a comprehensive numerical model for the determination of the electrical properties of carbon nanotube reinforced polymer composites. Procedures of this model are based on a new spanning network identification algorithm and the resistor network method. First, realistic nanotube geometry is generated from input parameters defined by the user. The spanning network algorithm then determines the connectivity between nanotubes in the representative volume element. Next, interconnected nanotube networks are converted to equivalent resistor circuits. Finally, Kirchhoff's Current Law is used in conjunction with finite element analysis to solve for the voltages and currents in the system and calculate the effective electrical conductivity of the nanocomposite. The Monte Carlo method is used to eliminate statistical variation by simulating five hundred random geometries. The model accounts for electrical transport mechanisms such as electron hopping and simultaneously calculates percolation probability, identifies the backbone, and determines effective conductivity. The accuracy of the model is validated by comparison to both models and experiments reported in the literature.

Acknowledgments

I would like to thank several important individuals for their contributions to my work at Rice University. First and foremost, I would like to sincerely thank my advisor and professor, Dr. Pol Spanos. He chose to offer me a scholarship and help me decide on a thesis topic. His guidance and leadership have been instrumental in the realization of this thesis. The lessons learned from his counseling have outweighed those learned in all the textbooks and classrooms.

I would also like to extend my gratitude to Dr. John Akin and Dr. Ilinca Stanciulescu for the significant amounts of their time and expertise consumed in the development of the technical aspects of this numerical model. I am appreciative of their willingness to sacrifice their time to help and also to be on my thesis committee. Further, this project would not exist if it were not for the previous works of Paul Elsbernd and Dr. Milton Esteva.

Additionally, many thanks also go to the innumerable conversations with Doctors Georgios Evangelatos and Ioannis Kougioumtzoglou. Your ideas and suggestions have helped shaped the success of this project. Thank you for taking your time and energy to ensure the success of a fellow student.

Ultimately, I would like to thank my incredible and beautiful wife Stephanie and my son Colton. Their unwavering support and love throughout my time at Rice has proved indispensible to my sanity and success.

Contents

List of Figures

List of Tables

Chapter 1

Introduction

1.1. Motivation

Extensive research effort has been focused on nanotechnology over the past two decades. Specifically, the properties and potential applications for nanoparticle-based composites have been of particular interest. Fullerenes, the original and one of the smallest nanoparticles, are capable of destroying harmful bacteria and fungi without damaging sensitive mammalian cells [1], and other important nanoparticles made from silver, gold, or platinum are being studied for their ability to deliver medicine and target cancer cells [2]. Carbon nanotubes, however, are one of the most commonly studied nanoparticles. This is due to their high electrical, mechanical, and thermal performance.

Nanotube-based polymer composites have a significant potential for application in electrical, mechanical, and thermal systems due to the exceptional physical properties of carbon nanotubes (CNTs). These multifunctional fibers have the ability to enhance more than one material property simultaneously [3]. More importantly, they have extremely high electrical conductivities. Intrinsic conductivity of CNTs is usually reported on the order 10^4 to 10^6 S/m [4]. Early measurements on individual nanotubes by Ebbesen et al. [5] produced conductivities of $1 \times 10^5 - 2 \times 10^7$ S/m. More recently, CNTs

were measured at 8 x 10^6 and 2 x 10^7 S/m in experiments executed by Wei et al. [6]. The current carrying capacity of nanotubes is even more remarkable. Nanotubes are capable of sustaining current densities above 10^9 A/cm^2 at high voltages and elevated temperatures for extended periods of time without any change in resistance or physical deterioration [6]. Frank et al. [7] and Yao et al. [8] measured sustained current densities of 10^7 A/cm^2 and 10^9 A/cm^2, respectively. These results indicate that CNTs have electrical current capacity 1,000 times that of copper wires [9] and at least two orders higher than typical superconductors [7]. Further, they have the potential to enhance polymer conductivities by as much as ten orders of magnitude [10].

In addition, carbon nanotubes have high thermal conductivities, large strength-to-weight ratios, and maintain their mechanical integrity under extreme loading [11]. Nanotubes have theoretical strengths of 150 GPa and elastic moduli on the order of 1 TPa, approximately three times larger than carbon fibers and five times that of steel at one-sixth the weight [12-13]. Theoretical thermal conductivity is over 6,000 W/mK [14], well above that of diamond. Experiments have reported conductivities of multi-walled CNTs of 3,000 W/mK at room temperature [15].

These properties make nanotubes ideal for a variety of interesting applications in thermal management, structural reinforcement, and electrical conduction applications. Specific applications include incorporation in field-emitting displays, photo-voltaic cells, corrosion resistance, aircraft skins, and even lightning protection [16-17]. Of particular interest to this study, however, are the potential applications involving CNT-filled polymer composites for electrical conduction. According to Li and Chou [18], unique properties give rise to use of CNT/polymer nanocomposites in structural health

monitoring. Percolation behavior, high aspect ratios, and high electrical conductivity make carbon nanotubes promising fillers for sensing damage and measuring stress and strain in bulk materials [18]. Furthermore, nanocomposites are ideally suited for electromagnetic interference shielding and electrostatic discharge applications [17]. The very low density and high conductivity of CNTs can convert an insulating polymer into an electrical conductor without negatively impacting the other desirable properties of the thermoplastic. Therefore, materials with these qualities are potentially valuable to the electronics, automotive, and aerospace industries [19].

The potential performance of these nanocomposites has motivated the need for accurate models to predict their effective electrical characteristics. Due to the copious different combinations of CNT and polymer constituent phases, numerical and analytical methods can help reduce the number of expensive and timely experiments. In addition, a manifold of controllable material parameters, such as CNT aspect ratio and volume fraction, need to be accounted for and studied. Finally, the probability a nanocomposite forms percolating networks of CNTs needs to be related to its effective electrical properties. Therefore, a new model is necessary to simultaneously predict percolation, identify conducting backbones, and estimate the electrical conductivity. These are the principal motivations for a comprehensive and versatile numerical method of accurately representing electrical behavior of CNT-based composites.

1.2. Electrical Conduction in Nanotube-based Composites

Electrical properties of nanocomposites are governed by a set of principles different from those that dictate elastic or thermal properties. Factors such as CNT

dispersion, embedment, and interface bonding are critical to both elastic and thermal performance. Contrastingly, the driving factors behind electrical behavior include the formation of conductive networks, percolation, and nanoscale effects. Conductive networks in a nanocomposite consist of interconnected strands of CNTs that have the potential to carry an electric current. Each nanotube in a network can be visualized as a cylindrical structure with 25 - 40% of their volume hollow [3]. Therefore, their large conductivities are concentrated in the axial direction and they function as one-dimensional conductors with very low resistances.

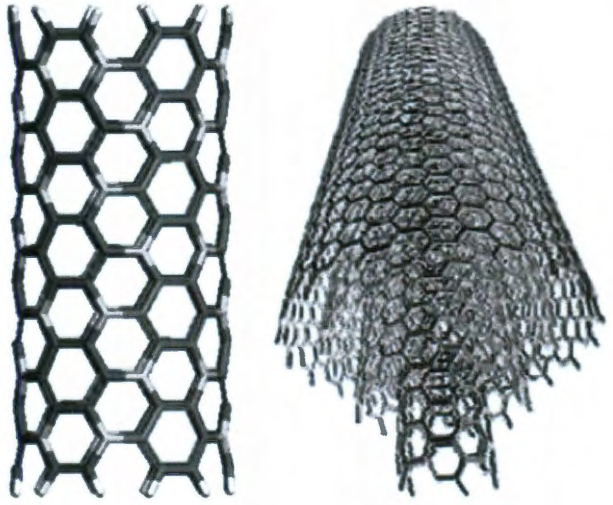

Figure 1. Carbon nanotubes consist of rolled sheets of graphene. Multi-wall CNTs (MWNTs) have several concentric layers, while single-wall CNTs (SWNTs) have only one [20].

When connected to an applied potential difference, CNT networks can form closed electrical circuits. However, only a relatively small portion of the CNTs in an entangled network will carry a current. This current carrying portion is known as the backbone of the nanocomposite [21-22]. Although both thermal and electrical

conduction problems form CNT networks and are described by the same constitutive equations, the notion of backbones and effective conductivity behavior differ drastically. The reason CNT/polymer composites form backbones and do not conduct electricity in the same manner as they conduct heat is a direct consequence of conductivity differences of the materials. The ratio of CNT to polymer thermal conductivity is on the order of 10^4 while for electrical it is much larger, on the order of 10^{12} - 10^{16} [23]. With such a large difference in electrical properties, only the CNTs contribute to current flow. However, in the thermal case the matrix material is able to contribute to heat conduction.

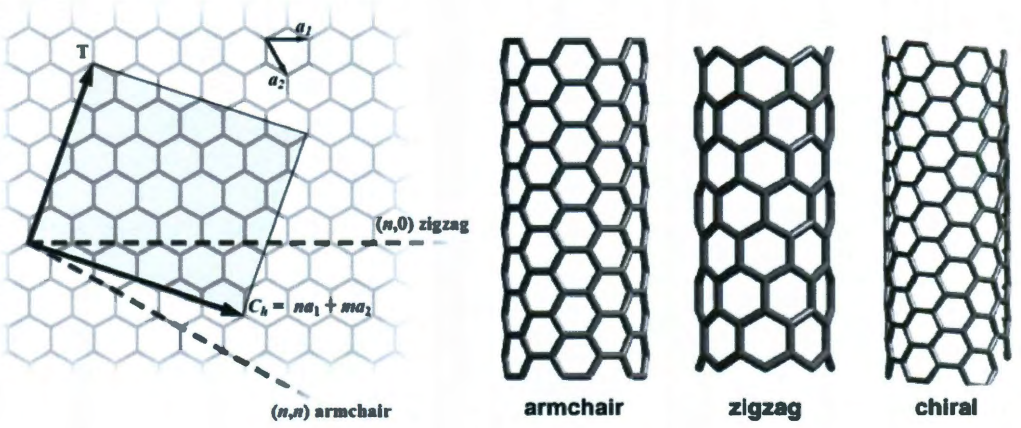

Figure 2. The three basic categories of nanotube structure are shown. Intrinsic electrical conductivity of a CNT depends on its chiral structure, or pattern of carbon-carbon bonds.

The lack of matrix participation in electron transport is the primary cause of percolation behavior in nanocomposites. Percolation is characterized by a sudden transition in effective conductivity over a very small increase in concentration of CNTs [3,10,24]. The volume fraction at percolation indicates the point at which the material transforms from an insulator to a conductor. This point is known as the percolation

threshold. Before the threshold, effective conductivity is dominated by the insulating matrix, which typically has conductivities below 10^{-12} S/m for polymers [25]. At the percolation threshold, conductivity can increase by more than six orders of magnitude. For volume fractions above the threshold, the conductivity is dominated by the CNT backbone and increases by another two to three orders of magnitude [10].

Percolation threshold is evidenced by a transition in macroscale physical properties. However, percolation jumps have been observed in materials at loadings well below the geometrical percolation threshold [26-28]. The geometric threshold is the volume fraction at which a complete network of connected CNTs spans the material. This lack of agreement between the macroscale and microscale thresholds signifies the presence of another electrical transport mechanism in the material. Electron tunneling or hopping is a phenomenological mechanism that allows current to flow between CNTs that are not in direct physical contact. Interestingly, electrons have demonstrated the ability to hop or tunnel from one conductor, through a finite length of insulator, to another conductor. The experiments of Postma et al. [29] and Park et al. [30] proved that crossed CNTs form tunnel junctions. Likewise, Ounaies et al. [31] reported a nonlinear current-voltage behavior above the percolation threshold. They attributed this to the electron tunneling effect.

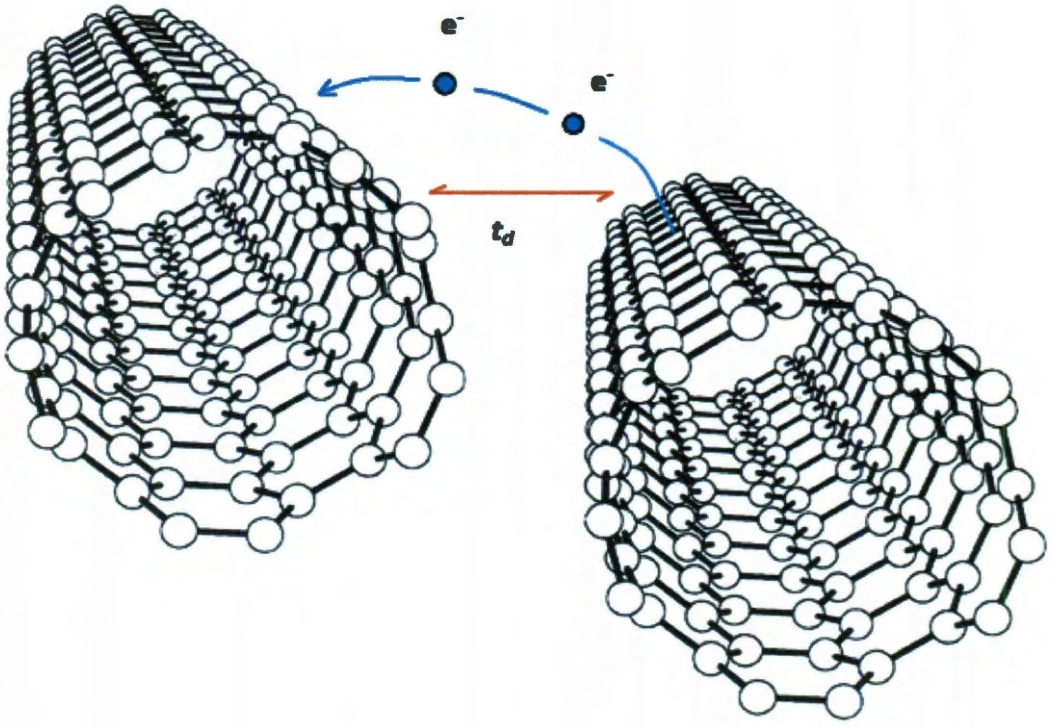

Figure 3. Electron tunneling between nanotubes is shown. The distance an electron can hop or tunnel through the matrix is represented by t_d.

Consequently, nanocomposites can achieve conducting status without the presence of a network of CNTs in direct contact. This has the effect of lowering the physical percolation threshold [32]. On the other hand, the insulating polymer in the tunneling region has a very high resistance. According to the work of Li et al. [33], the thickness of the insulating layer determines the tunneling resistance more than any other factor. High resistances between the CNTs in the backbone decrease effective conductivity of the composite as a whole. However, as the volume fraction increases more CNTs physically touch. Direct contacts have much lower resistances than tunneling contacts. Therefore, as more tunneling contacts in the backbone are replaced by direct contacts, effective conductivity in the nanocomposite increases. Unfortunately,

the mechanisms dominating electrical transport in nanotube/polymer composites are not fully understood. This is the foremost challenge to predicting their effective electrical properties. Incorporating complex transport effects using simple representations is a motive for developing a numerical nanocomposite model.

1.3. Current Electrical Models

A wide variety of analytical and numerical models have been developed to predict effective electrical conductivity, percolation threshold, and parametric relationships of nanotube composites. Balberg et al. [34] and Bug et al. [35] presented two of the early percolation models. Both models were based on the excluded volume approach and predicted percolation thresholds of disordered systems with different shaped fillers. The more recent model of Cai et al. [36] used a combination of effective medium theory and percolation equations to calculate both the threshold and the effective conductivity. Authors Deng and Zheng presented two electrical models. The first [25] used micromechanics equations to predict conductivity and percolation threshold of wavy CNTs. The second [10] was adapted from elastic analysis and used interaction direct derivation and Eshelby tensor equations. Lebovka et al. [37] developed a two-dimensional diffusion-limited aggregation model for colloidal dispersions. The model includes multiple-seed growth and particles that execute random walks in the lattice-type domain. Seidel and Lagoudas [3] used a micromechanics model based on the composite cylinders and Mori-Tanaka methods to calculate effective electrical properties of CNT/polymer composites. Seidel et al. [38] also reported a micromechanics model to calculate effective conductivity of straight, randomly oriented CNTs using the

generalized self-consistent composite cylinders approach. All of the models detailed above are analytical and provide valuable insight on electrical properties of nanocomposites. However, they use individual equations, many of which are based on only a single CNT or adapted from other applications such as thermal or elastic analysis. Original studies by Seager and Pike [39] suggested that due to the interplay of complex factors of disordered continuum composites, numerical approximations may be better suited to study electrical properties.

In addition to analytical methods, several numerical models provide good representations of nanocomposites. Pike and Seager [40] were the first to study percolation in random two-dimensional stick models using Monte Carlo simulations. One of the original resistor network models was developed by Kirkpatrick [41] as an extension to established lattice models. Both two- and three-dimensional disordered stick systems were simulated by the Monte Carlo method. More recently, Behnam and Ural [42] used Kirchhoff's laws and Monte Carlo simulations to calculate electrical properties of straight, randomly oriented CNTs in stacked two-dimensional layers. Dalmas et al. [4] presented a three-dimensional model of wavy, randomly oriented nanotubes using the resistor network method. They included constant contact resistance and solved the model by using the finite element method (FEM). Hakobyan et al. [24] also used FEM to determine effective conductivity and percolation threshold of a two-dimensional lattice of highly conductive triangles. Foygel et al. [11] only studied percolation threshold with their spanning network model of straight, randomly oriented, soft-core CNTs. Monte Carlo, statistical percolation, and resistor network methods were used by Hu et al. [16] to determine electrical conductivity and thresholds in polymer nanocomposites. The

pseudo-three-dimensional model of Jack et al. [43] is based on Kirchhoff's Current Law (KCL) and Monte Carlo simulations. Further, it included stochastic nanotube parameter inputs, properly scaled sample dimensions, and periodic geometry on the boundaries. Li and Chou [17] presented a novel method of representing contact resistances and used their direct electrifying algorithm to calculate effective conductivity and identify the backbone [22]. The three-dimensional model of Sun and Song [44] used the resistor network method and calculated contact resistances to find the effective conductivity and percolation threshold. Topinka et al. [45] also used the resistor network method combined with KCL and constant contact resistances to determine effective conductivity and visualize the currents and voltages in the CNT networks.

Each of these models gives important insights into the electrical conduction behavior of nanocomposites. The vast majority employ a combination of Monte Carlo and resistor network methods. Pike and Seager [40] were the first to establish Monte Carlo simulations as the primary method of analyzing random percolating systems. Kirkpatrick [41] was the first to prove the viability of a resistor network model in determining electrical properties of a system of random sticks. Though they use similar methods, all the models are unique in how details such as geometry, contact resistance, CNT morphology, and CNT resistance are represented. Only a few models use periodic geometric boundaries. By relocating the parts of fibers extending outside the sample to the opposite boundary, continuity between sample structures is maintained, insulating boundary conditions are validated, and the structure is representative of an infinite system [41,43]. Also, contact resistance between CNTs is one of the most crucial physical aspects of the problem and must be incorporated into the model [44]. Some numerical

models make broad assumptions about contact resistance or ignore the tunneling effect altogether. Several authors [18,20,41,45] emphasize the impact of the number of CNT contact points on the results. For this reason, it is important for models to incorporate nanotube waviness and realistically represent the number of contact points. The other major factor to include in a numerical model is intrinsic nanotube resistance [18]. Of the models detailed above, none incorporates all four of these important factors. This is one of the motivations for the method presented in this thesis.

The proposed model is extremely versatile and produces relevant results that are threefold; first, it calculates percolation probability, second, identifies the conducting backbone, and third, it calculates effective conductivity. All three results are obtained simultaneously and in an expeditious manner. The model is based on three of the methods introduced above: Monte Carlo simulations, spanning network identification, and the resistor network method. As explained above, Monte Carlo simulations are necessary for reducing statistical variation in the random system. A large number of random sample structures, hereafter referred to as representative volume elements (RVEs), are populated with wavy CNTs and periodic boundaries. Each RVE is solved and the results are averaged over all RVEs at a given volume fraction. The percolating behavior of nanocomposites causes two factors to be of extreme importance. The first is the formation of complete spanning networks in the material. The spanning network algorithm portion of the model detects the presence of CNT networks that extend the length of the RVE. Electron tunneling effect is incorporated through the criterion that determines the connection status between nanotubes. This allows CNTs to be considered in contact even without directly touching. An RVE with a full network has the capacity

to carry an electrical current between the simulated electrodes. The network of fibers is then converted into equivalent series and parallel resistor elements. Both intrinsic nanotube resistance and contact resistance due to tunneling are represented according to methods introduced in the literature. The system is assembled and solved using the matrix form of KCL and FEM. The use of KCL is valid because the system consists of only linear resistors and charge is neither generated nor stored within the RVE. Results of FEM include voltages and currents within the CNT network and effective electrical conductivity of the polymer nanocomposite. Currents within the fibers are used to identify the current carrying backbone of the material similar to the method developed by Li and Chou [22]. The most important feature of this model is the prediction of percolation probability and effective conductivity at a given volume fraction. To the author's best knowledge, these results have never been reported concurrently. The percolation probability and conductivity results are interpolated across all volume fractions near the percolation threshold using the cumulative density function fit method from Li and Chou [47] and the percolation power fit law, respectively. The model's calculations for a specific nanocomposite ultimately result in the ability to predict effective conductivity and probability of forming conducting CNT networks. Therefore, the nanocomposite is fully characterized by its electrical properties and the potential applications it is suited for can be determined. Each of these factors is presented as part of a model that is efficient and useful for the determination of electrical behavior of a polymer nanocomposite. In addition, the model's level of accuracy is determined via comparison to experimental and analytical results in the numerical results section of this thesis.

Chapter 2

The Representative Volume Element

The percolation portion of the model proposed in this thesis is based on a two step approach. First, the geometry of a CNT-based composite material is generated. Then, a spanning network algorithm determines the existence of a complete percolating nanotube network. For simplicity, the geometry of the nanocomposite is represented by a pseudo-three-dimensional representative volume element (RVE). The RVE is a two-dimensional square with an assumed thickness that approximates a three-dimensional structure. This RVE, which represents the bulk matrix material, is embedded with CNT fillers. The CNT fibers are randomly placed within the RVE at the desired concentration, or volume fraction. Next, each CNT is given extra nodes as searching points for the spanning network algorithm. Then, this algorithm uses the specified bond criteria to determine the connections between fibers. Finally, the algorithm determines whether a complete network of CNTs spans the longitudinal direction of the RVE.

2.1. Geometry Generation

The first step to accurately model the nanocomposite is to create a realistic representation of the filler geometry. The CNT fibers are modeled individually in the RVE and dispersed randomly. Each consists of a series of line elements that are controlled by length, diameter, and waviness parameters. Because this proposed model is based in part on the previous work of Elsbernd [48], the same method for creating CNT morphology is used. In addition to the shape of individual CNTs, the CNT locations in the matrix and RVE dimensions must also reflect realistic structures.

The length of individual CNTs varies greatly and depends on manufacturing and dispersion methods. Some can be as short as dozens of nanometers or as long as several microns within a given batch. Behnam and Ural [42] reported a SWNT average length of as high as 2 microns and MWNTs are usually even longer [49]. Publications, such as Wang et al. [50], have measured CNT lengths and reported large statistical length distributions. The Weibull distribution found by Wang et al. has scale and shape parameters of 5 x 10^{-6} and 2.4, respectively [50]. The inverse transformation method introduced by Elsbernd is used to randomly generate nanotube lengths for the RVE. The cumulative density function (CDF) for a Weibull distribution is given by the equation

$$F(x) = 1 - e^{-\left(\frac{x}{\alpha}\right)^{\gamma}}, \tag{1}$$

where α and γ are related to the scale and shape parameters. Solving for x in the CDF gives the equation

$$x = -\alpha[ln(1-u)]^{\frac{1}{\gamma}}. \quad (2)$$

The variable x is a random number from the Weibull distribution and the variable u is a random number from a uniform distribution. Now the distribution of lengths reported by Wang et al. can be stochastically sampled using random numbers from a uniform distribution. The distriubtion parameters are included through the equations

$$\alpha = e^{-\frac{ln\,a}{b}},\ \gamma = b, \quad (3)$$

where, a and b are the shape and scale parameters, respectively. Upper and lower length limits of 800 nm and 20 nm, respectively, are used in the inverse transformation method to generate random CNT lengths. A histogram of 8,054 random nanotube lengths is presented in Figure 4.

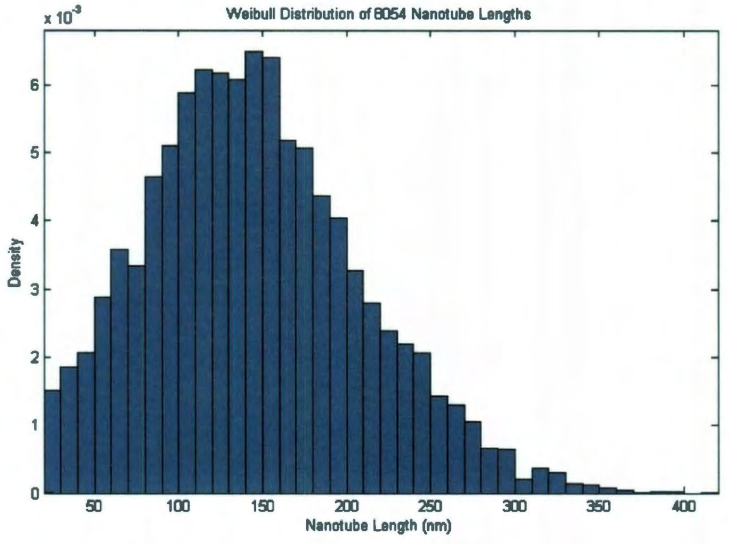

Figure 4. Example of 8,054 CNT lengths is presented as a histogram. The lengths follow a distinct Weibull distribution.

The next CNT geometrical parameter adopted from Elsbernd's model is the diameter distribution. Nanotube diameters vary as much as their lengths. Therefore, this variation is included in the model to reflect realistic nanocomposite structures. For SWNTs, diameters can range from less than one nanometer to several nanometers [49]. Grunlan et al. [51] found an average SWNT diameter of 1.2 nm and Behnam and Ural [42] reported SWNT diameters of 1.5 nm. Multi-walled nanotubes have reported experimental diameters of 7 – 20 nm [52], 50 nm [53], and even over 120 nm [49] due to their several tubular, concentric layers. Ziegler et al. [54] reported a lognormal distribution of CNT diameters ranging from about 0.5 to 2 nm. The inverse transformation method is again used for the CDF of a lognormal distribution:

$$F(x) = \frac{1}{2}\left(1 + erf\left[\frac{\ln x - \mu}{\sigma\sqrt{2}}\right]\right). \quad \textbf{(4)}$$

Isolating x in the CDF gives the equation

$$x = e^{(\sigma\sqrt{2}\, erfinv[2u-1]+\mu)}, \quad \textbf{(5)}$$

where u is a random number from a normal distribution, x is a random number from a lognormal distribution , and μ and σ are the distribution parameters.

Ziegler et al. did not report any parameters for the lognormal distribution. However, Elsbernd found them by using Matlab's "dfittool" feature on the CNT diameter histogram. The distribution fit generated values of 0.02847 and 0.33637 for μ and σ, respectively [48]. The lower limit on CNT diameters is 0.5 nm. However, the diameters must also include realistic atomic bond distances to properly account for the volume each

CNT occupies in the matrix. Carbon-carbon bond spacing is about 0.34 nm [48], which is significant compared to the diameter of nanotubes. Therefore, each CNT includes an additional 0.68 nm for bond spacing. This effect is portrayed in Figure 5.

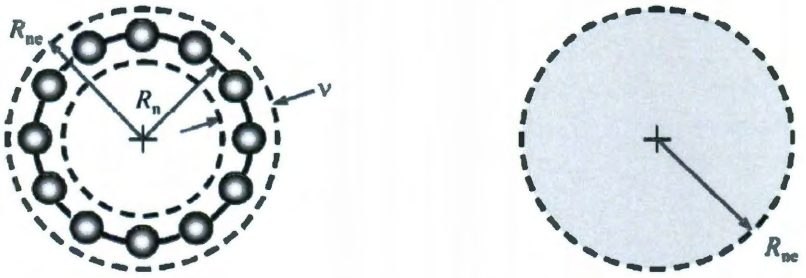

Figure 5. The structure on the left represents the cross section of a SWNT with its carbon atoms and hollow nature. The distance R_n indicates the physical CNT radius and R_{ne} is the effective radius accounting for carbon-carbon bond spacing, v.

The inverse transformation method including bond spacing generated random CNT diameters that are sampled from the lognormal distribution reported by Ziegler et al. A histogram of 1,536 diameters is shown in Figure 6.

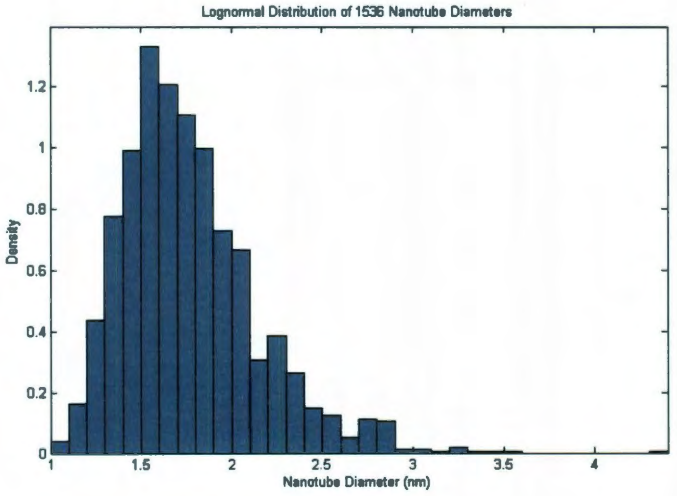

Figure 6. Example of 1,536 nanotube diameters is presented. The randomly generated values include carbon-carbon bond spacing and conform to a lognormal distribution.

The final morphological parameter included in the model accounts for the inherent waviness of nanotubes. The method utilized by Elsbernd is incorporated into the current model. Due to their low bending stiffness, matrix-embedded CNTs appear to be curved rather than straight. Further, longer fibers tend to be wavier than shorter ones. Therefore, this is accounted for in the model by creating each CNT from several, small, connected line segments. The sine of the deviation angle, $sin\,(\theta_i)$, between line segments is allowed to vary uniformly between $-sin\left(\frac{\theta_{max}}{2}\right)$ and $sin\left(\frac{\theta_{max}}{2}\right)$. The variable θ_{max} is the upper angle limit as determined by nanotube length according to the equation

$$\theta_{max} = \frac{180^{\circ}}{upper\ length\ limit} \times CNT\ length. \tag{6}$$

Therefore, the deviation angle between segments varies linearly with nanotube length. This has the effect of causing longer CNTs to be wavier and shorter ones to be straighter.

With these nanoscale characteristics of the CNTs defined, the microscale geometry of the composite structure is ready to be generated. Recent advancements in manufacturing techniques have made uniform dispersions of CNTs in thermoplastics possible [55-57]. In addition, good dispersion is one of the characteristics of a high performance nanocomposite. The nanotubes in the model are uniformly dispersed in the RVE using the following method. First, a random coordinate location is chosen within the RVE to be the first node of a fiber. Then, a second random coordinate is chosen, this time either inside or outside the RVE. The second coordinate determines the direction of the first fiber segment. Subsequent segments are added to the same fiber at random

angles within the waviness angle distribution described previously. When the specified fiber length is reached the fiber is terminated. If a fiber segment ends outside the RVE at any time, the fiber is ended at that boundary. The remainder of the segment and all subsequent segments of that fiber are transposed to the opposite boundary. This periodic boundary geometry creates a more realistic approximation of an infinite system [41]. Further, it justifies the assumption of insulating boundary conditions on the sides of the RVE [43]. Fibers are able to touch the electrodes for electrical measurement and thereby form complete spanning networks across the RVE. The process repeats until the desired volume fraction is reached for the material. Figure 7 shows the uniform dispersion of CNTs in an RVE at 0.017 volume fraction.

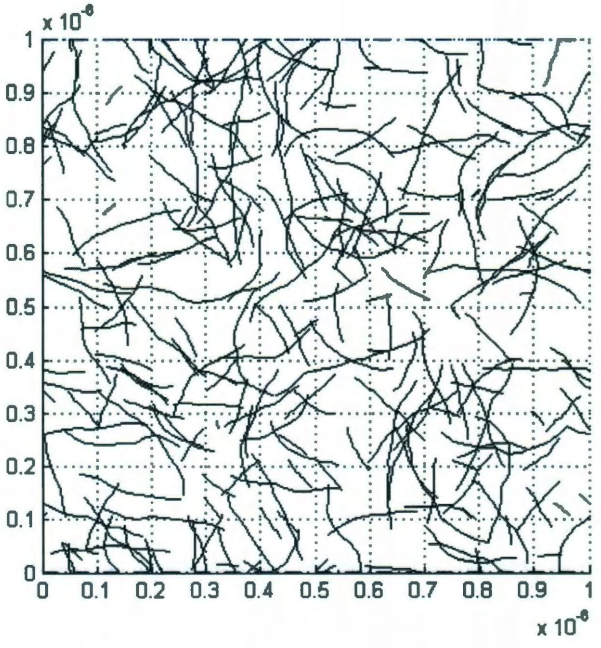

Figure 7. Nanotube geometry of an RVE with a volume fraction of 0.017 is shown.

Figure 7 is a good illustration of how short fibers tend to be straighter than long fibers. Also, several CNTs touch each boundary and the remainder of each is transposed to the opposite boundary. Figure 8 shows how the periodic geometry is generated.

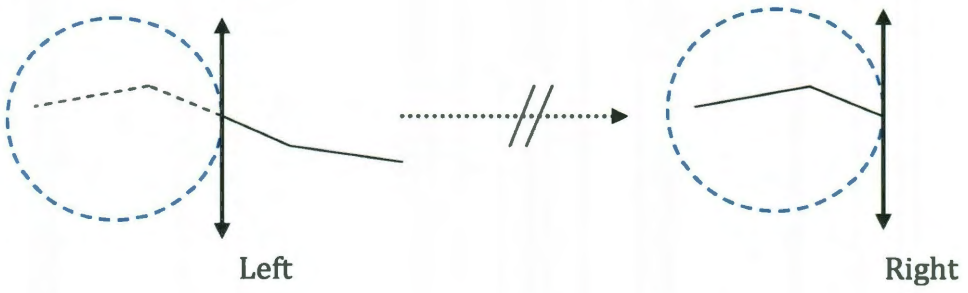

Figure 8. Diagram depicting the transposition of the fiber extending beyond the left boundary of the RVE to the right boundary edge is presented.

The dispersion of CNTs in the RVE is verified by analyzing the average number of fiber crossings along four axes of the simulated material. The average number of fibers that cross the top, right side, vertical midline, and horizontal midline for 500 random RVEs at nine different volume fractions is shown in Figure 9.

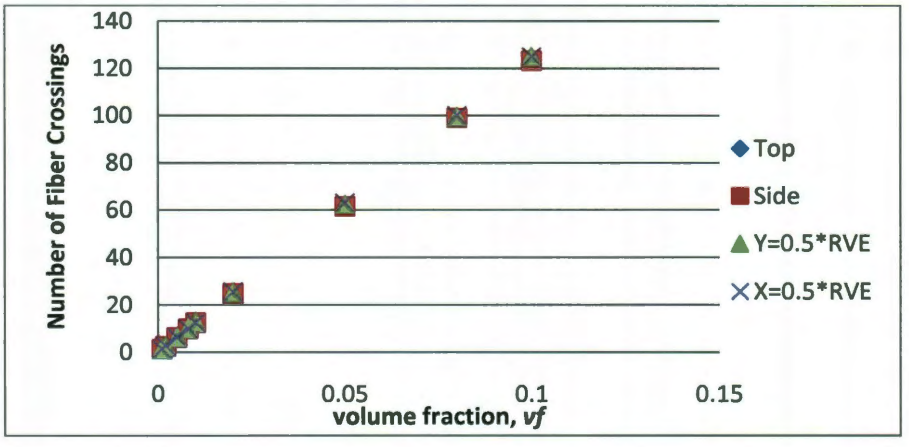

Figure 9. The number of fibers that cross the specified lines in the RVE is averaged over 500 samples. Volume fractions range from 0.001 to 0.1.

With excellent CNT dispersion in the RVE, the only geometric factor left to consider is the scaling of the RVE itself. Effective conductivity and percolation of a nanocomposite depend on fiber dimensions and interactions among CNTs. Therefore, the RVE dimensions must be large enough to capture the interactions and stochastic nature of the geometry. The goal of the pseudo-three-dimensional model is to approximate a full three-dimensional model at a fraction of the computational cost. If the RVE dimensions are too small, the effective conductivity and percolation probability will be overestimated. On the contrary, if they are too big, the computational time will be exaggerated [43]. The three-dimensional models of Dalmas et al. [4], Foygel et al. [11], and Hu et al. [16] were unit cubes. The ratio of the CNT length to RVE dimension ranged from 2.5 [4] to 5 [16] to 14 [11]. The two-dimensional model of Topinka et al. [45] had RVE dimensions of 40 x 40 μm^2 and CNT length of 4 μm. The pseudo-three-dimensional models of Li et al. [33], Li and Chou [17], and Jack et al. [43] also had RVE dimensions at least ten times CNT length. Therefore, RVE width and depth must be significantly larger than the CNT length and diameter, respectively. For this reason, dimensions of the RVEs in the present model are scaled to always be about ten times average CNT length and twice the diameter plus the tunneling distance according to the method of Li and Chou [17].

2.2. Spanning Network Algorithm

After creating realistic nanocomposite geometry in each RVE, the microstructure must be analyzed to determine the existence of a complete spanning CNT network. A complete spanning network allows an electrical connection to be made between the top

and bottom edges of the sample structure. This percolation condition is the determining factor in effective electrical properties of nanocomposites. Without percolation, no electrical current flows through the RVE. The spanning network algorithm is a searching process that determines whether a particular sample structure has percolated. In the algorithm, the CNTs are first sorted into bins and then extra nodes are added as additional searching points. The searching points are then checked from top to bottom for those that satisfy the bonding criterion and, finally, the electrical connections between CNTs are established to reflect the physics of the material.

The RVE is divided into a regular grid of searching bins. Each nanotube is assigned to a bin based upon its location in the RVE. The goal of using bins is to accelerate the searching process. Fiber nodes located in the upper left quadrant of the RVE will clearly not form connections with those located in the lower right quadrant. A typical RVE can have on the order of tens of thousands of nodes that must be analyzed in pairs. Therefore, the computational cost of the program is greatly reduced by testing only those node pairs that lie in the same region rather than searching each combination of node pair in the whole RVE. The fibers are sorted by checking the location of each node. This allows a CNT to be located in more than one bin if it crosses bin boundaries. Thus each bin will include all fibers that have at least one node in it. The redundancy introduced by this method guarantees no connections are omitted in the searching network algorithm. A visualization of a typical bin is presented in Figure 10.

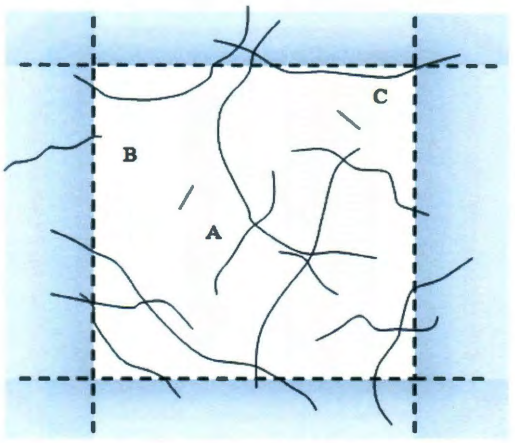

Figure 10. A typical bin with its inclusive nanotubes is presented. Each nanotube has at least one node within the bin boundaries. Fiber (A) is completely within only one bin, fiber (B) is in two bins, and fiber (C) is in four bins.

Figure 10 shows examples of fibers that fall in more than one bin. Even though fiber (B) is nearly entirely in the neighboring bin, it is also included in the example bin because it has at least one node in it. Despite this redundancy, bins greatly reduce computational time of the spanning network portion of the model. The use of a ten by ten grid, or 100 bins, decreases run time by as much as 68%, with no loss of connectivity between CNTs. When the number of bins gets too large, the possibility that connections are omitted from the network increases. Several connections that should have been included in the CNT network are missing when the number of bins exceeds 144 (12x12 grid). Therefore, 100 bins are chosen for model simulations.

Since the fibers are assembled into the bins, the remainder of the spanning network algorithm depends on the bonding criterion. This criterion determines whether any pair of points, each from a different CNT, is connected [40]. If multiple fibers and bonds belong to the same chain, they form a CNT network. A complete spanning

network consists of an unbroken series of fibers and connections that touch the top and bottom of the RVE. Theoretically, when this happens the RVE is percolated and electrical current may flow in the nanocomposite. The original method of Pike and Seager [40] is used to compare each node against all other nodes in the bin. If the bond criterion is satisfied, a connection is established between the node pair.

Traditional bond criteria fall into one of two categories: overlapping figure or inclusive figure [40]. Overlapping figure (OLF) specifies that two sites are connected if their individual searching regions intersect. Inclusive figure (IF) states that two sites are bound if each site falls within the searching region of the other. Examples of both criteria are shown in Figure 11.

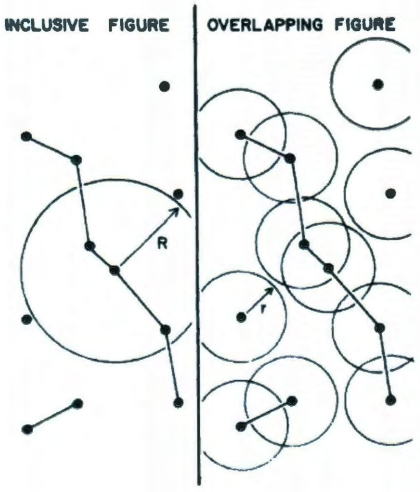

Figure 11. Both categories of bonding criteria are presented as explained by Pike and Seager [39]. The IF criterion only shows one searching region, though each node also has one for determining connections.

The work of Pike and Seager [40] found the OLF method to give a generally inaccurate approximation. On the other hand, the IF method is accurate and better suited

for random composite structures. Therefore, a pseudo-IF construct is used as a bonding criterion. For the purposes of the explanation of the method used in this model, a "lighthouse" is a searching point node that has a searching region centered on it. Likewise, a "vessel" node is any other node from the same bin, but not the same fiber, that is being compared to the lighthouse node. Thus, the model's criterion states that a connection is established between two nodes if the position of the vessel node is within the searching region of the lighthouse node. Each node in the RVE is used as a lighthouse and a vessel in the algorithm as connections between all combinations of fibers are searched for. Pike and Seager [40] proved that there is little difference between using circles or squares as searching regions. Therefore, squares are used in the proposed model for simplicity. Unlike the traditional IF criterion, the searching regions in this model are variable. The size of each variable searching region (VSR) depends on the diameter of each fiber that the pair of nodes belongs to plus the electron tunneling distance. Figure 12 illustrates how the VSR is used for fibers with different diameters.

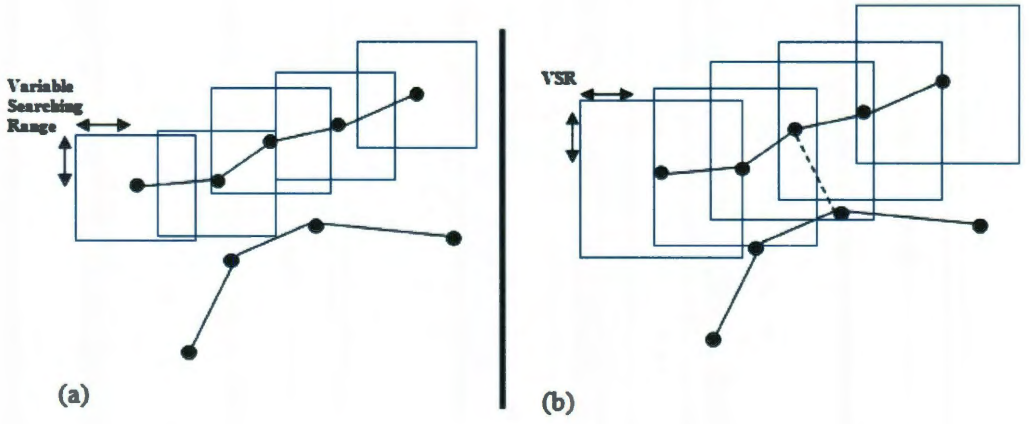

Figure 12. (a) Use of the VSR around lighthouse nodes of a fiber is shown. No vessel nodes from the other fiber satisfy the bond criterion. (b) The VSR for the same two fibers showing the impact of an increased CNT diameter. A vessel node satisfies the criterion allowing a connection to be made between the fibers.

After the fibers are sorted into bins and the bond criterion established, extra nodes are added along the fiber segments. These nodes are used as additional lighthouses and vessels for determining connections between fibers. Currently, nodes exist only at the ends of each CNT segment in the RVE. Adding additional nodes creates more VSR searching points, but also increases the number of node pairs that must be checked. Therefore, it is critical that the new nodes are properly spaced to minimize computational cost and simultaneously account for the effective tunneling region around each fiber. New node spacing is determined by the inequality

$$n \geq \frac{l_{seg}}{2(D_{min} + TunL)} - 1, \tag{7}$$

where n is the number of new nodes to add, l_{seg} is the original fiber segment length, D_{min} is the smallest possible fiber diameter, and $TunL$ is the electron tunneling distance. As long as the number of additional nodes satisfies Equation (7), the VSR boxes will leave no gaps along the fiber. This ensures all fiber connections are accounted for without increasing computational cost of the model more than necessary.

Finally, the spanning network algorithm sequentially searches the RVE for CNT clusters. This is accomplished in a series of steps beginning with determining if the random RVE has a potential spanning cluster. A complete CNT network only exists if at least one fiber is in contact with the top boundary and at least one other fiber is in contact with the bottom of the RVE. After all top and bottom edge fibers are identified, the top fibers are used as the building blocks for the CNT network. The VSR criterion is utilized to find other fibers connected to the top fibers. The nodes of the top fibers are the searching points for establishing these new connections. This part of the model is then

repeated and the newly found fibers become the searching points. With each new iteration, the fibers being added to the network approach the bottom boundary. If after any iteration no new fibers satisfy the bonding criterion, this part of the algorithm stops. Figure 13 illustrates how the network is identified in the model.

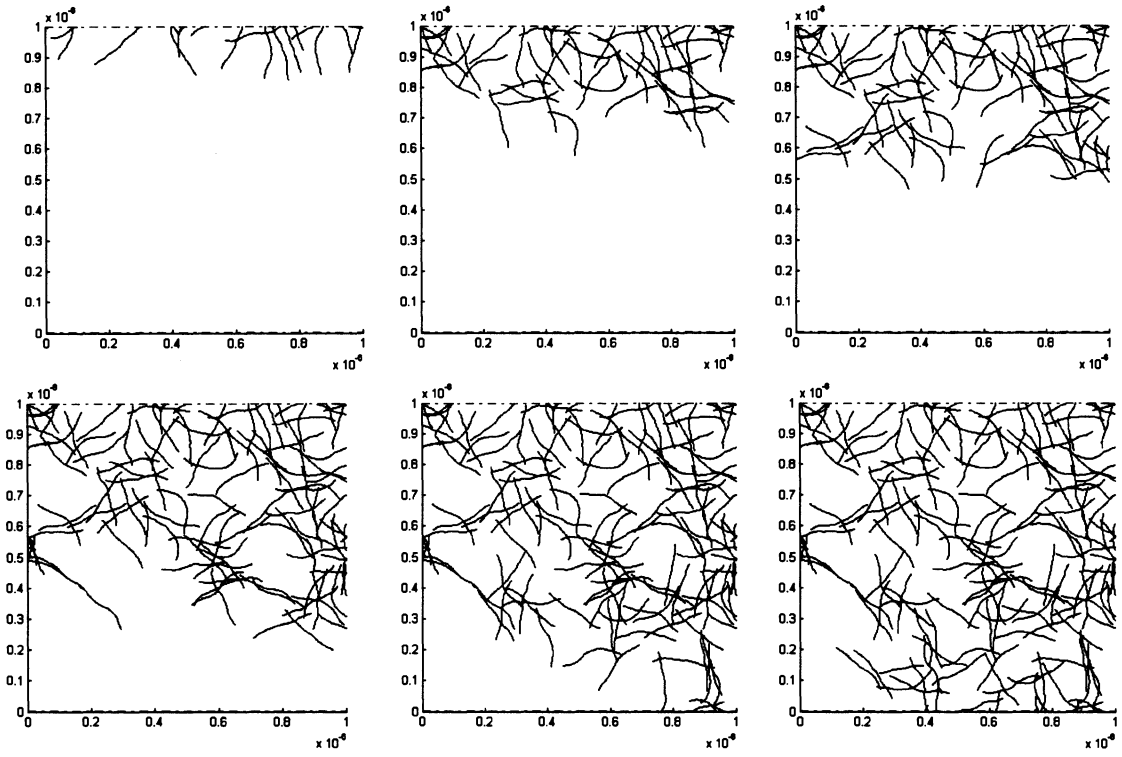

Figure 13. The progression of the spanning network algorithm is illustrated. The top left image represents the first iteration with only the top fibers shown. The bottom right image is after the last iteration showing all connected fibers in the network.

After the iterations are complete, the connections are checked for duplicates. Each fiber can have multiple connections with another fiber, but only one connection is made between the same two segments. This means CNTs that lie parallel to each other or cross multiple times will be modeled as parallel resistors. Finally, the percolation status

of the RVE is determined. If any fiber in the network is identified as touching the bottom edge, then a complete network of CNTs exists in the nanocomposite. Therefore, each RVE with a percolating network has the potential to conduct electrical current along the longitudinal direction, which is determined by the resistor network portion of the model.

Chapter 3

The Resistor Network Model

With the spanning network algorithm detailed, the resistor network and solver portion of the model can be presented. The first published application of the resistor network method is from the work of Kirkpatrick [41]. Electrical transport in inhomogeneous mixtures of conductors and insulators exhibiting percolation behavior was studied. Several two- and three-dimensional models were developed and compared to original lattice models and effective medium transport theory. As an extension of the lattice models, random resistor networks were shown to accurately simulate transport details in two-phase mixtures. This method is well suited for numerical methods involving finite element analysis (FEA) and Monte Carlo simulations. Kirkpatrick [41] demonstrated the accuracy of Monte Carlo simulations of resistor network models. The method of the proposed model uses equivalent resistors, FEA, and Kirchoff's Current Law (KCL) to determine the voltages and currents in the fiber network and effective electrical conductivity of the nanocomposite sample. First, conversion of the spanning

network into a resistor network is explained. Then, details of the use of KCL and FEA in solving the model are presented. Finally, post-processing of the data to determine effective conductivity and backbone of the RVE is discussed.

3.1. Electrical Resistance Modeling of CNTs and Contact Points

The most important portion of the resistor network model is the representing of fibers and contacts as electrical resistor elements. It is crucial that both the fiber and contact resistances are modeled accurately because they have a significant impact on the results. The intrinsic electrical properties of individual carbon nanotubes are well documented in the literature. There are numerous experiments on CNTs using a wide array of methods. The most challenging aspect of determining resistance or conductance of a CNT is in connecting a macro size measurement instrument to these nanoscale structures. Dai et al. [52] dispersed MWNTs in ethanol which was then deposited on an insulating, oxidized silicon substrate. A layer of gold strips was created on top of the CNT suspension using conventional lithography. This caused several MWNTs to touch the gold on one end and remain unconnected on the other. A coated cantilever assembly contacted the free end and applied an electrical voltage to the fiber. They were able to measure and report the resistances at several points along the CNT. Results indicated that CNT resistance is independent of applied voltage and ranges from 60 to 1930 kΩ/μm. Ebbesen et al. [5] used a similar experiment to measure electrical conductivity of individual annealed CNTs. They were able to attach four 80 nm wide tungsten leads to an individual CNT and apply small voltages across it. Multimeters recorded resistances of 0.2–43 kΩ/μm and conductivities of about 1-200 kS/cm. A more novel

approach of measuring straight MWNTs was taken by Frank et al. [7]. The CNTs were attached to the tip of a scanning probe microscope by a gold wire and colloidal silver paint to ensure good electrical contact. The probe was then lowered into a reservoir of liquid mercury to create a closed circuit. The position of the CNT in the reservoir was controlled so the current could be measured at several different locations along the fiber. Results proved the ballistic nature of electron transport in CNTs and confirmed their extremely high stable current carrying capacities. Further, resistance of the 4 μm long MWNTs was reported as 12.9 kΩ. The more recent work of Wei et al. [6] used a MWNT/chloroform solution deposited on an oxidized silicon wafer. Focused-ion-beam lithography was used to connect tungsten leads to a CNT approximately 2.5 μm apart. Two-terminal (constant voltage) and four-terminal (constant current) measurements gave similar average resistances of 2.4 kΩ and 1.7 kΩ, respectively. Additionally, experiments of Yao et al. [8] yielded two-terminal resistances of about 17 kΩ for individual metallic SWNTs. This value is slightly larger than the predicted resistance of 6.5 kΩ. Finally, Zhou et al. [58] performed two-terminal resistance measurements of SWNTs on oxidized silicon chips. The leads were gold and titanium and about 3 μm apart. They reported resistances of about 11.5 - 36 kΩ. Experimental arrangements for Wei et al. [6] and Frank et al. [7] are presented in Figure 14.

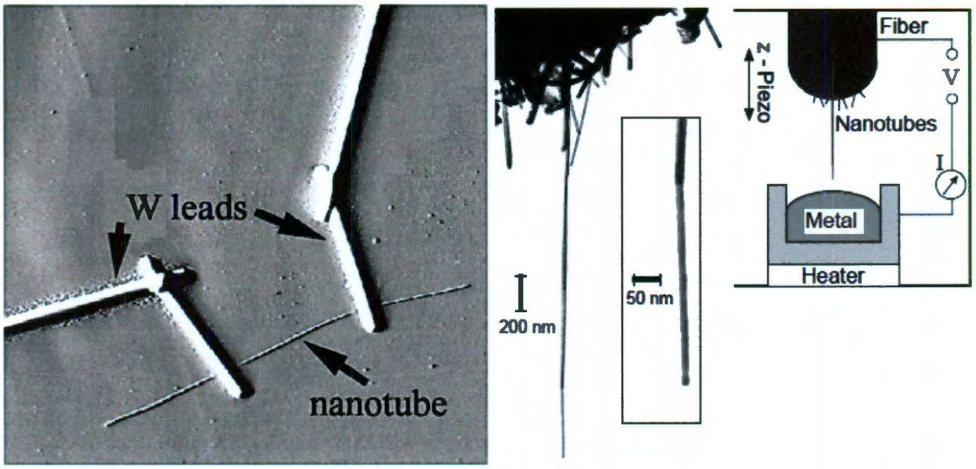

Figure 14. (a) The image from an atomic force microscope is presented showing the two tungsten leads connected to a CNT in the experimental set up of Wei et al. [6]. (b) Transmission electron micrograph of CNTs on the tip of a scanning probe microscope and a diagram of the experimental set up are presented from the work of Frank et al. [7].

The relationship between resistance and CNT dimensions appears conflicted from reported experiments. Some observations indicate a clear dependence of nanotube resistance on length and diameter while others indicate the opposite. Some report that SWNTs at least 1 μm long have constant resistance [7]. Unfortunately, the mechanisms of electrical transport in nanotubes are relatively little understood. This is most likely due to the differences in CNT types, manufacturing methods, and measurement procedures. However, several published models provide useful methods for estimating CNT resistance. Benham and Ural [42] calculated the resistance of a SWNT using its length, theoretical contact resistance at the ballistic limit (~6.5 kΩ) and the mean free path (1 μm). Theodosiou and Saravanos [59] assumed a constant resistance for all SWNTs longer than 1 μm. On the other hand, Topinka et al. [45] used a length-dependent resistance of 13 kΩ/μm. Meanwhile, the model developed by Jack et al. [43]

assumed nanotube resistance is small enough to ignore when compared to contact resistance. Most frequently, however, resistance is calculated by the equation

$$R_{CNT} = \frac{l}{\sigma A} = \frac{4l}{\sigma \pi d^2}, \tag{8}$$

where, l is the length of the CNT or CNT segment, d is nanotube diameter, and σ is CNT intrinsic conductivity [16,33,44]. Equation (8) is adopted in the present model for its simplicity and accurate representation of resistance. The nanotube resistances calculated for the model encompass a range from 0.16 to 52.33 kΩ with a mean of 5.89 kΩ. These values are similar to those reported in the experiments. Each CNT in the model is generated as a series of straight line segments connecting the fiber nodes. Therefore, each CNT is easily converted to a series of electrical resistor elements. Each segment's length and cross sectional area determine its equivalent resistance. Figure 15 illustrates the series of resistors that make up a single fiber.

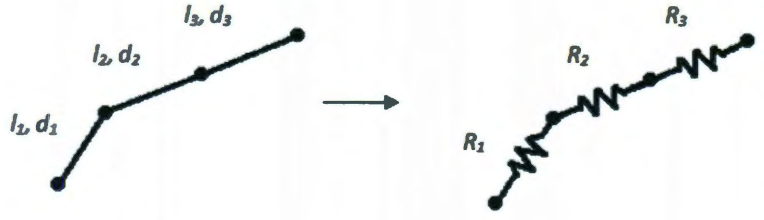

Figure 15. An illustration of a fiber being represented as a series of resistor elements is shown. The resistances of each element depend on that segment's length and diameter. The total resistance of the fiber equals the sum of its element resistances.

With all the fibers accurately represented as electrical resistors, the next step is to model the contact points in the resistor network. The contacts between CNTs throughout the RVE were determined in the spanning network algorithm. Pairs of fiber nodes,

including nodes added along the segments, were checked against the bonding criterion. For each pair of nodes that satisfied the criterion, a connection was established between the first nodes of the respective segments. Now these connections are converted to equivalent resistors to accurately reflect electrical transport behavior at CNT-CNT junctions.

Like individual nanotubes, significant experimental and numerical data exist on the characteristics of CNT junctions. Several authors [3,29,33,44,60,61] report that electrical properties of nanocomposites are governed by electron hopping or tunneling. Tunneling has the effect of lowering both percolation threshold [32] and effective conductivity [62]. The ability of an electron to jump from one CNT to another nearby CNT depends strongly on the length of insulating matrix material between the fibers [33], [38]. The resistance between nanotubes is a combination of direct contact resistance and tunneling resistance [36]. Direct contact resistance has been studied and measured by several authors. Fuhrer et al. [63] measured the direct contact resistances of crossed SWNT-SWNT junctions. They made both two- and four-terminal measurements on metal-metal, semiconducting-semiconducting, and metal-semiconducting junctions. Current-voltage measurements indicated junction resistances of about 100 - 2300 kΩ for SWNTs of the same type. Park et al. [30] also experimented on the electrical properties of crossed, metallic SWNTs. Nanotubes were ultrasonically dispersed in a silicon substrate and good contacts were made with gold-titanium electrodes using electron beam lithography. Current-voltage measurements indicated direct contact resistances of 22-26 kΩ at room temperature and 120-400 kΩ at lower temperatures. Postma et al. [29] reported electron transport properties between crossed SWNTs by using a similar method

to Park et al. Room temperature contact resistances were 12.5 MΩ, several orders higher than other experiments. This is due to the formation of a tunneling barrier in addition to the direct contact resistance between fibers. The atomic force microscope image of a crossed CNT experiment is presented in Figure 16.

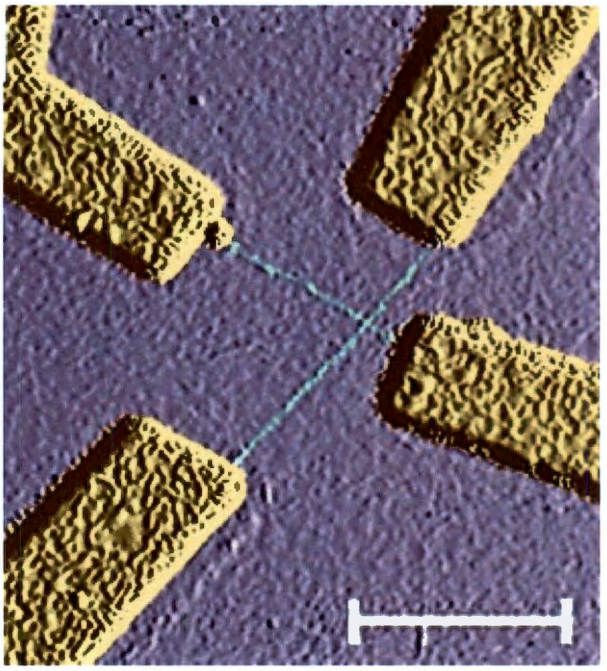

Figure 16. Crossed SWNTs with chromium/gold electrodes attached are shown in an atomic force microscope image from the experiments of Fuhrer et al. [62].

Obviously, contact resistances vary over a wide range and are influenced by a number of vaguely understood factors. Consequently, this presents challenges to modeling the contact resistors in the RVE. The direct contact resistance, tunneling distance, and tunneling resistance are all factors that determine the resistances existing at CNT junctions. Published models treat these factors in a variety of ways. Natsuki et al. [32] incorporated tunneling by assuming a penetrable soft-shell model. The thickness of the shell surrounding each CNT represents the tunneling distance. This allowed for a

qualitative study on the impact tunneling has on percolation threshold. The three-dimensional resistor network model of Sun and Song [44] incorporated tunneling resistance from the average voltage applied in the tunneling junction, length of polymer between CNTs, and current density. Further, they found tunneling distance limits of 2 - 2.5 nm based on the point where tunneling conduction equaled zero. Meanwhile, Hu et al. [16] did not include tunneling in their three-dimensional resistor network model and assumed perfect contact between CNTs. The micromechanics model presented by Seidel et al. [38] is based on the generalized self-consistent composite cylinders approach. The CNT phase was encapsulated by additional phases accounting for electron hopping. The model with hopping phases produced more accurate results than without hopping phases. However, the method to incorporate into the present model is taken from the work of Li et al. [33] and Li and Chou [17]. Both papers are based on the same pseudo-three-dimensional model utilizing the resistor network method. First, the effective tunneling distance limit is determined. Li et al. used the Simmons formula to calculate current density between crossed CNTs with a finite contact area. The current density was used to calculate tunneling resistivity and hence, tunneling resistance using the contact area. Their findings are presented in Figure 17.

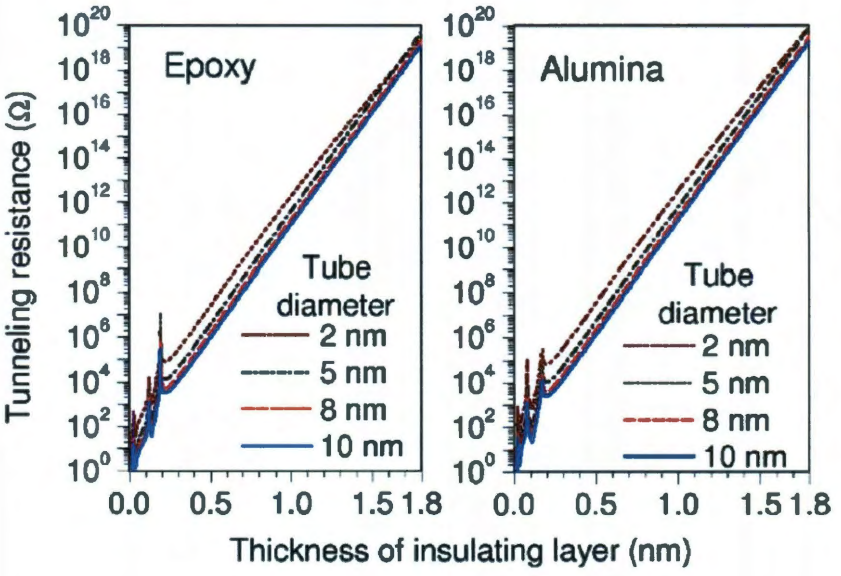

Figure 17. Calculated contact resistances for epoxy and alumina based nanocomposites are presented (Li et al. [32]). At tunneling distances greater than 1.8 nm, resistance exceeds 10^{19} Ω, which is essentially non-conducting.

From Figure 17, the tunneling resistance reaches 10^{19} Ω at a tunneling distance limit of 1.8 nm. This is close to the 2 - 2.5 nm limit found by Sun and Song [44]. A limit of 1.8 nm is used in the present model as the maximum polymer distance through which an electron can tunnel from one CNT to another. The 2 nm diameter CNT/epoxy curve in Figure 17 is used to calculate contact resistance from tunneling distance. This curve was imported using a coordinate finding program developed at Rice University [64] and approximated using Matlab's "polyfit" tool. The three-coefficient fit generated is shown in Figure 18.

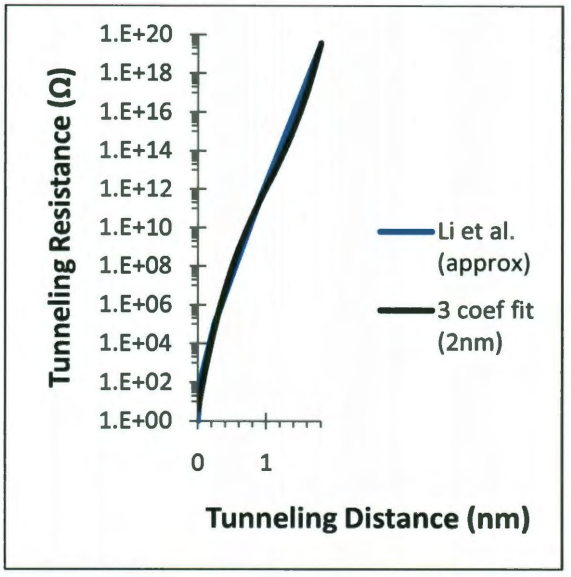

Figure 18. The approximate tunneling distance and resistance curve from Li et al. [32] is shown with the three–coefficient exponential curve fit.

Tunneling resistance is calculated in the model based on the equation from the curve fit. The three-coefficient fit is

$$R_c = e^{(ax^3+bx^2+cx+d)}, \tag{9}$$

where,

$$a = 9.3845,$$

$$b = -28.974,$$

$$c = 46.0367,$$

$$d = 1.3158,$$

and, x is the tunneling distance. The tunneling distance can vary from 0 nm to 1.8 nm. Therefore, the tunneling distances for all connections in the model are sampled randomly

from a normal distribution similar to the method of Li and Chou [17]. A mean tunneling distance of 0.8388 nm and standard deviation of 0.2243 are used. Figure 19 presents the resulting distribution.

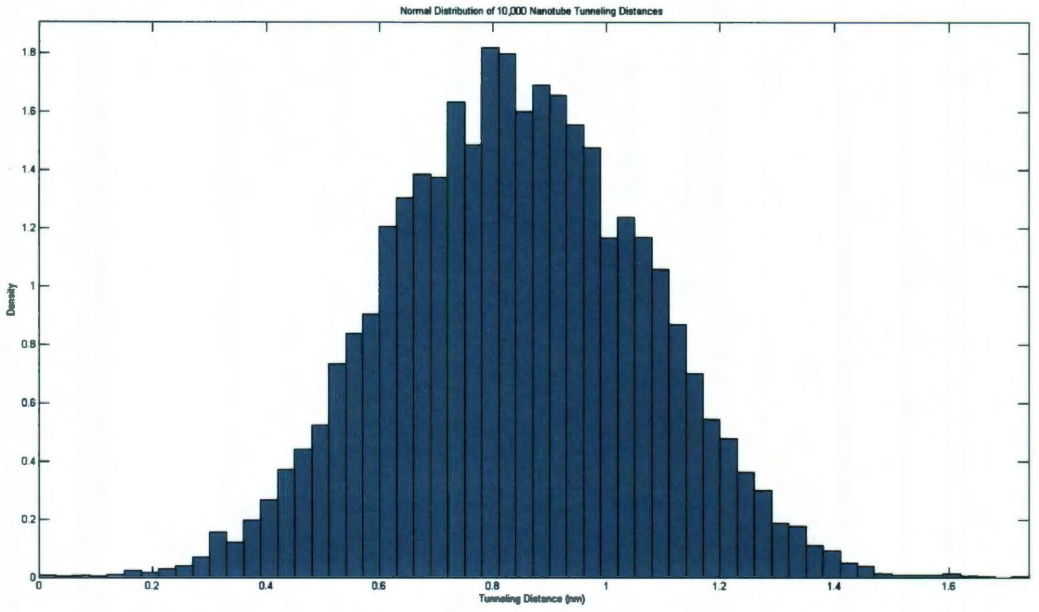

Figure 19. An example of a normal distribution used to sample tunneling distance is presented for 10,000 CNT-CNT connections in the model.

For each connection established in the resistor network, a random tunnel distance is generated from the assumed normal distribution. Then, this value is used to calculate a tunneling resistance from the exponential fit in Equation (9). The lower limit of contact resistance is set at 10^5 Ω to reflect direct contact. Maximum resistance is limited to be 10^{16} Ω to represent the highest possible tunneling distance and to prevent singularities in the solver. A distribution of contact resistances generated using this method is presented in Figure 20.

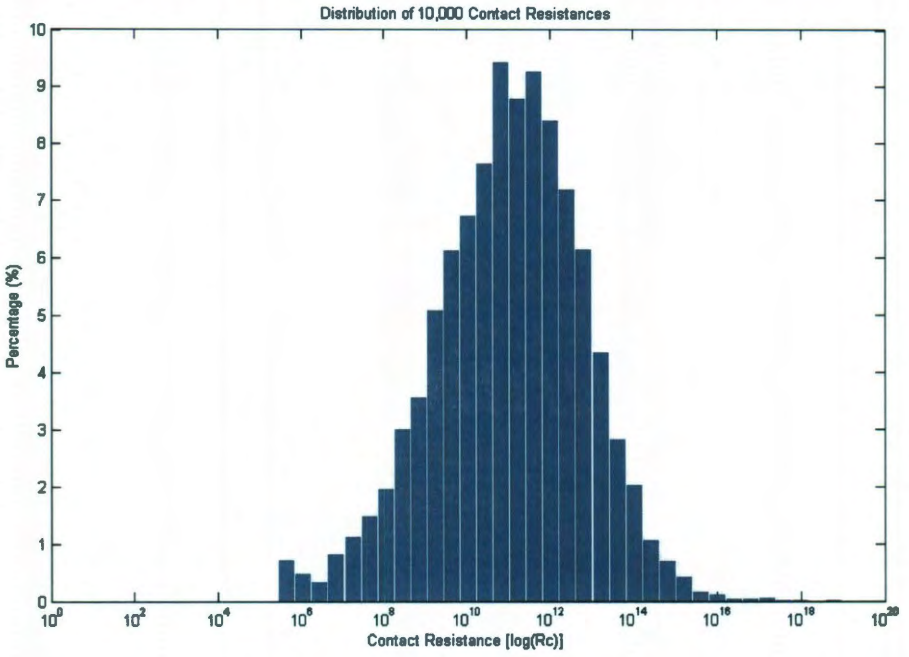

Figure 20. Contact resistance distribution for the method used in this model is shown for the same 10,000 nanotube contacts used in Figure 19.

Now, each CNT and connection in the spanning network is assigned a resistance. An example of connected fibers in the RVE is represented schematically in Figure 21.

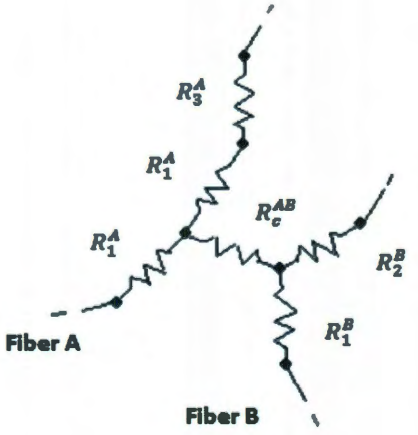

Figure 21. A schematic electrical diagram of the connection between two nanotubes in the model is shown.

The location of the contact is determined from the VSR and respective fiber dimensions in the spanning network algorithm as described in Chapter 2. The nanotube resistances and the contact resistance, R_C^{AB}, are calculated from the methods detailed above. After the complete spanning network is converted to an equivalent resistor network, the next step is to employ Kirchhoff's Current Law in conjunction with finite element analysis to solve for the system voltages and currents.

3.2. Details of the Model

The application of KCL to resistor networks is well established. Kirkpatrick [41] was among the first to use KCL on two- and three-dimensional site and bond percolation models based on resistor networks. The foundational principle of KCL is conservation of electrical charge. It states that the sum of the currents at a given point, or in this case node, must equal zero. Theoretically, an intersection of two or more electrical components cannot have a net positive or negative charge. Further, the current entering and exiting an individual component must the same. These basic laws of electrostatics also apply to the RVE as a whole. The total current entering and exiting the nanocomposite system must be the same so as to satisfy conservation of charge. Essentially, the movement of electrons through the percolating model can be viewed as a fluid flowing through the resistor network. Therefore, all electrons that enter the RVE must also exit because there are no storage or generation devices within the system. The process of applying KCL and solving the equivalent resistor network using FEA is presented.

The two pieces of information required to apply KCL and FEA are the calculated resistances from the previous section and nodal connection information from Chapter 2. Each component in the network is modeled as a one-dimensional linear resistor element. This includes both the nanotubes and the tunneling contacts. Figure 22 diagrams the features of a resistor element.

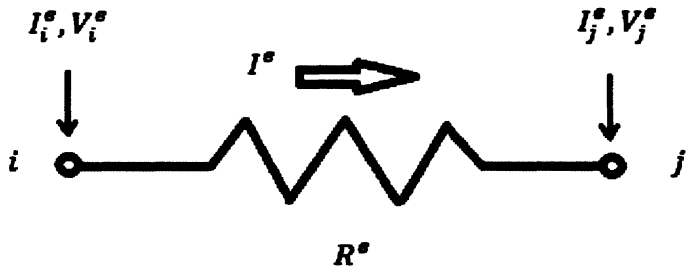

Figure 22. Visualization of a one-dimensional resistor element is shown. The nodal voltages and element current are governed by Ohm's Law and KCL.

Current is calculated *across* each resistor element. Therefore, current entering from node i and node j are equal in magnitude, but opposite in direction with respect to the resistor. Applying Ohm's Law at each node yields the equations

$$I_i^e = \frac{1}{R^e}(V_i - V_j), \tag{10}$$

$$I_j^e = \frac{1}{R^e}(V_j - V_i), \tag{11}$$

which can be represented in matrix form as

$$\begin{Bmatrix} I_i^e \\ I_j^e \end{Bmatrix} = [K_{ij}^e] \begin{Bmatrix} V_i \\ V_j \end{Bmatrix}, \tag{12}$$

where the element coefficient matrix is

$$[\boldsymbol{K}_{ij}^{e}] = \frac{1}{R^e}\begin{bmatrix} 1 & -1 \\ -1 & 1 \end{bmatrix}. \tag{13}$$

Equation (12) is the finite element formulation for a single resistor element. The nodal currents included in this equation are with respect to the particular resistor element of interest. The nodal results for the system must satisfy Equation (12). However, currents at the nodes may include contributions from more than two components. Because the net current at each node must be zero as explained previously, the total current at a node can be written using KCL at the nodes as:

$$I_i = \sum_{j=1}^{n} I_{ij} = \sum_{j=1}^{n} \frac{1}{R_{ij}}(V_i - V_j) = 0\,. \tag{14}$$

The total current at node *i* depends on *n* directly connected components, each with current I_{ij} and resistance R_{ij}, which always sum to zero. Therefore, nodal currents are summed at each system node using Equation (14) where the individual resistor element currents are represented by Equation (10). The complete CNT network is simply a system of linear algebraic equations. The assembly of nodal KCL equations is written in matrix form as

$$\boldsymbol{I} = \boldsymbol{K}\boldsymbol{V}\,, \tag{15}$$

where, $\boldsymbol{I}$ is the vector of external input currents, $\boldsymbol{V}$ is the vector of nodal voltages, and $\boldsymbol{K}$ is the global coefficient matrix. Because the boundary conditions for this problem do not include current inputs, $\boldsymbol{I}$ is simply a vector of zeros. The global coefficient matrix is built by assembling the coefficient matrices from Equation (13). This is accomplished for each resistor element in the network using connectivity information according to standard FEA procedures.

After assembling the global matrix equation, the next step is to apply the boundary conditions and solve the system. Essential boundary conditions are applied to the top and bottom of the RVE in the traditional FEA manner and can be found in any standard book on the finite element method, such as Akin [65] or Zienkiewicz et al. [66]. The system of equations is solved in skyline storage form by U^TDU – factorization and backsubstitution. Initial results consist of electric potentials at the CNT nodes. These voltages, V_i and V_j, are then used to calculate the current in each linear resistor, R^e, using the equation

$$I^e = \frac{1}{R^e}(V_i - V_j)\,. \tag{16}$$

Element currents provide the basis for two important results presented by the model. The first important result is backbone identification. Not all resistor elements, or fibers, in the network contribute to electrical properties. In fact, only a small fraction will make up the path of least resistance and carry the bulk of the electrical current. This fraction of nanotubes is known as the backbone [41]. Theoretically, the backbone consists of all fibers with nonzero currents [22]. Visualization of the backbone is

accomplished from the highest calculated currents in the fibers. In addition to identifying the backbone, the model simultaneously calculates the effective electrical properties of the composite. The total current entering the RVE is calculated by summing the element currents of resistors in contact with the top of the microstructure:

$$I_{total} = \sum_{j=1}^{m} I_j^e \,. \tag{17}$$

In Equation (17), m is the total number of linear resistors in contact with the top boundary of the RVE and I_j^e represents each of their calculated currents. Finally, the effective electrical properties of the system are calculated with the equations [17,43]

$$G_{eff} = \frac{I_{total}}{(V_{top} - V_{bottom})}, \tag{18}$$

$$R_{eff} = \frac{1}{G_{eff}}, \tag{19}$$

$$\sigma_{eff} = \frac{G_{eff}}{t}. \tag{20}$$

Equation (18) produces the effective electrical conductance of the system in units of Siemens (S), where V_{top} and V_{bottom} are the applied voltages on the RVE boundaries. Conductance measures how easily current flows in the system and is the inverse of Ohm's Law in Equation (19). Resistance measures strength of opposition to current flow in the system and is analogous to friction in mechanical systems. Equation (20) is the effective electrical conductivity of the nanocomposite where t is the RVE thickness.

Effective conductivity indicates the material's overall ability to conduct an electrical current and is measured in Siemens per meter (S/m).

With the basic model in place, effective nanocomposite properties can be estimated for any random microstructure. Due to the stochastic nature of system parameters, it is necessary to simulate the nanocomposites by using the Monte Carlo method. Statistical variation is eliminated in the results by averaging the effective conductivities for a sufficiently large number of random microstructures. The general procedure for the Monte Carlo simulations is illustrated in Figure 23.

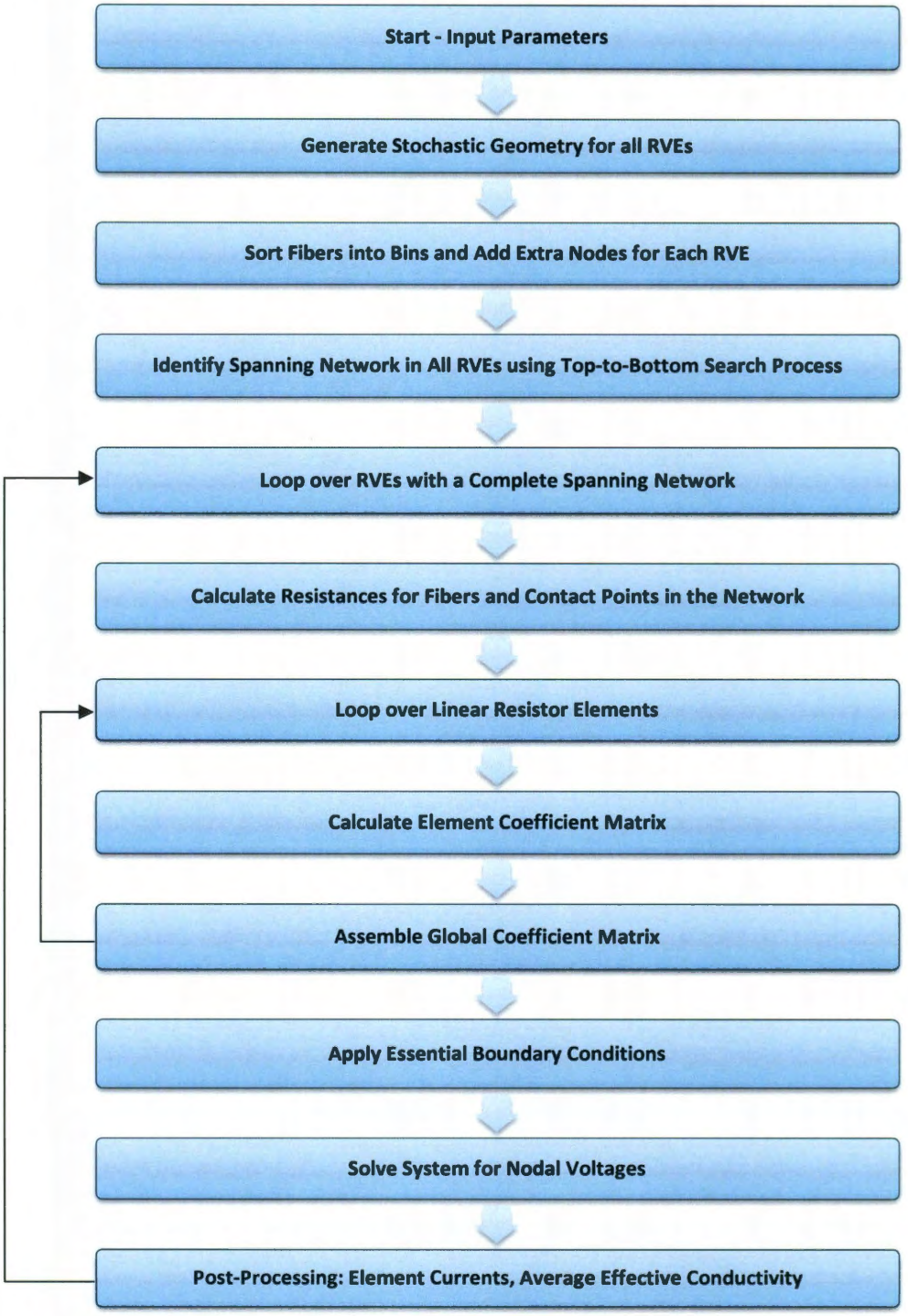

Figure 23. A block diagram of the process the resistor network model follows is shown. The program only enters the loops for RVEs that have complete spanning networks. All others are assumed to be non-percolating and insulating materials.

Monte Carlo analysis, KCL, and FEA are easily integrated in the model. The numerical process is straightforward and the results are simple. However, the real challenge and complexity of the model lie in the physical representation of the nanotubes and their electrical behavior. This leads to a multitude of controllable input parameters and variables. They include CNT dimensions, RVE dimensions, CNT morphology, number of bins, number of RVEs, boundary conditions, VSR tunneling distance, matrix and CNT conductivities, and fiber and contact resistances. The only ones kept constant for all studies are the boundary conditions, which are fixed at 100 V and 0 V for top and bottom, respectively, and number of bins, which is optimized at 10 from Chapter 2. All others must be determined. In all actuality, these variable parameters are what give the model its versatility and flexibility.

Chapter 4

Numerical Results

The results of the model proposed in this thesis are discussed in this chapter. First, numerical data from the model are verified through Monte Carlo convergence analysis. Several case studies on the general behavior of the model are then discussed. Subsequently, electrical percolation probability results are presented and compared to other available models. Finally, a comparison of effective electrical conductivity results to models and experiments is attempted including detailed summarized results for several specific simulated nanocomposites.

4.1. Model Convergence

The first results presented from the current model include effective electrical conductivity and percolation probability data for Monte Carlo simulations of 500 RVEs. In order to verify the characteristic behavior of the model, all stochastic input parameters must be held constant. With all input parameters fixed, the only variable behavior

inherent in the model involves the location and orientation of each CNT. Therefore, by executing the simulations at several different volume fractions and tunneling distances, it is possible to obtain important information about the electrical behavior of CNT nanocomposites.

An intrinsic benefit to the proposed model is the ability to obtain the ratio of percolated RVEs, which reflects the percolation probability, and effective electrical properties from the same simulation. Each unique analysis performed in this thesis had a potential difference of 100 volts applied to the boundaries. The specified boundary conditions for the RVE mirror those utilized in Elsbernd's model [48]. Analogous to his thermal model, an electric potential is applied across the intended measurement direction of the RVE. The top boundary, also referred to as the source, was given an input voltage of 100 volts. Likewise, the bottom boundary, or drain, acted as ground with 0 volts. Also similar to the thermal model, the sides of the RVE were insulated so that all electrical current was directed through the bottom boundary. Electrical conductance was calculated from the total flux, or current, at the drain. These boundary conditions for the electrical analysis are represented in Figure 24.

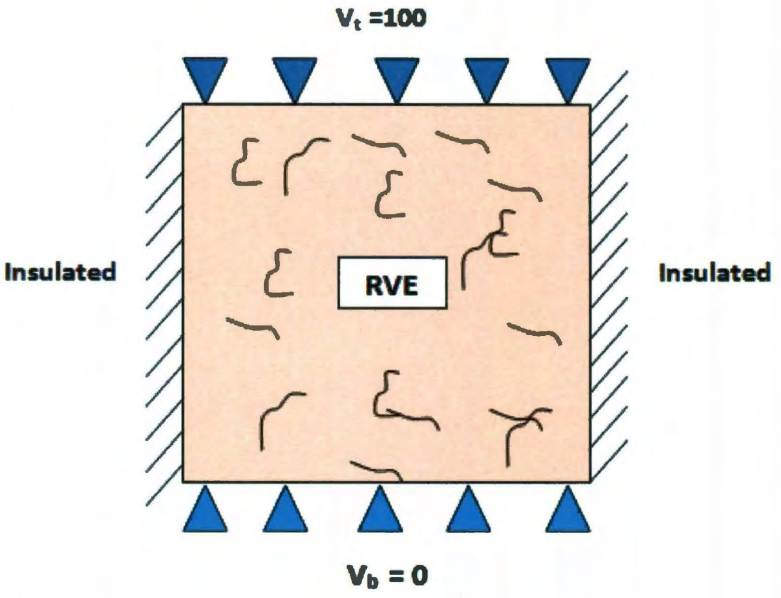

Figure 24. The boundary conditions for the electrical problem are shown. The top (source) has an applied voltage of 100 V, the bottom (drain) is grounded (0 V), and the sides are insulated.

The choice of potential difference applied across the RVE effects only the magnitude of the total current. The total current is then divided by the applied potential to obtain effective conductance. Therefore, the calculated conductance for a particular RVE is independent of the voltage applied to the boundary. To ensure valid comparison, however, the boundary conditions were kept the same for all analyses in this thesis.

The numerical model contains six distinct sources of stochastic behavior. Each is a random variable either sampled from a distribution or directly calculated from another stochastic variable. These inputs are easily controlled for the particular application or study. Location and orientation of the CNTs are stochastic parameters of interest for verifying convergence of the underlying model. Random dispersion and poorly controlled CNT alignment are fundamental characteristics of these materials. Therefore,

the percolation and resistor network algorithms must converge in a reasonable number of simulations for the model to be valid. All other parameters are held constant at the values shown in Table 1.

Table 1. Input parameters for the initial Monte Carlo convergence analysis.

INPUTS		
CNT length	200	nm
CNT diameter	2	nm
CNT conductivity	1E+07	S/m
Contact resistance	1E+06	ohms
Number of RVEs	500	
Number of bins	100	
RVE size	1E-06	m
RVE thickness	5	nm
Theta (CNT waviness)	0.0	deg
Applied potential	100	V
Tunneling distance	1.8	nm

The length and diameter are chosen to reflect typical short CNT fibers with an aspect ratio of 100. The fibers are perfectly straight when the variable "theta" is set to zero. Dimensions of the RVE are scaled to be at least 10 times the aspect ratio and 5 times the largest filler dimension according to the method of Hu et al. [16]. Thickness is approximately twice the CNT diameter plus the tunneling distance according to the model of Li and Chou [17]. The CNT conductivity is set at 10^7 S/m, a value typical of SWNTs, and tunneling distance is 1.8 nm as found in the study by Li et al. [33]. A microstructure created by the program with the geometrical inputs given above is shown in Figure 25.

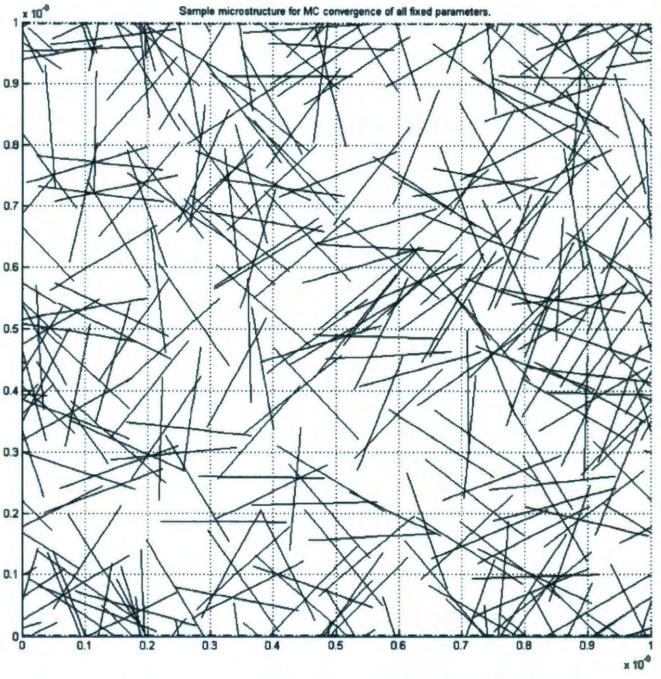

Figure 25. Shown is a sample microstructure with all stochastic variables fixed including CNT length, diameter, waviness, and contact resistance. Only the location and orientation of the fibers are randomly determined.

The convergence analysis performed in this section involved creating, analyzing, and solving 500 different random RVEs at chosen CNT volume fractions of 0.008, 0.01, 0.012, 0.014, 0.016, 0.018, 0.02, 0.022, 0.024, 0.026, 0.028, and 0.03. These values are chosen to span the percolation region of a material with the given input parameters. At 0.008 volume fraction, all RVEs are expected to be insulating and at 0.03 volume fraction, all are expected to be electrically conducting. For each RVE at each volume fraction, the percolation network algorithm evaluates the existence of a complete spanning network of CNTs. For each RVE without a complete CNT network, the material is assumed to be insulating and the effective conductivity equals the matrix conductivity. For each RVE with a complete percolating network, the nodal voltages are

solved using KCL as described in Chapter 3. Then the total electric flux at the drain is calculated according to Equation (17). Effective electrical conductivity of the nanocomposite is calculated from the equation

$$\sigma_{eff} = \frac{I_{tot}}{t(V_{source} - V_{drain})}. \tag{21}$$

In this equation, t represents the thickness dimension of the RVE and V_{source} and V_{drain} are the boundary condition voltages applied to the top and bottom of the RVE, respectively.

Before verifying the Monte Carlo convergence of effective electrical conductivity, the results of the percolating and resistor network algorithms are analyzed. Percolation behavior in two-phase materials where the inclusion phase has intrinsic physical properties several orders of magnitude larger than the bulk phase always exhibits a characteristic threshold region. This region has a large jump in the composite physical property over a very small range of filler concentration. The percolation ratio and effective conductivity results are presented in Figure 26.

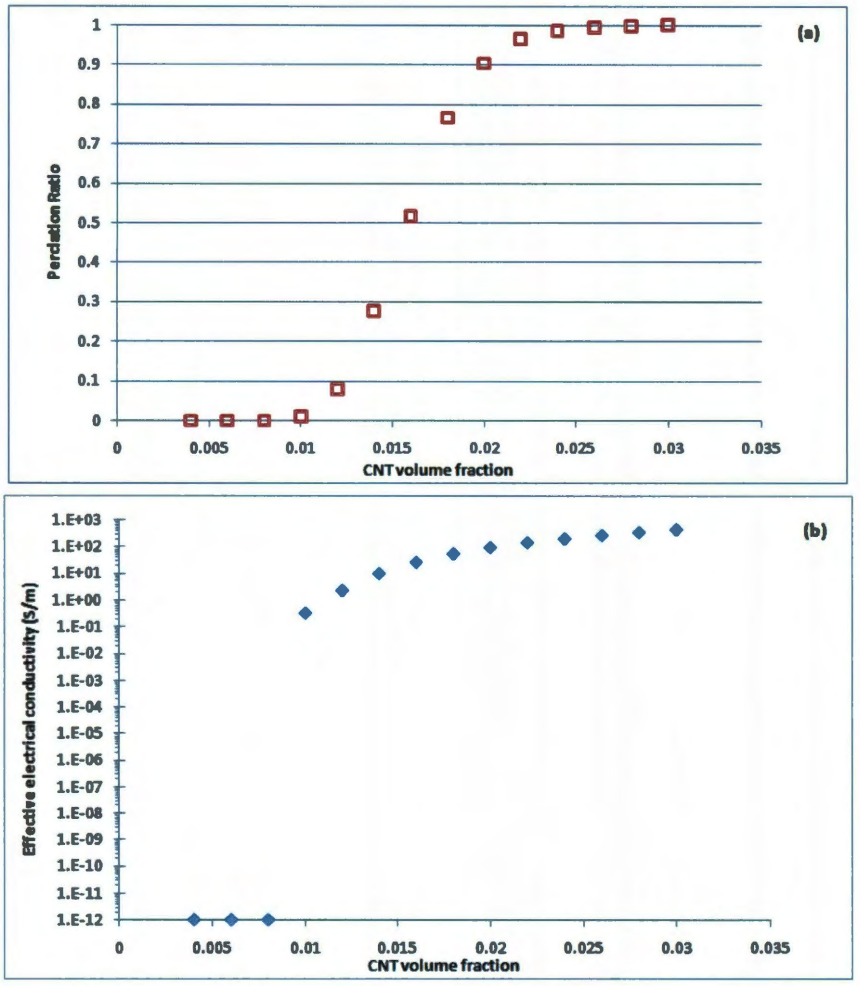

Figure 26. (a) The ratio of RVEs with complete spanning CNT networks at each simulated volume fraction is presented. (b) The effective electrical conductivities averaged over all 500 RVEs were simulated at the same volume fractions to capture the characteristics of the percolation threshold region.

Figure 26(a) shows that at 0.01 volume fraction a small number of RVEs in the simulation begin to form complete conductive networks. Between 0.012 and 0.024 volume fraction, 97.6% of the RVEs percolate. By 0.03 volume fraction, all 500 RVEs form a complete spanning CNT network in the simulation. Correspondingly, in the effective conductivity plot all RVEs at volume fractions below 0.01 are insulating. At 0.01 and higher, the average effective conductivities are at least eleven orders of

magnitude higher indicating electrically conductive behavior. After 0.01 volume fraction, the average conductivity increases only modestly by about three orders of magnitude. The effects CNT fillers have on the properties of an insulating matrix are confirmed by the significant enhancement of effective conductivity at relatively low CNT concentrations.

Results of Monte Carlo convergence analysis verify the number of random RVEs used in the simulation. The value of 500 was chosen based on the work of Esteva [64] and Elsbernd [48]. Their models used the same general methodology of generating and controlling creation of the RVE geometry. Contrastingly, the model presented in this thesis analyzes electrical behavior rather than thermal or elastic. The data from the above simulation and three additional simulations were used to confirm the choice of 500 RVEs for this model. The normalized average electrical conductivity convergence results are presented in Figure 27.

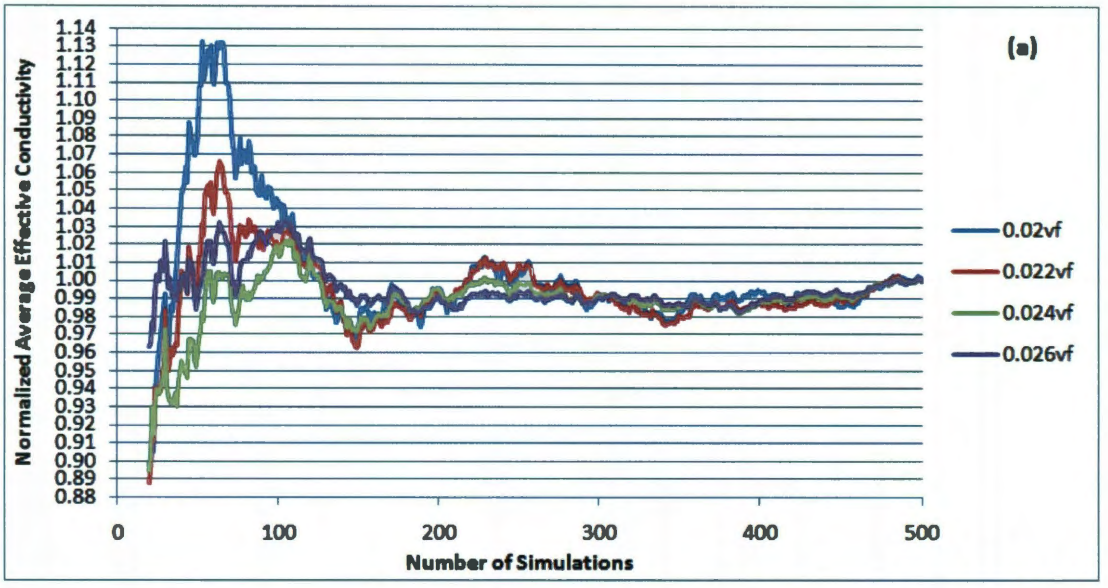
(a)
Normalized Average Effective Conductivity
1.14
1.13
1.12
1.11
1.10
1.09
1.08
1.07
1.06
1.05
1.04
1.03
1.02
1.01
1.00
0.99
0.98
0.97
0.96
0.95
0.94
0.93
0.92
0.91
0.90
0.89
0.88
0
100
200
300
400
500
Number of Simulations
0.02vf
0.022vf
0.024vf
0.026vf

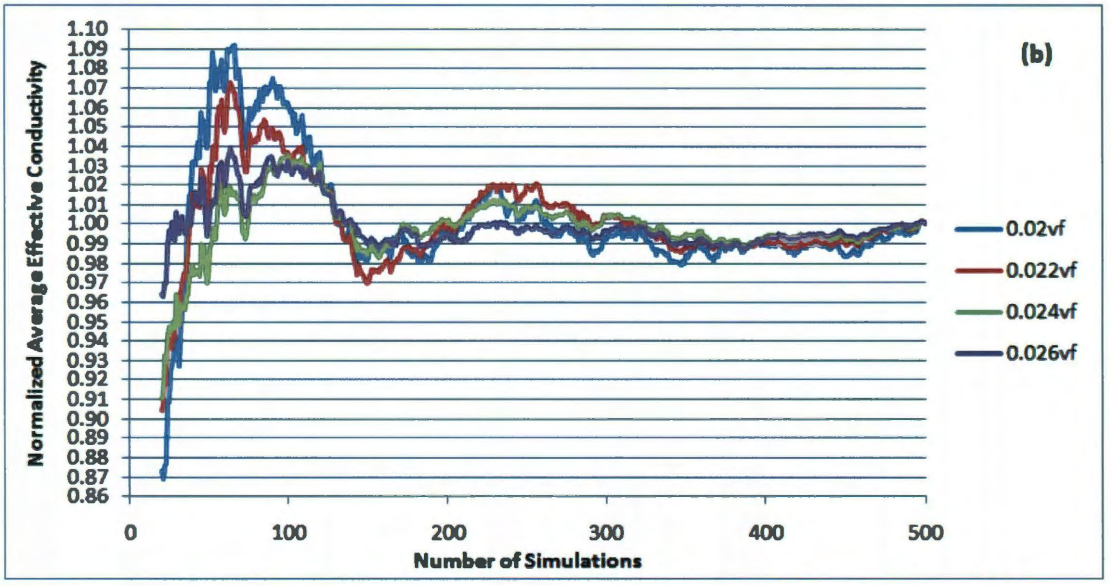
(b)
Normalized Average Effective Conductivity
1.10
1.09
1.08
1.07
1.06
1.05
1.04
1.03
1.02
1.01
1.00
0.99
0.98
0.97
0.96
0.95
0.94
0.93
0.92
0.91
0.90
0.89
0.88
0.87
0.86
0
100
200
300
400
500
Number of Simulations
0.02vf
0.022vf
0.024vf
0.026vf

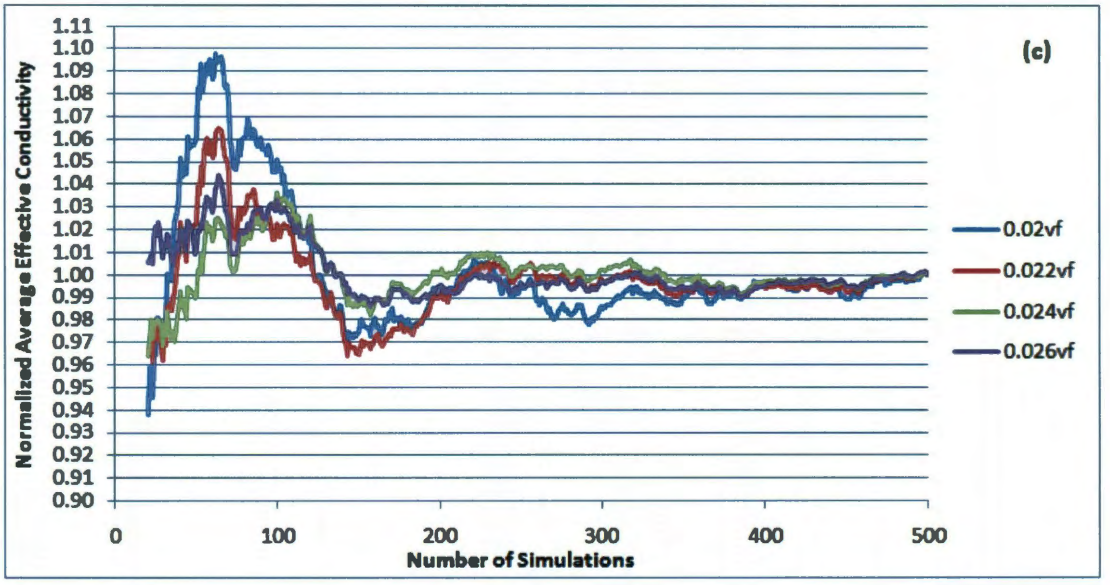

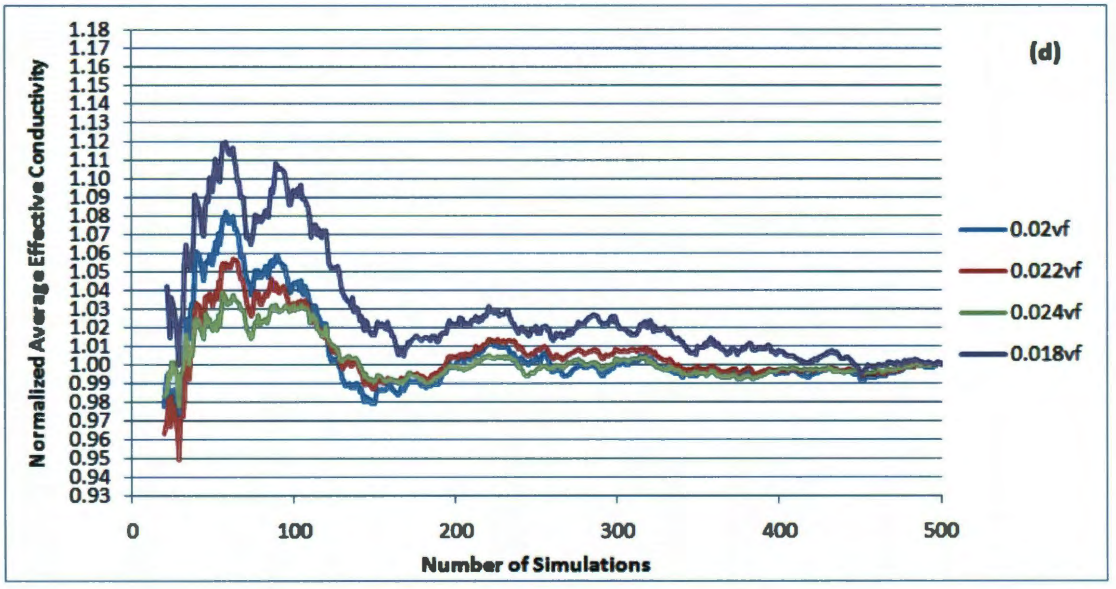

Figure 27. Normalized average mean is calculated over 500 random RVEs with fixed variables for searching (tunneling) distances of (a) 0 nm, (b) 1.8 nm, (c) 4 nm, and (d) 10 nm.

Each of the plots in Figure 27 indicates that at Monte Carlo simulations below about 450 there is considerable variation in the average effective conductivity results. Results are very erratic below about 250 RVEs, varying by as much as 13%. Above 450 RVEs all simulations at the given volume fractions are within 1% of the normalized mean. These results confirm the assumption of 500 RVEs for all simulations presented in this study. However, preliminary studies incorporating all aforementioned stochastic parameters indicate that up to twenty times more RVEs are necessary for acceptable convergence.

Information gleaned from the Monte Carlo convergence study also provides valuable insights on an important physical behavior of CNT/polymer composites. Discussion in Chapter 3 included the phenomenological nature of atomic-scale effects on electron transport. The model incorporated this physical attribute with the input variable of tunneling distance. Each of the four sets of simulations in the convergence study was conducted with a different tunneling distance ranging from 0 nm to 10 nm. Comparisons of the percolation ratio and electrical conductivity results are presented in Figure 28.

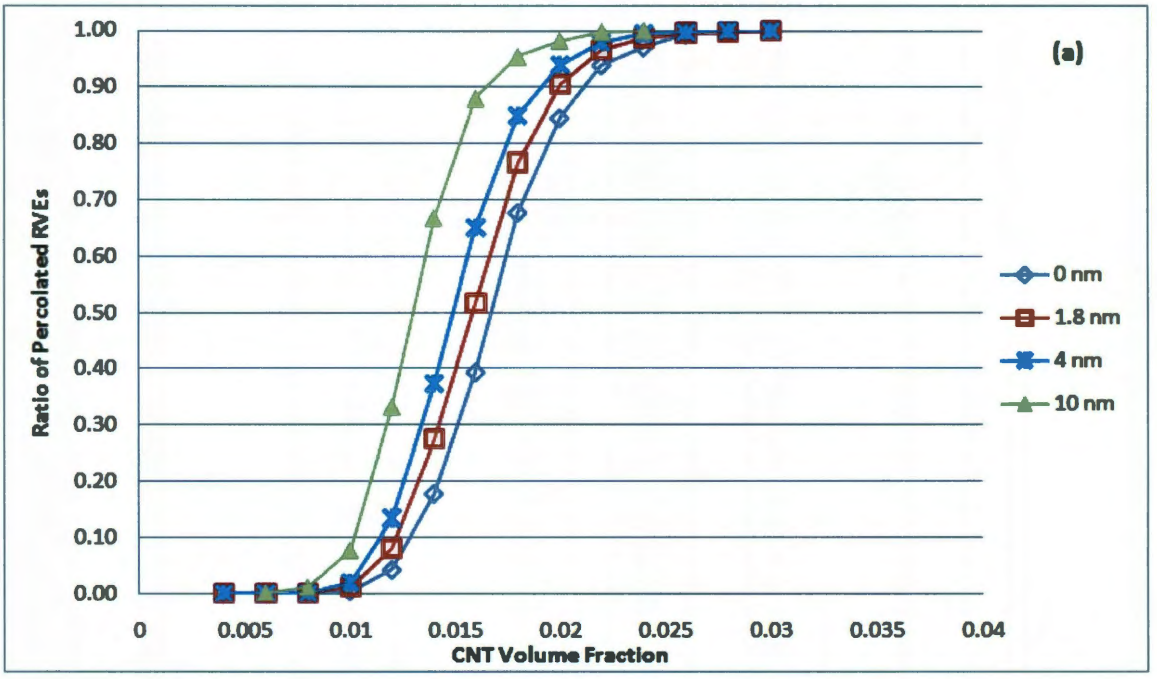

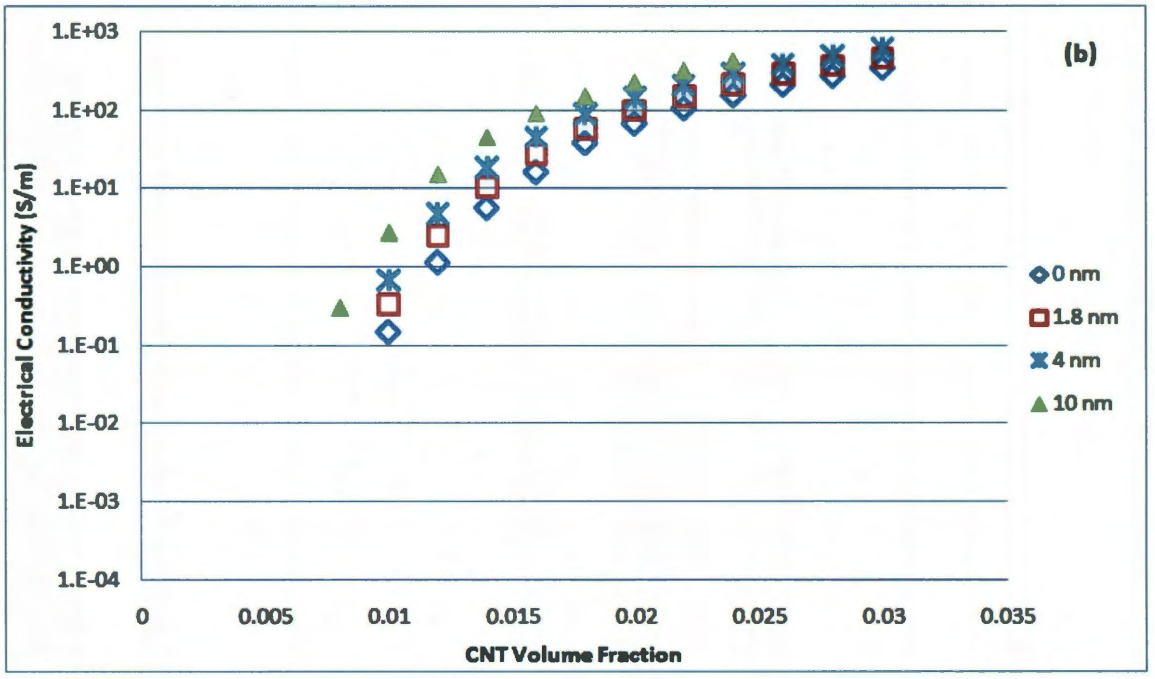

Figure 28. Effect of tunneling distance as part of the bond criteria on (a) the ratio of percolated RVEs out of 500, and (b) the effective electrical conductivity averaged over 500 RVEs.

It is readily determined from Figure 28 that percolation ratio and effective conductivity results mirror the physical behavior of the material. As tunneling distance increases, the ratio of percolated RVEs increases for each volume fraction. Increasing the tunneling distance allows more CNTs to meet the bonding criterion that previously had not formed connections. Thus, the probability of spanning network formation at a given volume fraction increases. The effective conductivity also increases at each volume fraction shown in Figure 28(b). This result reflects an increase in RVEs containing complete spanning networks and an increase in the number of percolation paths available for current to flow. The differences in percolation and conductivity results are amplified for the case of 10 nm. The significantly larger tunneling distance causes a pronounced reduction in the percolation threshold. The material is completely insulating at 0.008 volume fraction when tunneling is less than 10 nm. However, at 10 nm, 1% of the RVEs form complete networks at the same concentration. Lower percolation thresholds and higher effective electrical conductivities are fundamental aspects the electron tunneling phenomenon in nanocomposites.

The final study on the stochastic behavior of this model determined the impact of the random CNT length and diameter variables. For this study, two sets of simulation data are gathered. For the first, CNT length and diameter are sampled from Weibull and lognormal distributions, respectively. For the second set, CNT dimensions are fixed at 149.5 nm and 1.77 nm for length and diameter, respectively. These chosen values maintain the same average aspect ratio for both sets of data. This allows the statistical variation between the two sets to be restricted to the variables themselves and to isolate

the effects they have on the results. The convergence behavior for 500 RVEs at volume fractions from 0.006 to 0.03 is depicted in Figure 29.

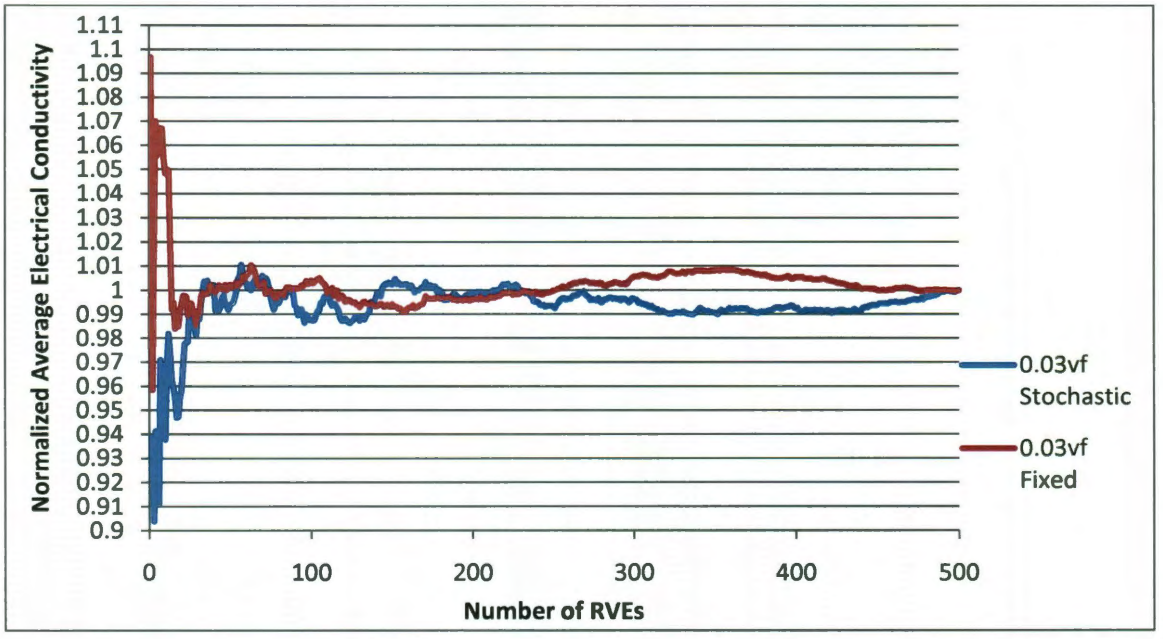

Figure 29. Normalized average mean over 500 RVEs for the case of stochastic and fixed CNT length and diameter is presented. Nanotubes in both sets have average aspect ratios of approximately 85.

Eliminating the length and diameter random variables has a noticeable effect on the convergence behavior in Figure 29. At lower numbers of RVEs, there is less variation in the normalized average conductivity for fixed length and diameter. Additionally, the model converges faster and is within 1% variation by 360 samples. The impact of fixing CNT dimensions on percolation ratio and average effective conductivity is shown in Figure 30.

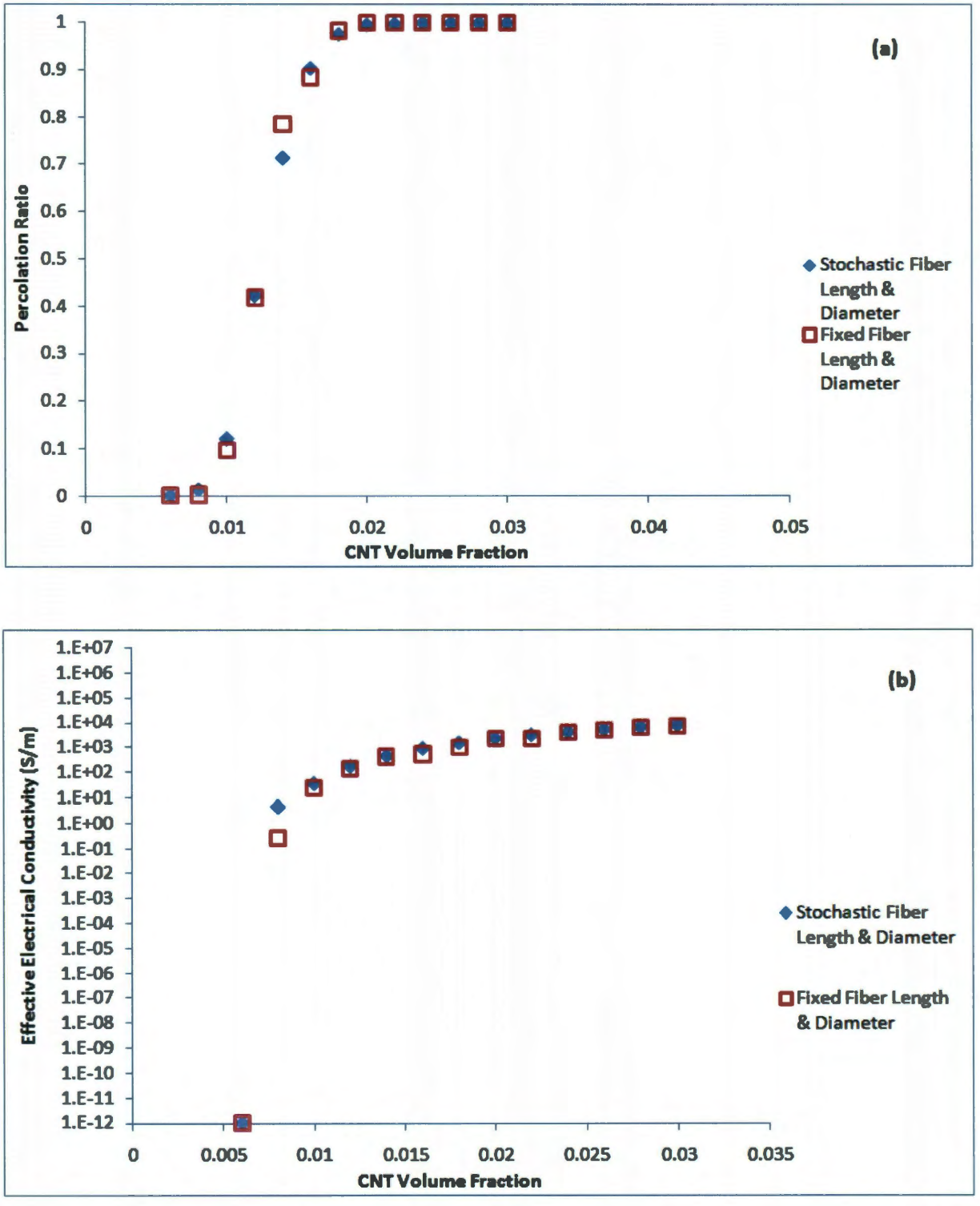

Figure 30. Impact of fixed CNT length and diameter on (a) effective electrical conductivity and (b) percolation ratio of the model is presented.

Results in Figure 30 confirm that eliminating the randomness in CNT dimensions has minimal impact on the percolation ratio and electrical conductivity of the nanocomposite. Both sets percolate all 500 RVEs in the volume fraction range of 0.008 to 0.024 with most data points differing by a few percent of each other. The effective conductivity is nearly the same with only one data point that differs by an order of magnitude. Incorporating all six stochastic features of the model would theoretically produce the most accurate representation of the real world nanocomposite system. For the purpose of this thesis, however, it is only important to demonstrate accurate qualitative results and quantitative estimates of effective electrical properties. Thus, it is beneficial to reduce the number of random variables in the model to reduce the computational cost of the program and improve the convergence performance of 500 RVEs.

4.2. Verification of Results

Model verification results are presented including effective conductivity at 1.0 volume fraction, comparison of total electric flux at the source and drain, and identification of the conducting backbone in each RVE. These outputs of the model were verified as a quality control measure and to confirm system specifications were met. The results proved that the model meets all requirements and that it is qualified for comparison to published models and experiments. Running the model at 1.0 volume fraction, or 100% concentration by volume of CNTs, is a very useful technique for investigating the calculated effective conductivity. A similar approach was used by Li et al. [33] to explore the importance of CNT resistance. They extrapolated an effective

conductivity for a CNT mat (100% concentration) and concluded that intrinsic CNT resistance is the dominant factor in very high volume fraction nanocomposites. Due to the extreme computational cost associated with generating, analyzing, and calculating results at 1.0 volume fraction in this model, the RVE dimensions are reduced to 300x300x3 nm^3. In addition, the number of bins is increased from 100 to 400 to enhance the efficiency of the percolation algorithm. The CNTs are modeled as straight, 300 nm long, and 3 nm in diameter fibers. These dimensions represent realistic nanotubes with aspect ratios of 100. Conductivity of the fibers is input at 10^7 S/m and contact resistances of 1, 10, 100, and 1000 Ω are used. Effective conductivity results of the model at 1.0 volume fraction are presented in Table 2.

Table 2. Effective conductivities for two random RVEs with 100% volume fraction at several different contact resistances.

Contact Resistance (Ω)	RVE #1 σ_eff (S/m)	RVE #2 σ_eff (S/m)	Average σ_eff (S/m)
1	8.38E+06	4.14E+06	6.26E+06
10	8.41E+06	4.79E+06	6.60E+06
100	7.76E+06	6.97E+06	7.37E+06
1000	5.89E+06	7.11E+06	6.50E+06

The effective electrical conductivity was calculated for two random RVEs at each chosen contact resistance. The contact resistance shows little correlation with the effective conductivity of each RVE. They all average to about 6 or 7 x 10^6 S/m. More importantly, all conductivities are very close to the intrinsic CNT input of 10^7 S/m. Resistance of the nanotubes themselves causes the results to be below CNT conductivity despite a large number of parallel, current carrying pathways in the RVEs.

The next analysis that verifies the results of the model presented in this thesis involves an examination of the total electric flux on the boundaries. The boundary conditions imposed on the model should yield matching total fluxes along the top and bottom RVE edges. The results confirm the correct electrical behavior of the model, specifically the use of the resistor network algorithm. Total fluxes are calculated along the top and bottom edges of the RVE for 500 random microstructures at volume fractions from 0.008 to 0.028. Average calculated top and bottom edge currents are presented in Table 3 along with their ratios and standard deviations.

Table 3. Total average currents along top (source) and bottom (drain) of the microstructure for 500 RVEs with standard deviations.

	Average Currents (Amps)		
Volume Fraction	**Top**	**Bottom**	**Standard Deviation**
0.008	9.914E-11	1.002E-10	7.301E-13
0.012	2.166E-09	2.201E-09	2.479E-11
0.016	1.706E-08	1.715E-08	5.972E-11
0.02	5.132E-08	5.124E-08	5.946E-11
0.024	1.972E-07	1.971E-07	9.419E-11
0.028	4.437E-07	4.430E-07	5.305E-10

It is easily determined from Table 3 that almost no variation exists between the average source and drain electric fluxes. The top to bottom ratios are all nearly equal to one and the largest standard deviation in the data is 5.3×10^{-10} at a volume fraction of 0.028. The results are presented graphically in Figure 31.

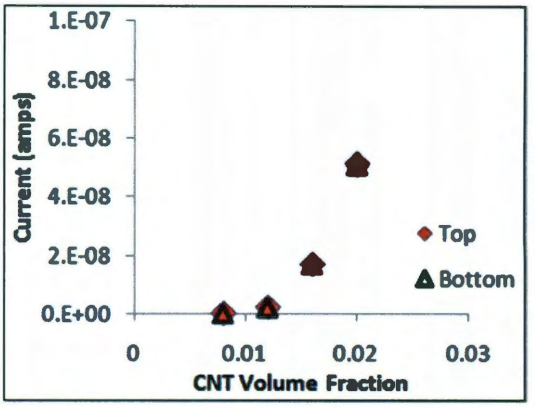

Figure 31. Total electric flux at the source and drain are averaged over 500 RVEs. Overlap of average top and bottom edge currents is shown.

Comparison of total average electric flux at the source and drain in Figure 31 verify that the model reflects correct physical behavior of charge conservation in a closed electronic circuit. There is no significant net gain or loss of electric flux, and hence electrical energy, within the system. Therefore, it is reasonable to assume that all current entering the RVE at the source exits at the drain. These results also confirm the applicability of KCL, which is based on conservation of charge.

The final results presented are potential and flux verification through visualization of nodal voltages and element currents in the RVE. For this study, CNTs are wavy with fixed lengths and diameters. They are randomly dispersed in a 1 μm^2 RVE at a high enough volume fraction for complete percolating networks to form. The geometries of two RVEs are shown in Figure 32.

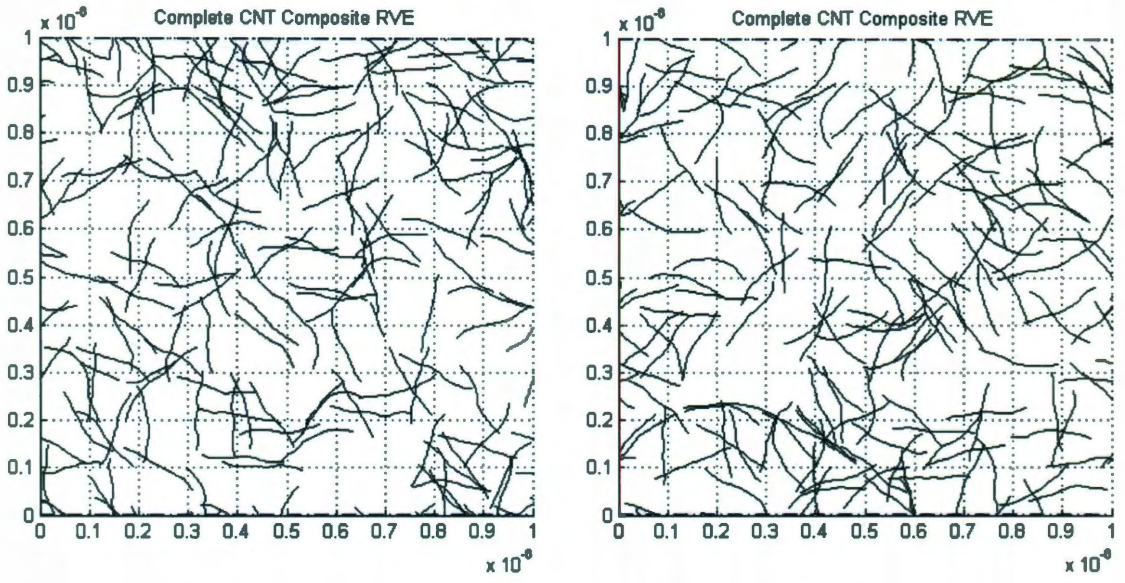

Figure 32. Two random RVEs were selected for verification of voltage and flux results.

The first step to determine nodal voltages and element fluxes is to identify the complete spanning network of CNTs. The percolation algorithm described in Chapter 2 identifies all CNTs in contact or within tunneling distance of each other and establishes connection points for creation of a resistor network. The percolation network identified for each RVE is presented in Figure 33.

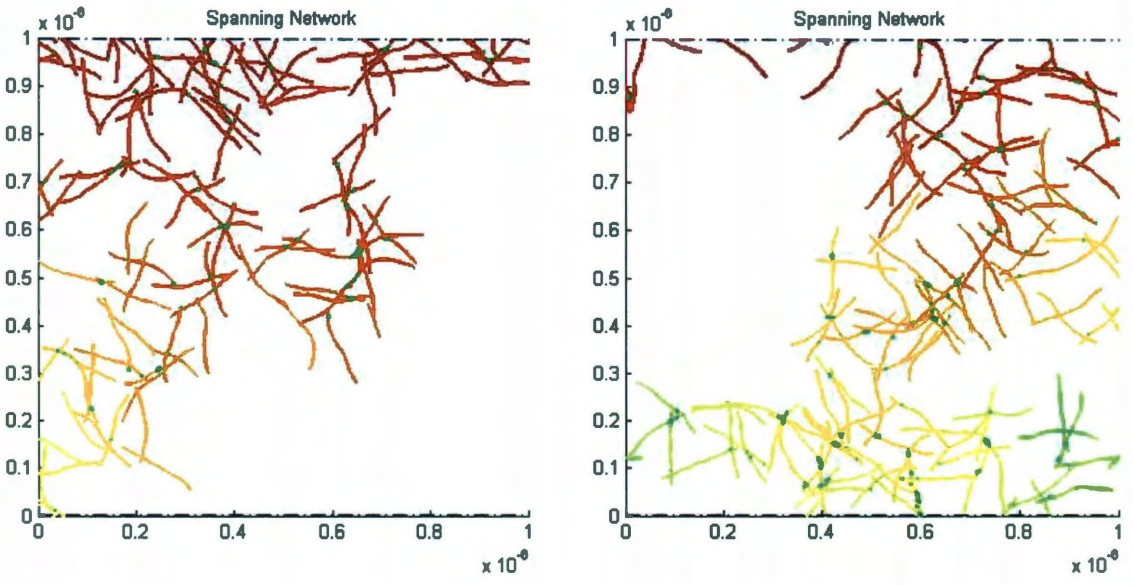

Figure 33. The complete spanning network of each RVE is highlighted including the established connection points (green).

Figure 33 indicates that there are continuous CNT structures spanning the longitudinal direction of both RVEs. Each highlighted CNT met the bonding criteria with either another nearby CNT or the voltage source at the top of the RVE. Consequently, there are fibers included with the spanning network that clearly will not carry any current and may not be near another fiber. The voltage and current results confirm that these CNTs are not part of the conducting backbone and have minimal impact on the effective conductivity.

With the spanning networks in hand, the next step is to represent the CNTs and connections as resistor elements as described in Chapter 3. The resistances, currents, and unknown nodal voltages are assembled into a system of linear algebraic equations according to KCL. Factorization and matrix multiplication give the electric potentials at the discretized system nodes. The nodal voltages are presented in Figure 34.

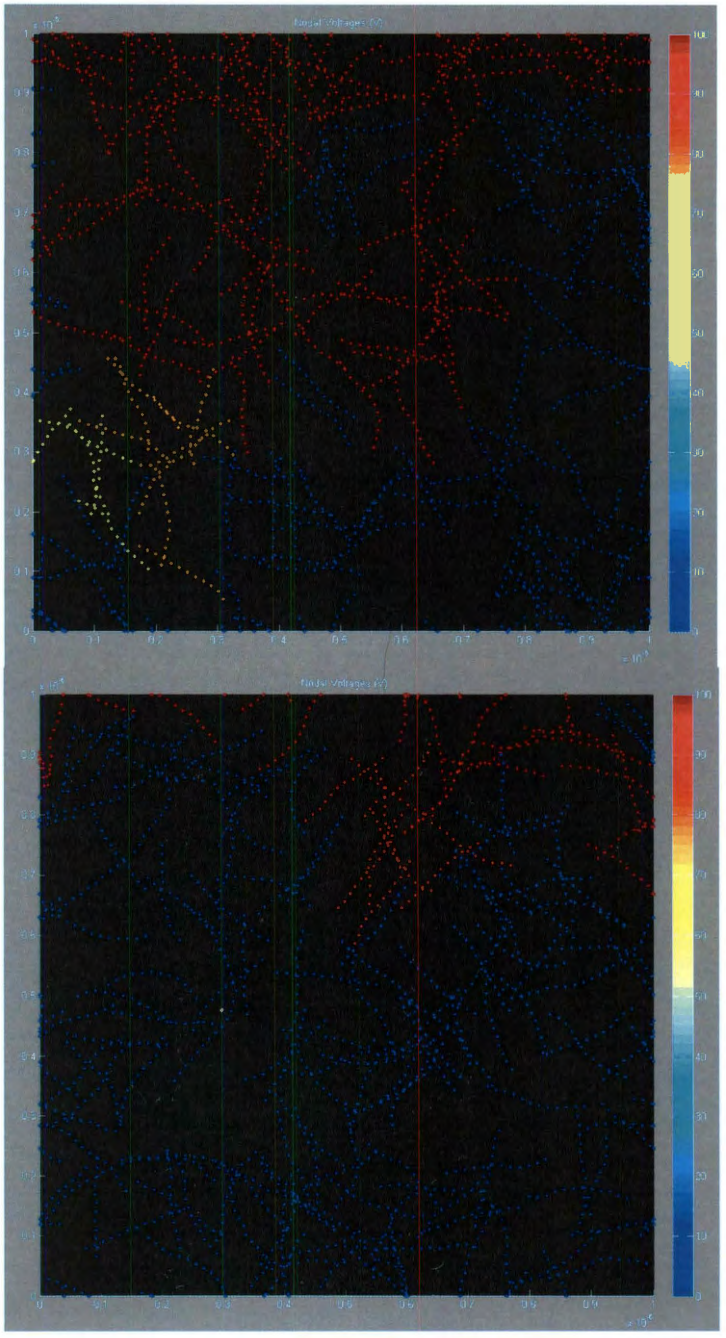

Figure 34. Nodal voltage results for both RVEs are presented. The red CNT nodes are at around 100 volts and the blue nodes are close to 0 volts.

Results in Figure 34 indicate that RVE #1 has more CNTs at a high voltage than RVE #2. Many have potentials close to 100 V that extend more than half way to the

bottom of the RVE. Also, the transition from source to drain voltage is much smoother for RVE #1 with several CNTs in the mid voltage range. RVE #2 is characterized by a very sharp voltage transition near the source. Topinka et al. [45] observed similar activity and inferred that these transitions, or cliffs, occurred in regions with few connecting CNTs. It is also observed from the figure that voltage is virtually unchanged along the length of the CNT due to low CNT resistances. The one-dimensional conductors of the model are successfully approximating the ballistic nature of charge transport in CNTs discussed in Chapter 3.

A key feature of the model proposed in this thesis is its ability to identify the conducting backbone of a complete CNT network. Simply stated, the backbone is the current carrying part of the percolating network [41]. The final step in this process is to indentify this backbone. The nodal voltages are used to calculate the current in each resistor element using Equation (16). Then, the currents are used to determine the path of concentrated electric flux connecting the source and drain. Results show that the largest currents in RVE #1 occur close the left side and, in RVE #2, they are toward the right side as depicted in Figure 35.

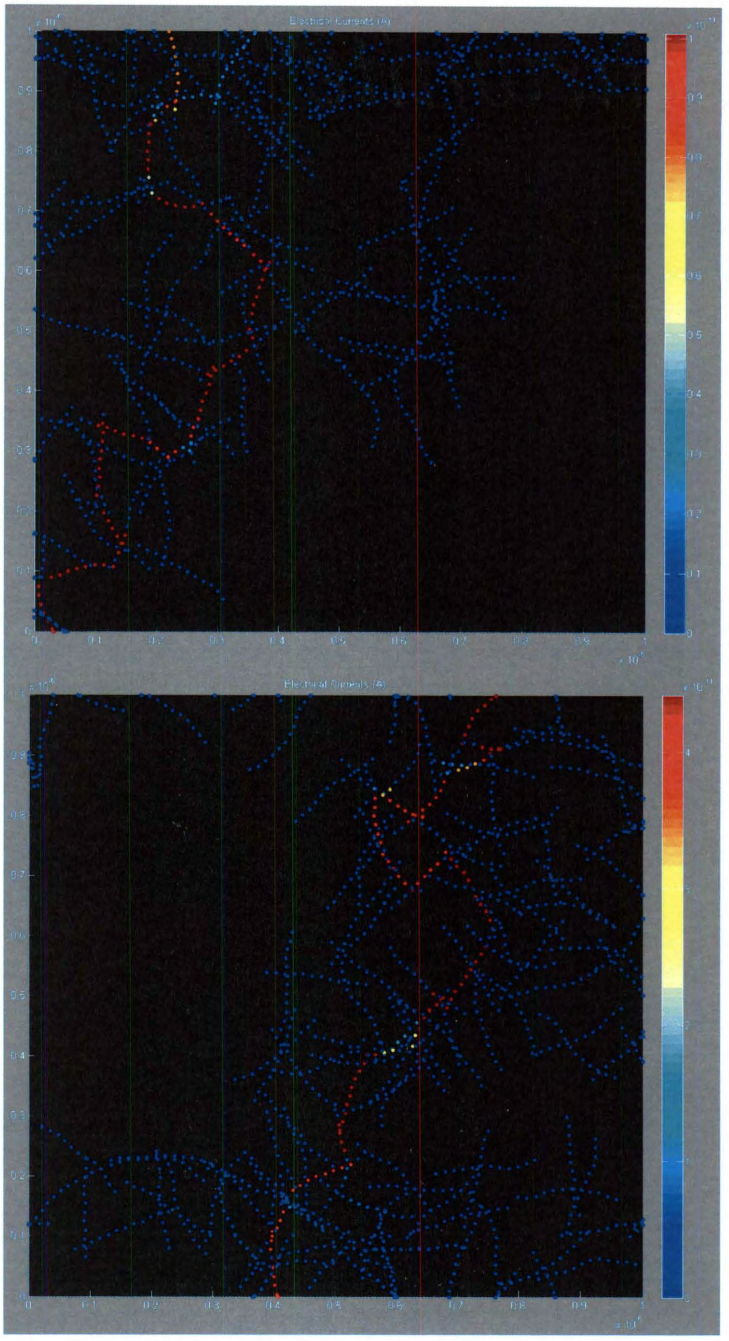

Figure 35. The currents calculated in each resistor element are shown for both RVEs. The higher currents correspond to the percolating backbone.

The backbone is easily identified in each RVE in Figure 35. The regions of relatively high flux indicate the path of least resistance through the entangled mass of

CNT fibers. Current drops are visible in the backbone. These indicate the existence of parallelism in the circuit where charge flows through multiple CNTs at the same time near a junction. Though each RVE in this study contains one backbone, it is possible for multiple parallel backbones or branches to occur at higher volume fractions. The model is proven to successfully estimate electrical behavior in CNT-based nanocomposites and identify the current carrying backbone.

4.3. Percolation Probability

The results presented in this section include percolation probability curves for high aspect ratio CNTs, low aspect ratio CNTs, and a MWNT/polycarbonate (PC) composite. Comparison to published models is attempted for the high and low aspect ratio results. Broadbent and Hammersley [41], who first studied percolation thresholds, presented the idea of percolation probability. It is a measure of the chance a given material region forms enough connections to conduct electrical current. Thus, this probability is one of the most important calculations of the proposed model. The output consists of the total number of RVEs with a complete spanning network of CNTs for a given volume fraction. This number is the direct result of the percolation network algorithm described in Chapter 2. The ratio of percolated RVEs to total RVEs at several volume fractions gives a comprehensive estimate of the probability a nanocomposite of given properties will form conducting networks of CNTs.

The first results reported are for straight, small aspect ratio CNTs. The input parameters are chosen based on information from the publication of Li and Chou [47]. The CNT length is input at 100 nm, diameter at 5 nm, and conductivity at 10^7 S/m. The

coordinate finding program [64] was used to obtain the data points from Li and Chou. The results for 500 RVEs are compared to the data in Figure 36.

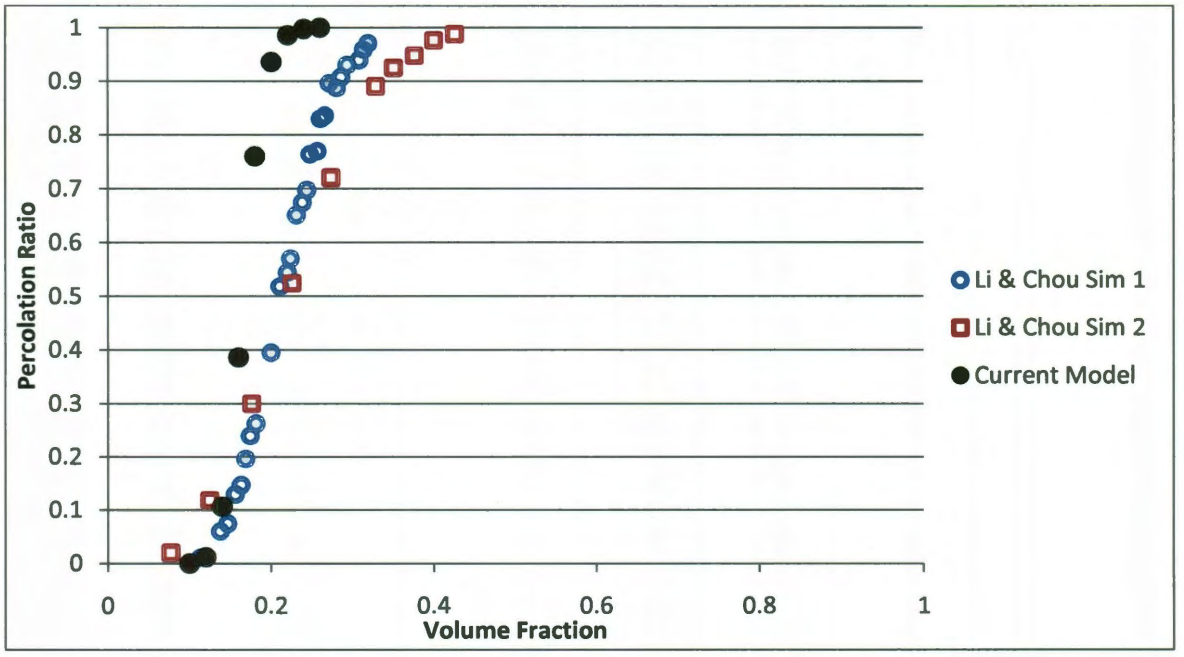

Figure 36. Percolation ratio results from the current model are compared to numerical results published by Li and Chou [46].

From the data points in Figure 36, it is evident that the proposed model overestimates the percolation probability at volume fractions above 0.14. The Li and Chou model appears to transition over a wider range of volume fractions. Both of their simulations do not approach full percolation until volume fractions over 0.3 and 0.4, respectfully. The lack of agreement between models should not be interpreted as poor accuracy in either. Instead it is indicative of the complexity of the problem due to the numerous input parameters. Li and Chou reported only a limited number of their parameters making comparison difficult. However, the purpose of the comparison is to

demonstrate the general behavior of the model and provide an estimate of percolation probability for a low aspect ratio fiber-based material.

The second percolation probability results are obtained for large aspect ratio CNTs. The RVEs are populated with straight nanotubes with aspect ratios of 250. Fiber lengths are set at 1 micron, diameters at 4 nm, and conductivity at 10^7 S/m. Simulations of 500 RVEs are executed at CNT concentrations ranging from 0.2% to 4.4%. Data points from Theodosiou and Saravanos were obtained by using the coordinate finding program [64]. Comparison of the results to the reported model is shown in Figure 37.

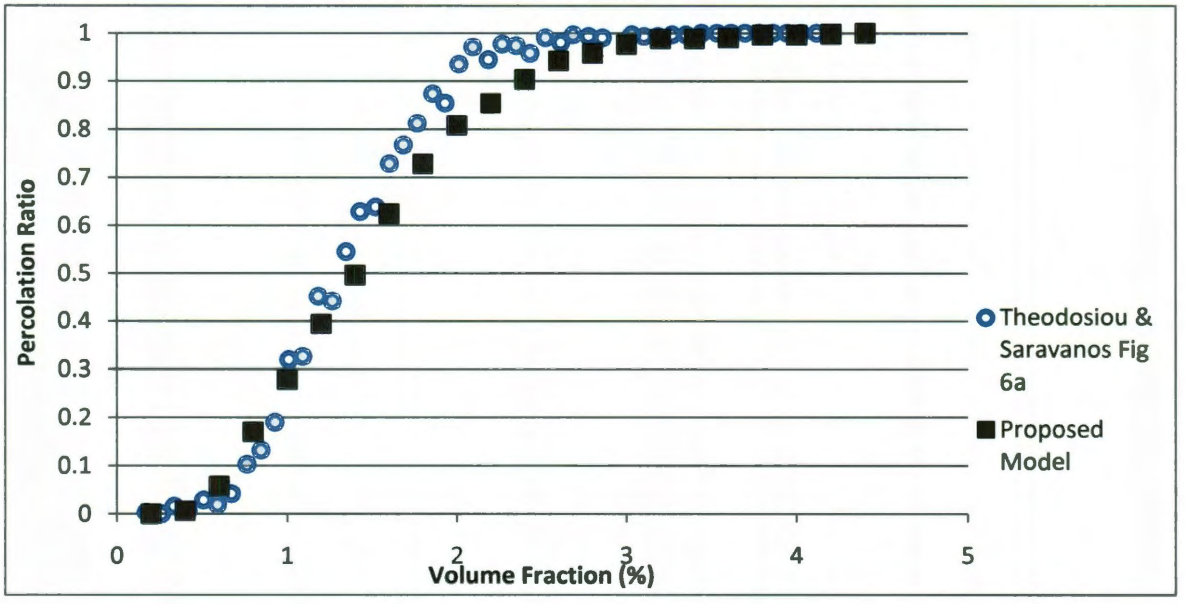

Figure 37. Percolation probability of 500 RVEs with CNTs of aspect ratio of 250 is compared to results published by Theodosiou and Saravanos [58].

The results in Figure 37 are in good agreement with the published model. Theodosiou and Saravanos are one of few to report a percolation probability curve. With the few available details they reported, the current model is able to mirror their results for

the same material. The model has the ability to estimate percolation probability of randomly dispersed and oriented CNTs of given dimensions.

The final percolation probability results presented are for a typical MWNT/PC material. Inputs to the model reflect those of real constituent materials and are summarized in Table 4.

Table 4. Inputs for percolation probability runs simulating a MWNT/PC material.

INPUTS		
CNT length	1E-07	m
CNT diameter	2E-10	m
CNT conductivity	1E+04	S/m
Contact resistance	(stochastic)	ohms
Number of RVEs	500	
Number of bins	100	
RVE size	1E-06	m
RVE thickness	1E-09	m
CNT waviness	(stochastic)	deg
Applied potential	100	V
Tunneling distance	6E-10	m

Contact resistance is randomly assigned based on the method introduced in Chapter 3. The RVEs are sampled at volume fractions in the range 0.001 - 0.0045 and, unlike the previous two simulations, the CNTs are wavy. In addition to reporting the percolation probability at several volume fractions, a method for accurately interpolating the results at all volume fractions is introduced. Li and Chou proposed that percolation probability of a composite with random arbitrary filler shapes can be closely approximated by the CDF of the volume fraction according to the equation

$$F(f;\mu,\sigma) = \frac{1}{2}\left[1 + \text{erf}\left(\frac{f-\mu}{\sigma\sqrt{2}}\right)\right]. \quad \textbf{(22)}$$

In this equation f is the volume fraction, μ is the mean percolation volume fraction, and σ is the standard deviation [47]. Li and Chou successfully fit a CDF to their simulations shown in Figure 38.

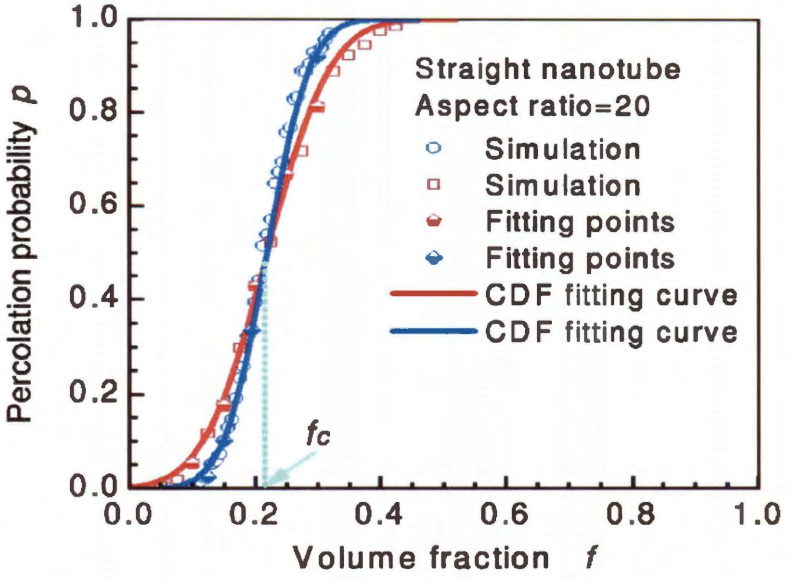

Figure 38. Percolation probability of a nanocomposite can be approximated by a normal distribution CDF curve with five fitting points or less (Li and Chou [46]).

The method of Li and Chou to approximate probability using a CDF is implemented in this model to provide information at all volume fractions. The mean and standard deviation of percolation volume fraction are 0.0018128 and 0.000195327, respectfully. Using Equation (22), the results are fit with the CDF for a normal distribution and are shown in Figure 39.

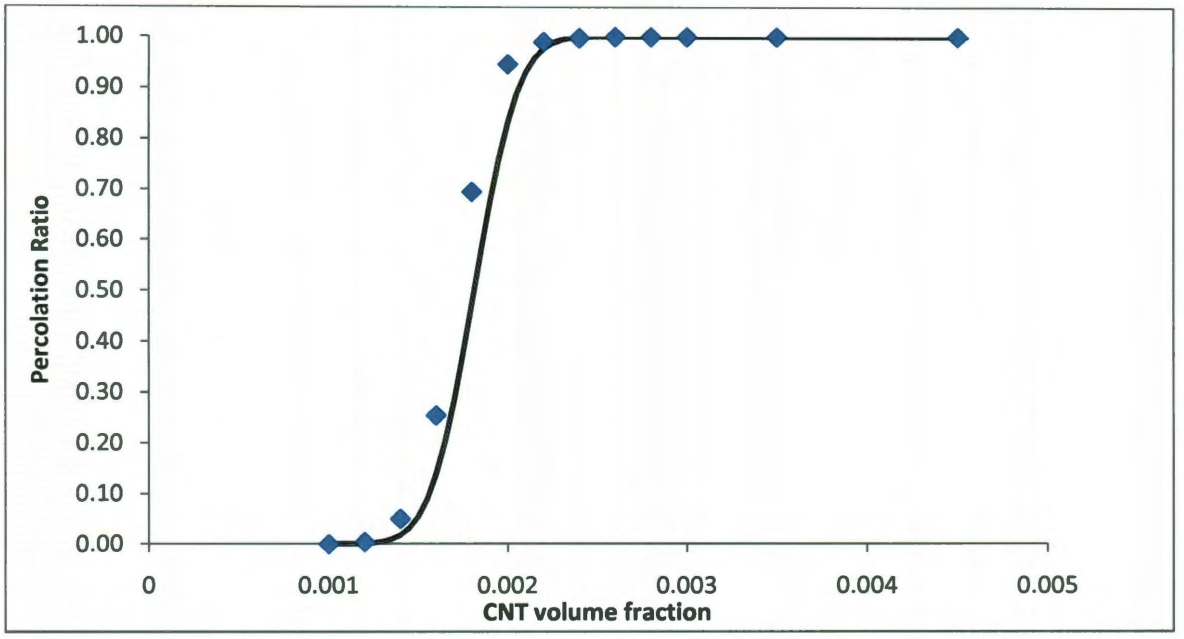

Figure 39. Percolation probability of 500 RVEs for a simulated MWNT/PC composite are shown with a normal distribution CDF using the mean and standard deviation from the simulation data.

The CDF fit shown in Figure 39 is in good agreement with the model results in the percolation region. The region spans volume fractions of 0.0012 to 0.0026 with both the data and CDF curves converging to 1.0 by 0.0026 volume fraction. The volume fractions at which probabilities occur differ by up to 0.0001 between the model and the CDF fit for this material. However, at this low of a CNT concentration the difference is a matter of a few MWNTs. Though there are clear differences between the data and CDF fit, the method is a simple and useful estimate of the probability of percolating at a given CNT concentration for a simulated material.

4.4. Effective Electrical Conductivity Results

The effective electrical conductivity results presented in this section include comparison of data to published models and experiments and presentation of a new approach to characterize CNT-based nanocomposites. First, model outputs are compared to the numerical work of Hu et al. [16] and Dalmas et al. [4]. The parameters given in their publications are adopted in the proposed model. These comparisons show the versatility and accuracy of the model presented in this thesis.

First, comparison to the results of Hu et al. is presented. The characteristics and parameters from their model are incorporated to provide a basis for comparison. Hu et al. reported a three-dimensional resistor network model with periodic geometry. They used straight MWNTs with conductivity of 10^4 S/m, aspect ratio of 100, and no tunneling distance. Therefore, the same values are input into the present model as shown in Table 5.

Table 5. Inputs chosen based on Hu et al. [16] for effective conductivity comparison.

PARAMETRIC INPUTS		
CNT length	200	nm
CNT diameter	2	nm
CNT conductivity	1E+04	S/m
Contact resistance	1E+05	ohms
Number of RVEs	500	
Number of bins	100	
RVE size	1E-06	m
RVE thickness	5	nm
Theta (CNT waviness)	0	deg
Applied potential	100	V
Tunneling distance	0	nm

Fiber length and diameter are set at 200 nm and 2 nm, respectively, to give an aspect ratio of exactly 100. Consequently, the RVE dimensions are scaled to 1,000 x 1,000 x 5 nm^3. Hu et al. assumed perfect contacts between CNTs and did not include any contact resistors in their network. The proposed model, however, does incorporate resistor elements between all CNT junctions. Therefore, contact resistance is fixed at 100 kΩ in the model, in the generally accepted range for direct CNT-CNT contacts [21,30,67]. The numerical results of Hu et al. depicted in Figure 40 shows the effective conductivity approaching 10^3 S/m as volume fraction exceeds 0.08. Further, they defined the percolation threshold as the point when conductivity reached 10 S/m. By this definition, their reported threshold is 0.013 volume fraction.

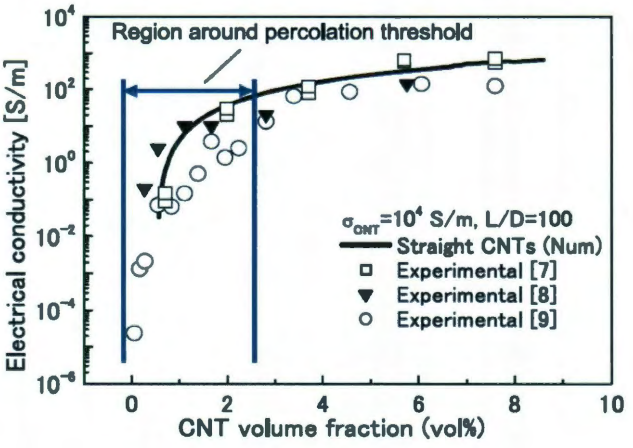

Figure 40. Model and comparison to experimental results published by Hu et al. [16] are shown.

If the same definition of percolation threshold is used, comparison results give a threshold volume fraction between 0.018 and 0.02. The effective conductivity at higher volume fractions follows a similar power law curve and would seem to also approach 10^3 S/m. By using the coordinate finding program [64], the reported data from Hu et al. were

obtained. The effective conductivity and percolation probability results are presented in Figure 41.

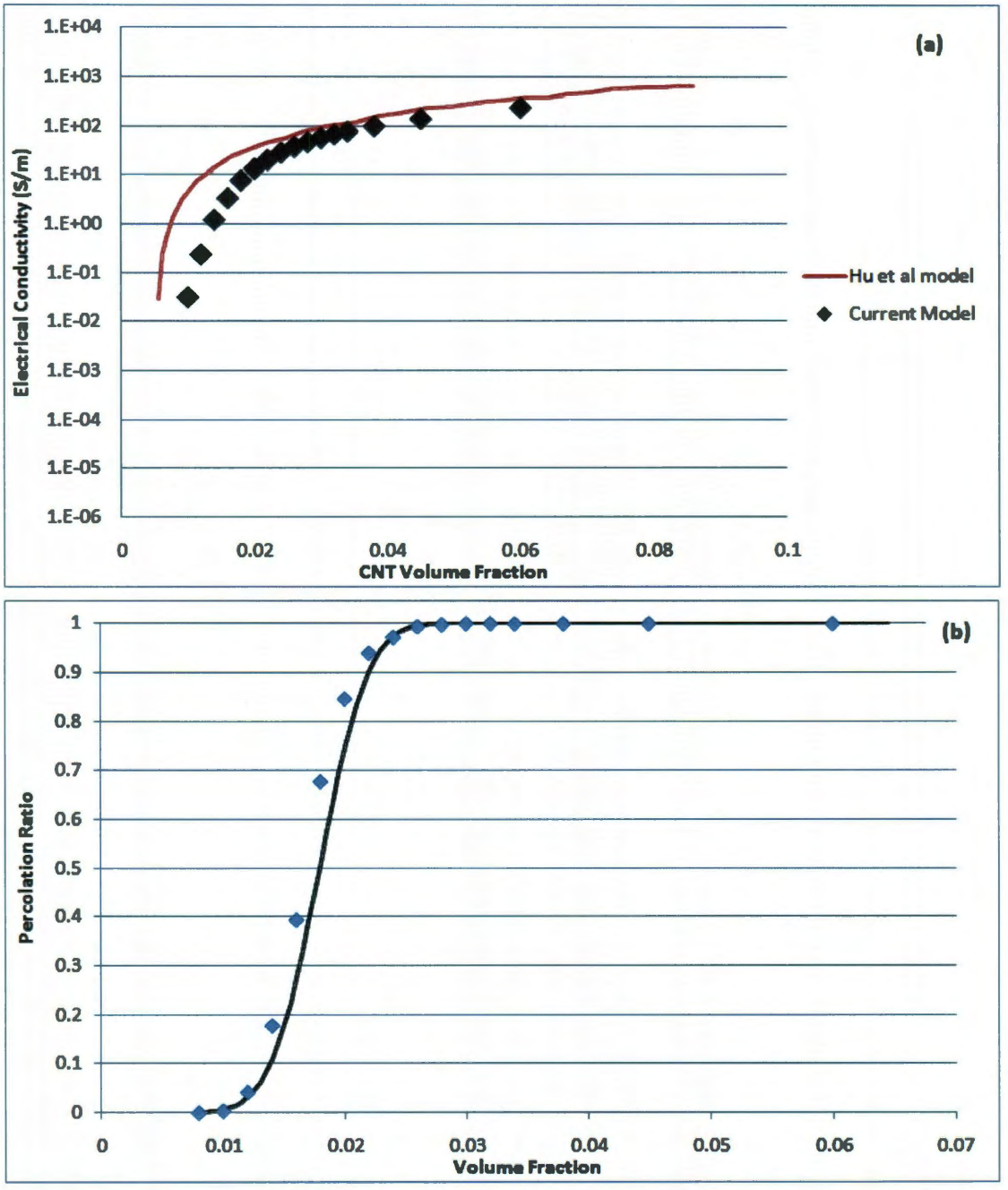

Figure 41. (a) Comparison of current numerical results to the model published by Hu et al. [16] is shown. (b) Percolation ratio results with CDF fit curve are also presented.

The proposed model slightly underestimates electrical conductivities at all volume fractions. This is likely a direct consequence of the 100 kΩ resistors between all CNT contacts in the resistor network. It appears from Figure 41(a) that these resistors have the affect of simultaneously increasing percolation threshold and decreasing effective conductivity. The difference is less apparent at higher volume fractions. Perhaps this is due to the increased number of percolating pathways in the RVEs. Behnam et al. [46] studied the impact of contact resistance on SWNT films using Monte Carlo simulations. They found that the impact any given parameter has on effective conductivity depends on how much that parameter alters the number of conductive paths. Further, they concluded that if CNT resistance is greater than contact resistance, like in this simulation, the effective conductivity depends on the length of conducting paths. Percolation probability results are also presented in Figure 41(b). CDF curve fitting used a mean volume fraction of 0.017908 and standard deviation of 0.003178.

Electrical conductivity results appear to follow a power law curve. According to percolation theory, conductivity in the threshold region can be fit by the percolation power law equation [36-37],

$$\sigma_{eff} = \sigma_o \left(\frac{p - p_c}{1 - p_c}\right)^t . \tag{23}$$

The variable p is CNT volume fraction, p_c is the percolation threshold, σ_o is a coefficient that depends on nanotube conductivity, and t is the critical exponent. Equation (24) expresses the dependence of a macroscopic property, effective conductivity, on microscopic properties, namely volume fraction and percolation threshold. The

relationship between them is characterized by the critical exponent, *t*. The critical exponent is determined from the reduced volume fraction plot shown in Figure 42.

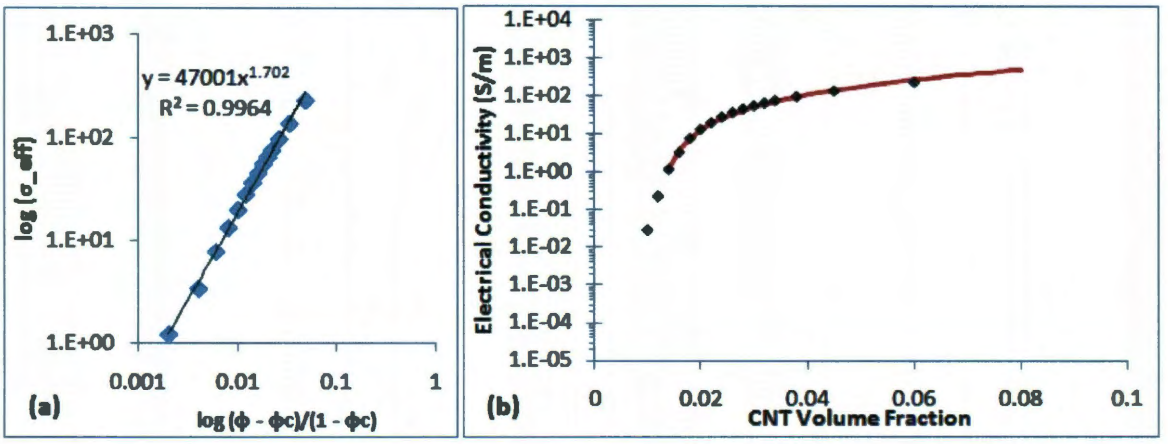

Figure 42. (a) The reduced volume fraction and effective conductivity are plotted on a log-log scale to determine the power law critical exponent *t*. (b) Simulation results are fitted well by the percolation power law.

The critical exponent and coefficient are 1.702 and 4.7 x 10^4, respectfully. Figure 42(a) shows a good power fit with an R-squared value of 0.9964. The resulting power law fits very well with original simulation data points for volume fractions above the percolation threshold, p_c.

The second numerical model used for comparison is from the work of Dalmas et al. [4]. They use a three-dimensional micromechanics approach that utilizes finite element software to solve an equivalent resistor network. The input parameters for this comparison are set according to findings in Section 4.1 and those used in Section 4.3. They are summarized in Table 6. Data from Dalmas et al. were obtained using the coordinate finding program [64]. Results of 500 RVEs at several volume fractions ranging from 0.001 to 0.0045 are compared to FEM results of Dalmas et al. in Figure 43.

Table 6. Input parameters used for comparison to the results of Dalmas et al. [4].

INPUTS		
CNT length	1E-07	m
CNT diameter	2E-10	m
CNT conductivity	1E+04	S/m
Contact resistance	(stochastic)	ohms
Number of RVEs	500	
Number of bins	100	
RVE size	1E-06	m
RVE thickness	1E-09	m
CNT waviness	(stochastic)	deg
Applied potential	100	V
Tunneling distance	6E-10	m

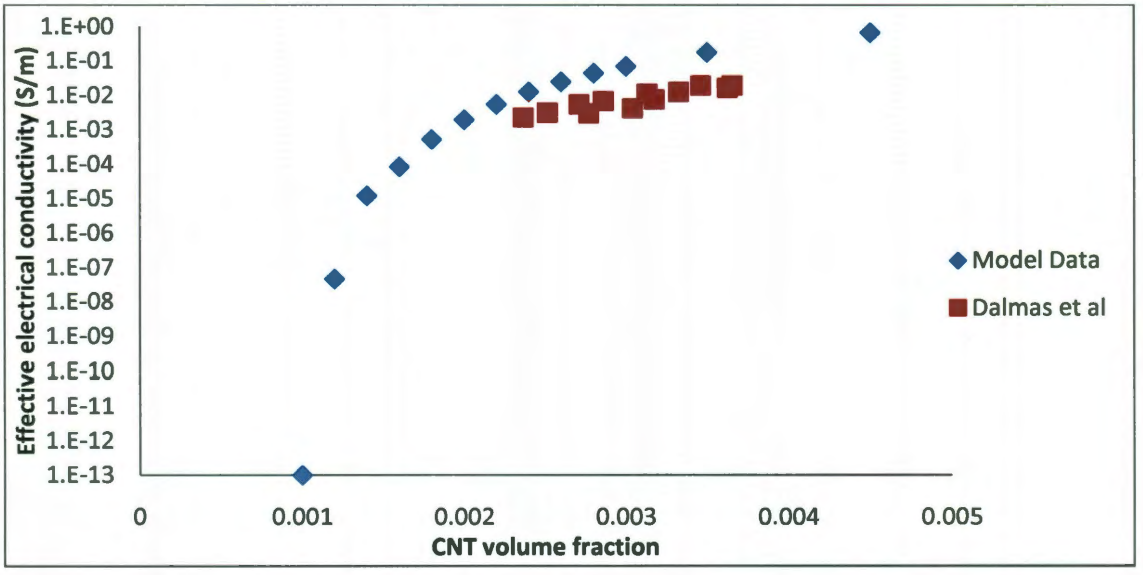

Figure 43. Comparison of current model results to numerical results of Dalmas et al. [4] is shown.

Figure 43 indicates that the numerical results are in close agreement with Dalmas et al. The data points between 0.002 and 0.0035 volume fractions slightly overestimate the published data and follow the same trend. This comparison indicates the method proposed in this thesis is capable of producing results in line with published models for

wavy CNTs and realistic material inputs. The inputs for this comparison reflect a MWNT/PC material. Further, the close comparison confirms the viability of a pseudo-three-dimensional model at significantly lower computational cost than a full three-dimensional model.

The most important comparisons for the proposed model are now presented. First, effective conductivity data from several experiments are compared to the numerical data. Then, percolation thresholds and critical exponents are compared to experimentally determined values. Experiments chosen for effective conductivity comparison include Ramasubramaniam et al. [68], Ounaies et al. [31], Skakalova et al. [69], Hu et al. [53], Sandler et al. [61], and Gojny et al. [26]. These experiments provide a wide range of nanocomposite combinations for comparison. All types of CNTs are included in variation with five different matrix materials. In addition, several different processing methods are represented by the data. Ramasubramaniam et al. produced undamaged, non-covalently functionalized SWNTs for dispersion in thermoplastics without sonication. The SWNT/polyimide samples of Ounaies et al. were prepared by in situ polymerization with sonication. Hu et al. also manufactured their nanocomposites by in situ polymerization with a variety of curing processes, mixing speeds, and mixing times. Skakalova et al. compared a PMMA composite prepared with pristine SWNTs to one with thionyl chloride doped SWNTs. A process of shear-intensive mechanical stirring and curing of an epoxy and amine hardener was used by Sandler et al. And Gojny et al. prepared nanocomposites with a variety of CNT types, some amino-functionalized, by a three-roll mill process. Some experimental data is reported in terms of weight or mass

fraction instead of volume fraction. Conversion requires only the matrix material density, ρ_m, and CNT density, ρ_{nt}, according to the equation [48,70]

$$vf = \frac{wf\rho_m}{(wf\rho_m + (1 - wf)\rho_{nt})}, \tag{24}$$

where, vf is CNT volume fraction and wf is CNT weight or mass fraction. The densities of matrix material and nanotubes are seldom reported. Therefore, approximate values were chosen and are summarized in Table 7.

Table 7. Approximate material densities for the nanotubes and thermoplastics used in this study.

Material	Approximate Density (g/cm^3)
SWNT	1.3
MWNT	1.75
Polycarbonate (PC)	1.22
Polystyrene (PS)	1.05
Polyimide (PI)	1.4
Poly (ethylene terephthalate) (PET)	1.4
Epoxy	1.17

The coordinate finding program [64] was used to gather data points for the experimental comparisons. The proposed model simulates 500 random RVEs of wavy MWNTs embedded in a PC matrix material. A 100 V potential difference is applied across the boundaries and the contact resistances are sampled stochastically as described in Chapter 3. Comparison of the effective conductivity results are presented in Figure 44.

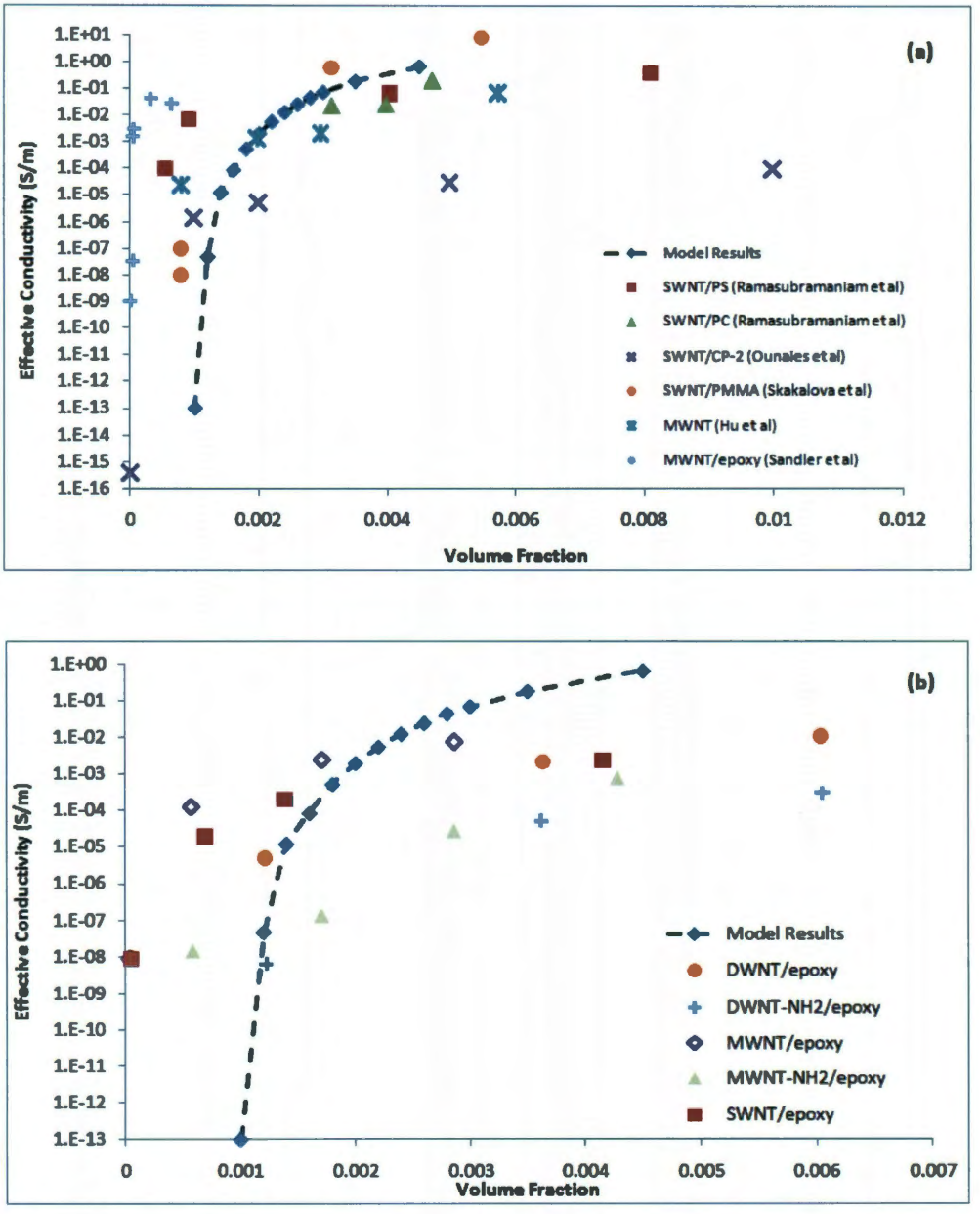

Figure 44. (a) Comparison of the model with six different experiments is presented. (b) Comparison of the same model results with the experiments of Gojny et al. [25] is depicted.

Figure 44 illustrates the wide variation in reported experiments. The model results appear to be close in magnitude to the experiments. Unfortunately, only few data points exist for each material. This makes a close comparison difficult. What is

important to note is that the model follows the same trend as experimental results. Both have the characteristic jump in effective conductivity near the percolation threshold and continue to increase modestly according to the percolation power law. Because CNT type and morphology dominate effective electrical properties, it is important to take a closer look at material results using MWNTs. Only the data of Hu et al. in Figure 44(a) give a percolation threshold close to the model. The MWNT materials of Sandler et al. and Gojny et al. in Figure 44 all have thresholds at lower volume fractions. This may indicate that a tunneling distance of 6 nm is insufficient to capture electron transport behavior between MWNTs. Moreover, the disagreement may be symptomatic of the model's inability to account for manufacturing processes of nanocomposites. However, the differences do not disprove the model's accuracy and versatility. They merely show that more studies can be done to determine the impact of processing conditions on input parameters and how the model can be tuned to better account for them.

Next, percolation thresholds and critical exponents of the model and experiments are compared. Numerical results for five simulation sets, each at several volume fractions with 500 RVEs are used. The first comparison is made with CNTs with aspect ratio of 500. The other four simulation sets have aspect ratios of about 100. Results show good agreement of percolation threshold and critical exponent between the model and multiple experiments at both aspect ratios. Percolation threshold is compared to twenty-two reported experiments in Figure 45.

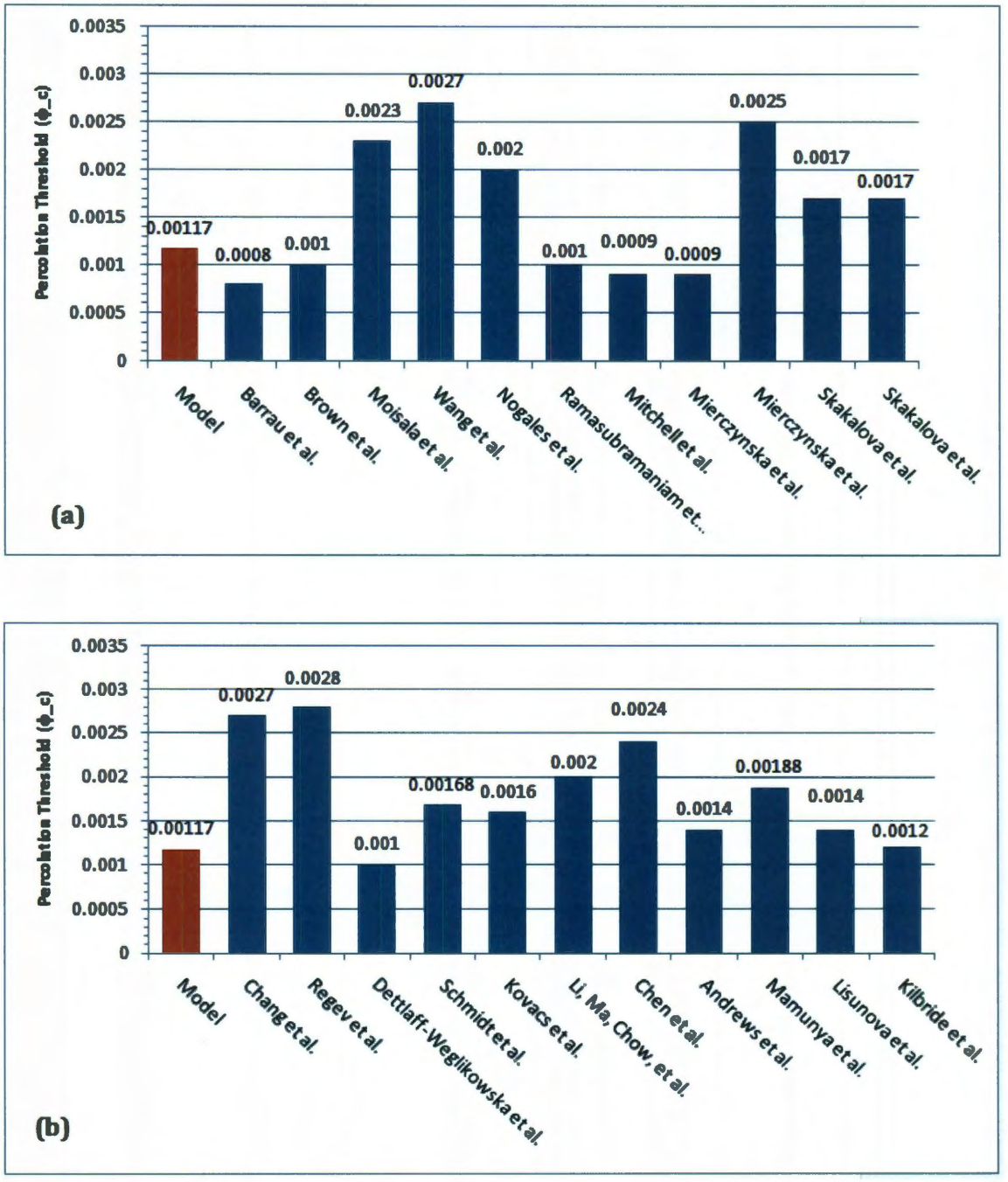

Figure 45. Percolation threshold for CNTs with aspect ratio of 500 are compared to twenty-two different experiments [19,67-85].

Figure 45 shows that results from the model are in good agreement with experiments. Experimental percolation thresholds are between 0.008 and 0.028 volume

fraction. The model estimated a percolation threshold of 0.00117 for CNT aspect ratio of 500. The relatively high aspect ratio nanotubes used in these composites percolate at very low volume fractions. Critical exponent, t, for the same simulation set is compared to thirteen of the twenty-two experiments in Figure 46.

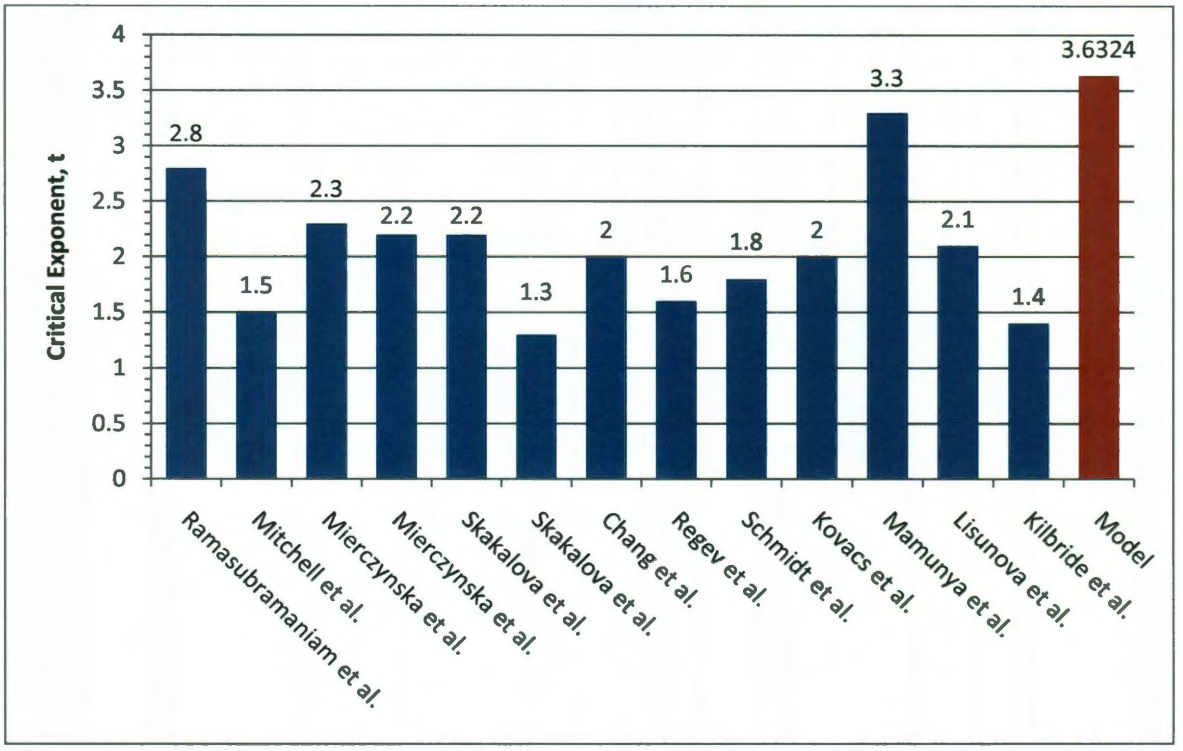

Figure 46. The estimated t value for CNTs with aspect ratio of 500 is compared to thirteen experiments [67-68,73-76,78-79,83-85].

The model overestimates the critical exponent for the simulation set in Figure 46. It is predicted to be 3.63, while experimental values range from 1.3 to 3.3. Although the predicted critical exponent seems high, it is within the 1.3-4 range frequently reported in experiments [62]. Further, values tend to be dimensionally dependent with $t = 1.33$ to coincide with two-dimensional and $t = 2$ for three-dimensional models [62]. Therefore, the high value from the pseudo-three-dimensional model suggests its capability to reflect

electrical behavior of a full three-dimensional model. Next, the other four simulation sets with aspect ratios of about 100 are presented. Each simulation set had minor differences in input parameters. Predicted percolation thresholds from each simulation are compared to eleven experiments in Figure 47.

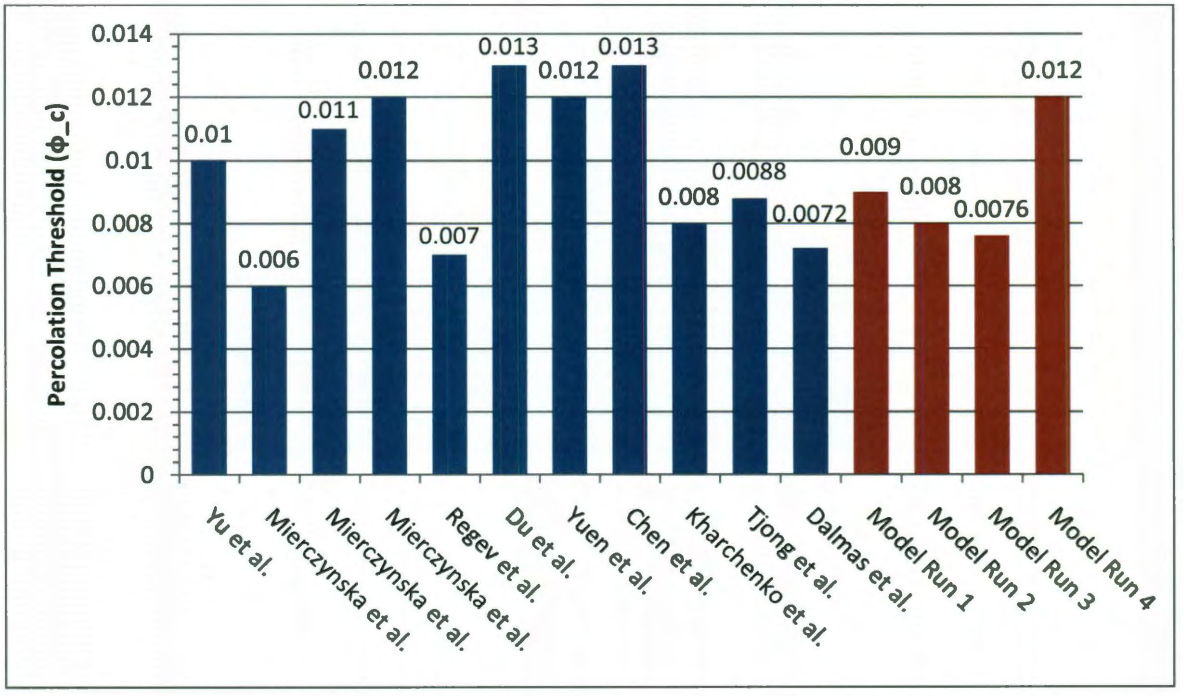

Figure 47. Percolation threshold results for CNTs with aspect ratios close to 100 are compared to eleven different experimental results [74,76,81,86-91].

It is readily observable in Figure 47 that model results agree well with experiments with CNT aspect ratios of about 100. Experimental thresholds range from 0.006 to 0.013 volume fraction and the model predicted thresholds from 0.0076 to 0.012 for various input parameters. Critical exponents calculated from the four simulation sets are compared to seven experiments in Figure 48.

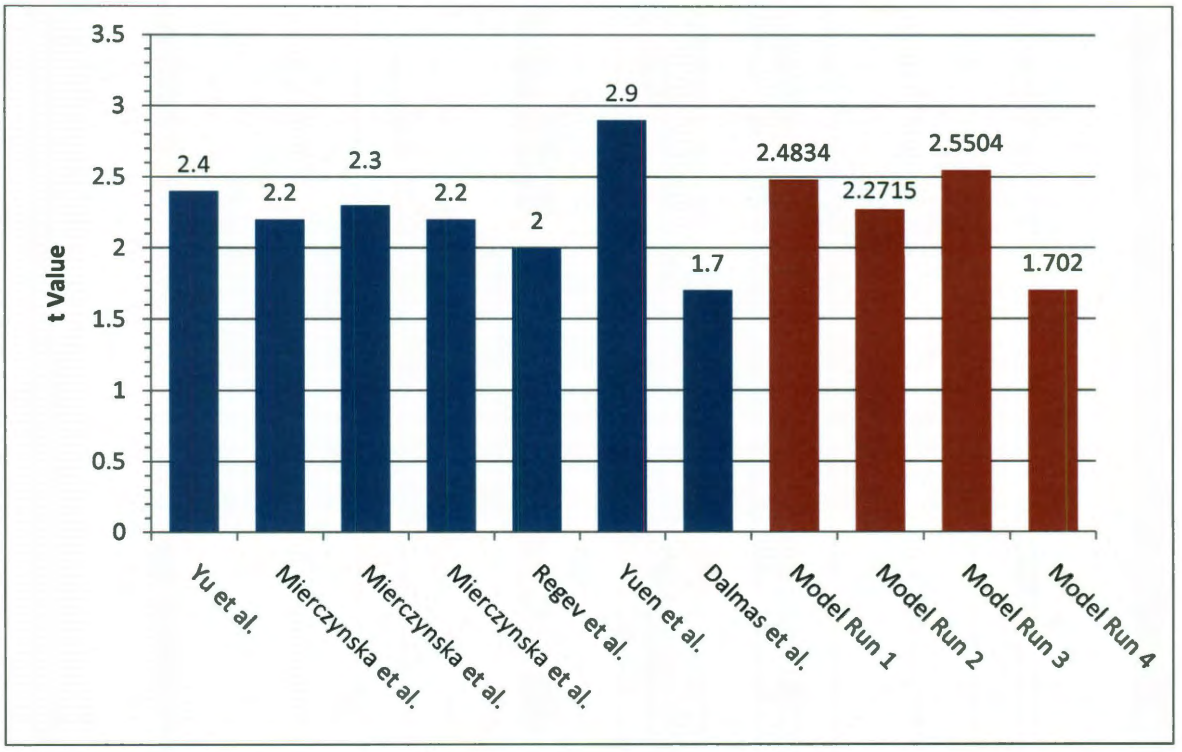

Figure 48. Calculated *t* values for CNTs with aspect ratios around 100 are compared to experimental results [74,76,86-88].

Figure 48 shows that experiments with similar CNT types have critical exponents in the range 1.7 to 2.9. All four model simulations have predicted exponents well within that range. In addition, they are close to the generally accepted value of 2 for three-dimensional models. Results from the five simulation sets presented in this section prove the accuracy of the model. Both the percolation thresholds and critical exponents determined from the percolation power fit agree well with those determined from experimental data.

A novel method for characterizing the electrical properties of CNT-based nanocomposites is now presented. Benefits of the current model include the ability to estimate percolation probability and effective electrical conductivity at volume fractions

in the percolation region. The CDF fit to percolation ratio data predicts the percolation probability using Equation (22). Therefore, the likelihood the input material will form conductive networks of CNTs at any given volume fraction is known. Further, the effective electrical conductivity is estimated from the power fit according to Equation (23). By combining these results-based fits, the electrical characteristics of the input material are known at any volume fraction in the percolation region. The first material characterized is a typical SWNT/epoxy or SWNT/alumina with filler aspect ratio of 100. Table 8 summarizes this input nanocomposite.

Table 8. Input parameters for simulating a SWNT/epoxy or SWNT/alumina material.

Run 1 Material		
Matrix	**Type**	epoxy, alumina *
	Conductivity (S/m)	1E-12
Filler	**Type**	SWNT
	Conductivity (S/m)**	1E+07
	Aspect Ratio	100
	Length (nm)	200
	Diameter (nm)	2
* Reference Hu et al. [53] and Kumari et al. [56]		
** Reference Li and Chou [18]		

The model predicts a percolation threshold of 0.009 volume fraction, critical exponent of 2.4834, and coefficient of 6.59×10^{6}. The CDF fit has a calculated mean volume fraction of 0.017 and standard deviation of 0.00311. The fits are interpolated over the percolation threshold region of 0.008 – 0.03 volume fraction. Materials for electrostatic discharge (ESD) applications typically require conductivities of at least 10^{-6} S/m [27,67,86]. At these low conductivities, the material gradually dissipates electrical charge build up on devices such as electronic components. For applications involving

electromagnetic interference (EMI) shielding, conductivities greater than 1 S/m are necessary [68]. These types of protective materials and films are essentially electrically conducting. The interpolated probabilities, effective conductivities, and potential applications for a SWNT/epoxy are presented in Table 9.

Table 9. Interpolated results for a SWNT/epoxy material with aspect ratio of 100 are shown. Percolation probability is interpolated using the CDF fit and effective conductivity is interpolated by the percolation power law.

Volume Fraction (φ)	Percolation Probability (F)	Expected Effective Electrical Conductivity (σ_{eff}')	Range of Application
0.008	0.0019	1.000E-12	Insulator
0.009	0.0050	1.000E-12	Insulator
0.01	0.0122	2.389E-01	ESD/Weak EMI
0.011	0.0268	1.336E+00	ESD/Weak EMI
0.012	0.0538	3.657E+00	ESD/Weak EMI
0.013	0.0990	7.471E+00	ESD/Weak EMI
0.014	0.1671	1.300E+01	EMI
0.015	0.2597	2.045E+01	EMI
0.016	0.3734	2.999E+01	EMI
0.017	0.4995	4.178E+01	EMI
0.018	0.6256	5.597E+01	EMI
0.019	0.7395	7.271E+01	EMI
0.02	0.8323	9.213E+01	EMI
0.021	0.9005	1.144E+02	EMI
0.022	0.9459	1.395E+02	EMI
0.023	0.9731	1.677E+02	EMI
0.024	0.9877	1.990E+02	EMI
0.025	0.9949	2.336E+02	EMI
0.026	0.9981	2.716E+02	EMI
0.027	0.9993	3.130E+02	EMI
0.028	0.9998	3.580E+02	EMI
0.029	0.9999	4.066E+02	EMI
0.03	1.0000	4.590E+02	EMI

Table 9 shows that at low volume fractions, such as 0.01, the given SWNT/epoxy material is expected to have an effective conductivity of about 0.24 S/m. Therefore, this

material is suitable for ESD applications. However, it has only a 1.22% probability of forming the spanning CNT networks required to achieve that conductivity. Electrical conductivity and percolation probability are visualized in Figure 49.

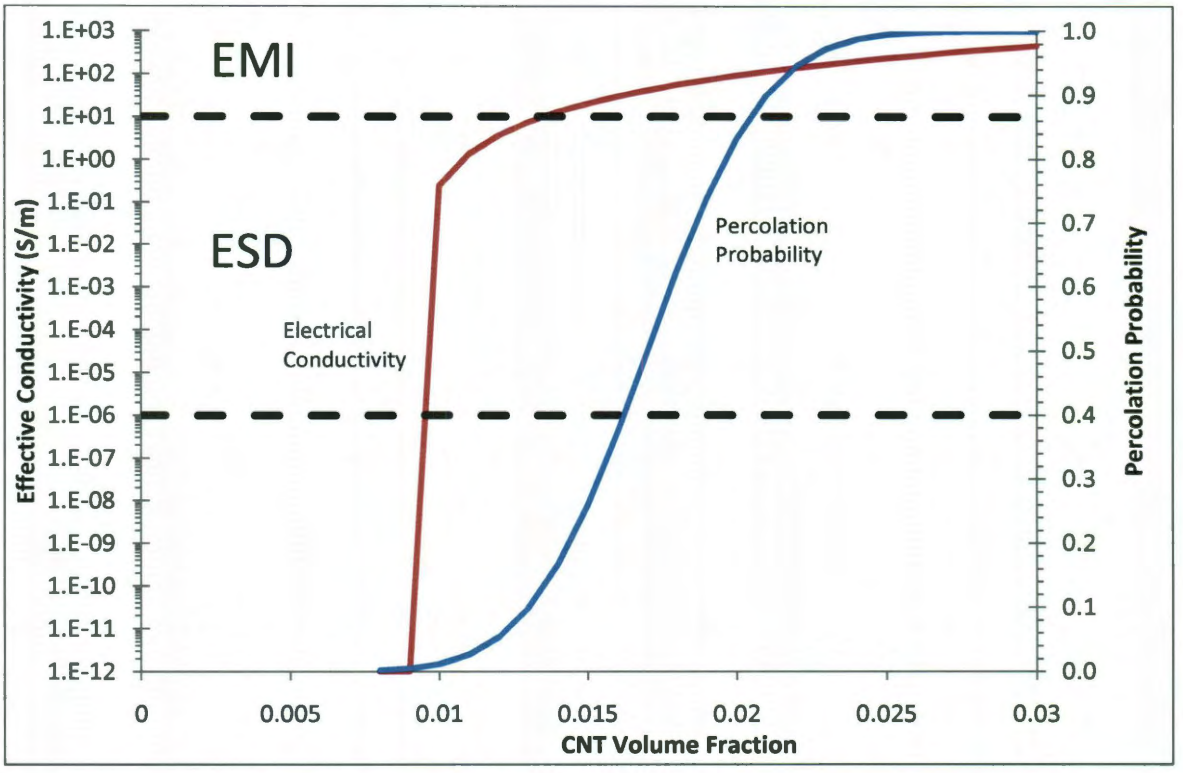

Figure 49. The predicted electrical performance for a SWNT/epoxy or SWNT/alumina material with aspect ratio of 100 is interpolated over volume fractions 0.008-0.03.

Figure 49 presents a measure of a nanomaterial's electrical performance. The probability that conducting networks of CNTs exist increases rapidly over a small range of volume fractions. Comparatively, effective electrical conductivity of the materials with spanning networks increases from the ESD to EMI range over the same span of volume fractions.

The final results presented in this thesis are for a MWNT/PC material simulated with 500 random RVEs. The material electrical properties were predicted over a volume fraction span of 0.001 - 0.0045. The input parameters for this simulation set are summarized in Table 10.

Table 10. Input parameters simulating a large aspect ratio MWNT/PC material.

Run 2 - Material		
Matrix	**Type**	polycarbonate *
	Conductivity (S/m)	1E-13
Filler	**Type**	MWNT
	Conductivity (S/m)**	1E+04
	Aspect Ratio	500
	Length (nm)	1000
	Diameter (nm)	2
* Reference Ramasubramaniam et al. [68]		
** Reference Hu et al. [16]		

This material has a much larger aspect ratio and lower CNT conductivity in contrast to the SWNT/epoxy material analyzed previously. Percolation probability has a CDF fit with calculated mean volume fraction of 0.00181 and standard deviation of 0.000195. A percolation threshold of 0.00117 volume fraction, critical exponent of 3.63, and coefficient of 4.6×10^8 are calculated for the power fit curve. Both fits are interpolated over the volume fraction range in Figure 50.

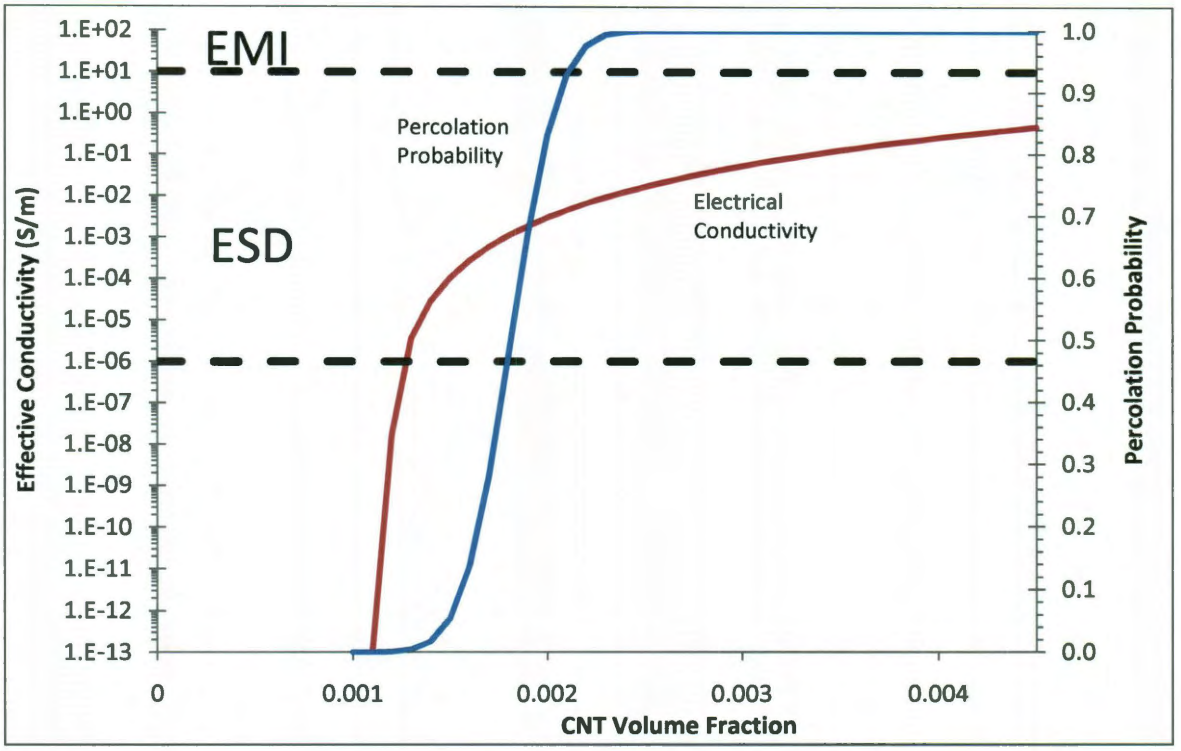

Figure 50. Predicted electrical performance for a MWNT/PC material with aspect ratio of 500 is interpolated over volume fractions 0.001-0.0045.

Electrical conductivity for this material is predicted to never exceed the required amount for EMI applications at volume fractions below 0.0045. Rather, it is obvious from Figure 50 that this material is best suited for ESD applications. Also, the material percolates at a volume fraction nearly ten times lower than the SWNT/epoxy nanocomposite. The lower effective conductivity and percolation threshold are likely due to lower intrinsic conductivity and higher aspect ratio of MWNT over SWNT.

In conclusion, the scaled resistor network model utilizing KCL produced effective electrical conductivities and percolation probabilities for a variety of CNT-based nanocomposites in the percolation region. Percolation probability curves compared well with published models and the usefulness of CDF curve fitting was demonstrated.

Further, predicted effective electrical conductivities, percolation thresholds, and critical exponents for several specific materials compared well with both models and experiments. Therefore, the accuracy and versatility of the model have been verified. The accuracy of the model, however, could be improved with better understanding of both the nanoscale physics that govern electron transport and the impact manufacturing techniques have on electrical properties.

Chapter 5

Concluding Remarks

Modern research efforts have been focused on the development and understanding of promising new nanomaterials. Experiments on carbon nanotube based polymer composites are time consuming, expensive, and complex. Additionally, analytical and numerical models have struggled to replicate and predict their physical behavior. Regardless, these fascinating materials have demonstrated high potential for multifunctional applications, especially for their electrical properties. The model presented in this thesis has addressed the need for a reliable, versatile, and accurate method of predicting nanocomposite electrical properties.

The model used Monte Carlo simulations, a spanning network algorithm, and the resistor network method to characterize electrical behavior of a nanotube composite. Monte Carlo simulations eliminated the statistical variation in the randomly generated microstructures. The spanning network algorithm incorporated the electron tunneling effect to identify complete CNT networks. The results of this algorithm led to the

estimation of percolation probability in the material. Finally, the resistor network method was used to represent the CNTs and contact points in the identified network. Kirchhoff's Current Law and the finite element method were used to assemble and solve the system equations. From the results, the current carrying backbone and effective conductivity of the RVE were calculated at each volume fraction.

This model has four primary advantages. First, it is a fast and flexible representation of very complex materials. The use of searching bins, skyline storage format, and optimization of the number of searching nodes in the program increase its overall processing speed. The model is flexible because it can be scaled to represent both small and large aspect ratio nanotubes. The input parameters include CNT conductivity, polymer conductivity, CNT morphology, and tunneling distance. Other characteristics of the model are easily modified as well. Beyond the material inputs, no user interaction with the model is needed.

The second advantage to the model lies in the opportunity to perform parametric studies. Any combination of the input parameters can be controlled or randomly varied in the system. This provides the opportunity to study the impact different factors have on the electrical results. These results lead to the discovery of dependencies and relationships between parameters to aid in development of nanocomposites. Further, the ability to minimize variation in the system by fixing low-impact parameters such as CNT length and diameter has been demonstrated in the results.

Third, the model has the ability to produce visualizations of several results and relationships. Using the spanning network algorithm for a large number of random

simulations, the probability a given nanocomposite formed a complete percolating network of CNTs was shown for several volume fractions. These results are seldom reported by other models. Results showed good agreement with probability curves produced by Li and Chou [47] and Theodosiou and Saravanos [59]. In addition, the resistor network results led to several excellent visualizations. The voltages and fluxes in the CNT network were shown. These plots clearly indicated the location of the conducting backbones of the RVE. Effective conductivity results were also presented graphically. They evidenced the expected percolation jump and power law relationship of nanocomposites. Conductivity results agreed well with several different experiments.

The final main advantage to the model detailed in this thesis is the ability to characterize the overall electrical performance of a nanocomposite. Results of the model simulations were used to calculate fitting curves for both percolation probability and effective conductivity. The curve fits interpolated results for all volume fractions within the percolation region. The probability that a given nanocomposite formed conductive pathways of CNTs in the material was estimated from the cumulative density function fit for a normal distribution. The percolation power law equation showed excellent fitting to effective conductivity results. Therefore, the electrical conductivity of a nanocomposite and its chances of percolating were gleaned simultaneously at any volume fraction in the percolation region.

The new technique given herein was developed when the embedded fiber approach described by Spanos et al. [89] for structural and thermal applications failed when extended to electrical CNT applications. Clearly, the numerical ill-conditioning found in that prior approach was due to the extreme ratios of the electrical conductivities

between the binding matrix material and the CNT combined with the lack of a percolation path. That percolation path shortcoming was due to the lack of a priori representation of contact and tunneling electrical connections between the CNTs. Obviously, extending the embedded fiber approach to also include a tunneling element, and the new algorithm for the identification of their connection points, would cause that approach to duplicate the results presented herein. However, the contribution of the matrix vis-à-vis the contribution of the CNT, while being non-negligible for the case of the effective mechanical and thermal properties, would be minimal for the case of the effective electrical conductivity problem considered in this thesis.

In conclusion, all the advantages and characteristics of the numerical model have provided valuable insights and accurate predictions of the electrical performance of nanotube composites. The resistor network and spanning network methods have proven they can accurately account for both microscale and nanoscale electrical conduction effects. This model provides a way to validate experimental results and potentially predict the performance of new materials. It is capable of quickly identifying CNT networks, calculating effective electrical conductivity, and locating current-carrying backbones over several volume fractions for any number of fiber-filled composite materials.

Future research related to the work in this thesis may include any number of studies based on the input parameters of the model, modifications to allow more accurate representation of nanotube contacts, expansion of the model to three full dimensions, and inclusion of metallic and semiconducting CNTs in the model.

References

[1] G. P. Tegos et al., "Cationic Fullerenes Are Effective and Selective Antimicrobial Photosensitizers," *Chemistry & Biology*, vol. 12, no. 10, pp. 1127-1135, 2005.

[2] W. H. De Jong and P. J. Borm, "Drug delivery and nanoparticles: Applications and hazards," *International Journal of Nanomedicine*, vol. 3, no. 2, pp. 133-149, Jun. 2008.

[3] G. D. Seidel and D. C. Lagoudas, "A Micromechanics Model for the Electrical Conductivity of Nanotube-Polymer Nanocomposites," *Journal of Composite Materials*, vol. 43, no. 9, pp. 917-941, May. 2009.

[4] F. Dalmas, R. Dendievel, L. Chazeau, J. Cavaillé, and C. Gauthier, "Carbon nanotube-filled polymer composites. Numerical simulation of electrical conductivity in three-dimensional entangled fibrous networks," *Acta Materialia*, vol. 54, no. 11, pp. 2923-2931, Jun. 2006.

[5] T. W. Ebbesen, H. J. Lezec, H. Hiura, J. W. Bennett, and et al, "Electrical conductivity of individual carbon nanotubes," *Nature*, vol. 382, no. 6586, p. 54, Jul. 1996.

[6] B. Q. Wei, R. Vajtai, and P. M. Ajayan, "Reliability and current carrying capacity of carbon nanotubes," *Applied Physics Letters*, vol. 79, no. 8, p. 1172, 2001.

[7] S. Frank, P. Poncharal, Z. L. Wang, and W. A. D. Heer, "Carbon Nanotube Quantum Resistors," *Science*, vol. 280, no. 5370, pp. 1744-1746, Jun. 1998.

[8] Z. Yao, C. L. Kane, and C. Dekker, "High-Field Electrical Transport in Single-Wall Carbon Nanotubes," *Physical Review Letters*, vol. 84, no. 13, p. 2941, Mar. 2000.

[9] H. Cebeci, R. G. D. Villoria, A. J. Hart, and B. L. Wardle, "Multifunctional properties of high volume fraction aligned carbon nanotube polymer composites with controlled morphology," *Composites Science and Technology*, vol. 69, no. 15, pp. 2649-2656, Dec. 2009.

[10] F. Deng and Q. Zheng, "Interaction models for effective thermal and electric conductivities of carbon nanotube composites," *Acta Mechanica Solida Sinica*, vol. 22, no. 1, pp. 1-17, Feb. 2009.

[11] M. Foygel, R. D. Morris, D. Anez, S. French, and V. L. Sobolev, "Theoretical and computational studies of carbon nanotube composites and suspensions: Electrical and thermal conductivity," *Physical Review B*, vol. 71, no. 10, p. 104201, Mar. 2005.

[12] T. Natsuki, K. Tantrakarn, and M. Endo, "Effects of carbon nanotube structures on mechanical properties.," *Applied Physics A: Materials Science & Processing*, vol. 79, no. 1, pp. 117-124, Jun. 2004.

[13] T. Belytschko, S. P. Xiao, G. C. Schatz, and R. S. Ruoff, "Atomistic simulations of nanotube fracture," *Physical Review B*, vol. 65, no. 23, p. 235430, Jun. 2002.

[14] S. Berber, Y. Kwon, and D. Tomanek, "Unusually High Thermal Conductivity of Carbon Nanotubes," *Physical Review Letters*, vol. 84, no. 20, p. 4613, May. 2000.

[15] P. Kim, L. Shi, A. Majumdar, and P. L. McEuen, "Thermal Transport Measurements of Individual Multiwalled Nanotubes," *Physical Review Letters*, vol. 87, no. 21, p. 215502, Oct. 2001.

[16] N. Hu, Z. Masuda, C. Yan, G. Yamamoto, H. Fukunaga, and T. Hashida, "The electrical properties of polymer nanocomposites with carbon nanotube fillers," *Nanotechnology*, vol. 19, no. 21, p. 215701, 2008.
[17] C. Li and T. Chou, "Electrical Conductivities of Composites with Aligned Carbon Nanotubes," *Journal of Nanoscience and Nanotechnology*, vol. 9, pp. 2518-2524, Apr. 2009.
[18] C. Li and T. Chou, "Modeling of damage sensing in fiber composites using carbon nanotube networks," *Composites Science and Technology*, vol. 68, no. 15, pp. 3373-3379, Dec. 2008.
[19] A. Moisala, Q. Li, I. Kinloch, and A. Windle, "Thermal and electrical conductivity of single- and multi-walled carbon nanotube-epoxy composites," *Composites Science and Technology*, vol. 66, no. 10, pp. 1285-1288, Aug. 2006.
[20] A. Andreescu, A. Savin, R. Steigmann, N. Iftimie, E. Mamut, and R. Grimberg, "Model for thermal conductivity of composites with carbon nanotubes.," *Journal of Thermal Analysis & Calorimetry*, vol. 94, no. 2, pp. 349-353, Nov. 2008.
[21] C. Li, E. T. Thostenson, and T. Chou, "Effect of nanotube waviness on the electrical conductivity of carbon nanotube-based composites," *Composites Science and Technology*, vol. 68, no. 6, pp. 1445-1452, May. 2008.
[22] C. Li and T. Chou, "A direct electrifying algorithm for backbone identification," *Journal of Physics A: Mathematical and Theoretical*, vol. 40, no. 49, pp. 14679-14686, 2007.
[23] N. Shenogina, S. Shenogin, L. Xue, and P. Keblinski, "On the lack of thermal percolation in carbon nanotube composites," *Applied Physics Letters*, vol. 87, Sep. 2005.
[24] Y. Hakobyan, K. D. Papoulia, and M. D. Grigoriu, "Physical and geometrical percolations of effective conductivity on a lattice," *Physical Review B*, vol. 76, no. 14, p. 144205, Oct. 2007.
[25] F. Deng and Q. Zheng, "An analytical model of effective electrical conductivity of carbon nanotube composites," *Applied Physics Letters*, vol. 92, no. 7, p. 071902, 2008.
[26] F. H. Gojny et al., "Evaluation and identification of electrical and thermal conduction mechanisms in carbon nanotube/epoxy composites," *Polymer*, vol. 47, no. 6, pp. 2036-2045, Mar. 2006.
[27] C. A. Martin et al., "Formation of percolating networks in multi-wall carbon-nanotube-epoxy composites," *Composites Science and Technology*, vol. 64, no. 15, pp. 2309-2316, Nov. 2004.
[28] J. Sandler, M. S. P. Shaffer, T. Prasse, W. Bauhofer, K. Schulte, and A. H. Windle, "Development of a dispersion process for carbon nanotubes in an epoxy matrix and the resulting electrical properties," *Polymer*, vol. 40, no. 21, pp. 5967-5971, Oct. 1999.
[29] H. W. C. Postma, M. de Jonge, Z. Yao, and C. Dekker, "Electrical transport through carbon nanotube junctions created by mechanical manipulation," *Physical Review B*, vol. 62, no. 16, p. R10653, Oct. 2000.
[30] J. W. Park, J. Kim, and K. Yoo, "Electrical transport through crossed carbon nanotube junctions," *Journal of Applied Physics*, vol. 93, no. 7, pp. 4191-4193.

[31] Z. Ounaies, C. Park, K. E. Wise, E. J. Siochi, and J. S. Harrison, "Electrical properties of single wall carbon nanotube reinforced polyimide composites," *Composites Science and Technology*, vol. 63, no. 11, pp. 1637-1646, Aug. 2003.
[32] T. Natsuki, M. Endo, and T. Takahashi, "Percolation study of orientated short-fiber composites by a continuum model," *Physica A: Statistical Mechanics and its Applications*, vol. 352, no. 2, pp. 498-508, Jul. 2005.
[33] C. Li, E. T. Thostenson, and T. Chou, "Dominant role of tunneling resistance in the electrical conductivity of carbon nanotube–based composites," *Applied Physics Letters*, vol. 91, no. 22, p. 223114, 2007.
[34] I. Balberg, C. H. Anderson, S. Alexander, and N. Wagner, "Excluded volume and its relation to the onset of percolation," *Physical Review B*, vol. 30, no. 7, p. 3933, Oct. 1984.
[35] A. L. R. Bug, S. A. Safran, and I. Webman, "Continuum Percolation of Rods," *Physical Review Letters*, vol. 54, no. 13, p. 1412, Apr. 1985.
[36] W. Cai, S. Tu, and J. Gong, "A Physically Based Percolation Model of the Effective Electrical Conductivity of Particle Filled Composites," *Journal of Composite Materials*, vol. 40, no. 23, pp. 2131 -2142, Dec. 2006.
[37] N. I. Lebovka, S. Tarafdar, and N. V. Vygornitskii, "Computer simulation of electrical conductivity of colloidal dispersions during aggregation," *Physical Review E*, vol. 73, no. 3, p. 031402, Mar. 2006.
[38] G. D. Seidel, Y. Bisrat, and D. C. Lagoudas, "Electrical and Thermal Conductivities of Carbon Nanotube-Epoxy Composites: Modeling and Characterization," 11-Nov-2007.
[39] C. H. Seager and G. E. Pike, "Percolation and conductivity: A computer study. II," *Physical Review B*, vol. 10, no. 4, p. 1435, 1974.
[40] G. E. Pike and C. H. Seager, "Percolation and conductivity: A computer study. I," *Physical Review B*, vol. 10, no. 4, p. 1421, 1974.
[41] S. Kirkpatrick, "Percolation and Conduction," *Reviews of Modern Physics*, vol. 45, no. 4, p. 574, Oct. 1973.
[42] A. Behnam and A. Ural, "Computational study of geometry-dependent resistivity scaling in single-walled carbon nanotube films," *Physical Review B*, vol. 75, no. 12, p. 125432, Mar. 2007.
[43] D. A. Jack, C. Yeh, Z. Liang, S. Li, J. G. Park, and J. C. Fielding, "Electrical conductivity modeling and experimental study of densely packed SWCNT networks," *Nanotechnology*, vol. 21, no. 19, p. 195703, May. 2010.
[44] X. Sun and M. Song, "Highly Conductive Carbon Nanotube/Polymer Nanocomposites Achievable?," *Macromolecular Theory and Simulations*, vol. 18, no. 3, pp. 155-161, 2009.
[45] M. A. Topinka, M. W. Rowell, D. Goldhaber-Gordon, M. D. McGehee, D. S. Hecht, and G. Gruner, "Charge Transport in Interpenetrating Networks of Semiconducting and Metallic Carbon Nanotubes," *Nano Letters*, vol. 9, no. 5, pp. 1866-1871, May. 2009.
[46] A. Behnam, J. Guo, and A. Ural, "Effects of nanotube alignment and measurement direction on percolation resistivity in single-walled carbon nanotube films," *Journal of Applied Physics*, vol. 102, no. 4, p. 044313, 2007.

[47] C. Li and T. Chou, "Continuum percolation of nanocomposites with fillers of arbitrary shapes," *Applied Physics Letters*, vol. 90, no. 17, p. 174108, 2007.
[48] P. Elsbernd, "A Non-Linear Finite Element Model for the Determination of Elastic and Thermal Properties of Nanocomposites," Master of Science, Rice University, 2009.
[49] J. B. Bai and A. Allaoui, "Effect of the length and the aggregate size of MWNTs on the improvement efficiency of the mechanical and electrical properties of nanocomposites--experimental investigation," *Composites Part A: Applied Science and Manufacturing*, vol. 34, no. 8, pp. 689-694, Aug. 2003.
[50] S. Wang, Z. Liang, B. Wang, and C. Zhang, "Statistical characterization of single-wall carbon nanotube length distribution," *Nanotechnology*, vol. 17, no. 3, pp. 634-639, 2006.
[51] J. Grunlan, A. Mehrabi, M. Bannon, and J. Bahr, "Water-Based Single-Walled-Nanotube-Filled Polymer Composite with an Exceptionally Low Percolation Threshold," *Advanced Materials*, vol. 16, no. 2, pp. 150-153, 2004.
[52] H. Dai, E. W. Wong, and C. M. Lieber, "Probing Electrical Transport in Nanomaterials: Conductivity of Individual Carbon Nanotubes," *Science*, vol. 272, no. 5261, pp. 523-526, Apr. 1996.
[53] N. Hu, Z. Masuda, G. Yamamoto, H. Fukunaga, T. Hashida, and J. Qiu, "Effect of fabrication process on electrical properties of polymer/multi-wall carbon nanotube nanocomposites," *Composites Part A: Applied Science and Manufacturing*, vol. 39, no. 5, pp. 893-903, May. 2008.
[54] K. J. Ziegler et al., "Statistically Accurate Length Measurements of Single-Walled Carbon Nanotubes," *Journal of Nanoscience and Nanotechnology*, vol. 7, no. 8, pp. 2917-2921, Aug. 2007.
[55] Q. Wang, J. Dai, W. Li, Z. Wei, and J. Jiang, "The effects of CNT alignment on electrical conductivity and mechanical properties of SWNT/epoxy nanocomposites," *Composites Science and Technology*, vol. 68, no. 7, pp. 1644-1648, Jun. 2008.
[56] L. Kumari et al., "Synthesis, microstructure and electrical conductivity of carbon nanotube-alumina nanocomposites," *Ceramics International*, vol. 35, no. 5, pp. 1775-1781, Jul. 2009.
[57] F. Du, R. C. Scogna, W. Zhou, S. Brand, J. E. Fischer, and K. I. Winey, "Nanotube Networks in Polymer Nanocomposites: Rheology and Electrical Conductivity," *Macromolecules*, vol. 37, no. 24, pp. 9048-9055, Nov. 2004.
[58] C. Zhou, J. Kong, and H. Dai, "Intrinsic Electrical Properties of Individual Single-Walled Carbon Nanotubes with Small Band Gaps," *Physical Review Letters*, vol. 84, no. 24, p. 5604, Jun. 2000.
[59] T. Theodosiou and D. Saravanos, "Numerical investigation of mechanisms affecting the piezoresistive properties of CNT-doped polymers using multi-scale models," *Composites Science and Technology*, vol. 70, no. 9, pp. 1312-1320, Sep. 2010.
[60] E. S. Choi et al., "Enhancement of thermal and electrical properties of carbon nanotube polymer composites by magnetic field processing," *Journal of Applied Physics*, vol. 94, no. 9, p. 6034, 2003.
[61] J. Sandler, J. Kirk, I. Kinloch, M. Shaffer, and A. Windle, "Ultra-low electrical

percolation threshold in carbon-nanotube-epoxy composites," *Polymer*, vol. 44, no. 19, pp. 5893-5899, Sep. 2003.
[62] W. Bauhofer and J. Z. Kovacs, "A review and analysis of electrical percolation in carbon nanotube polymer composites," *Composites Science and Technology*, vol. 69, no. 10, pp. 1486-1498, Aug. 2009.
[63] M. S. Fuhrer et al., "Crossed Nanotube Junctions," *Science*, vol. 288, no. 494, pp. 494-497, Apr. 2000.
[64] M. Esteva, "Hybrid Finite Elements Nanocomposite Characterization by Stochastic Microstructuring," PhD, Rice University, 2008.
[65] J. Akin, *Finite Element Analysis With Error Estimators: An Introduction to the FEM and Adaptive Error Analysis for Engineering Students*. Elsevier Butterworth-Heinemann, 2005.
[66] O. Zienkiewicz, R. Taylor, and J. Zhu, *The Finite Element Method: Its Basis and Fundamentals*, 6th ed. Elsevier Butterworth-Heinemann, 2005.
[67] A. Buldum and J. P. Lu, "Contact resistance between carbon nanotubes," *Physical Review B*, vol. 63, no. 16, p. 161403, Apr. 2001.
[68] R. Ramasubramaniam, J. Chen, and H. Liu, "Homogeneous carbon nanotube/polymer composites for electrical applications," *Applied Physics Letters*, vol. 83, no. 14, p. 2928, 2003.
[69] V. Skakalova, U. Dettlaff-Weglikowska, and S. Roth, "Electrical and mechanical properties of nanocomposites of single wall carbon nanotubes with PMMA," *Synthetic Metals*, vol. 152, no. 1, pp. 349-352, Sep. 2005.
[70] P. Spanos and M. Esteva, "Effect of Stochastic Nanotube Waviness on the Elastic and Thermal Properties of Nanocomposites by Fiber Embedment in Finite Elements," *Journal of Computational and Theoretical Nanoscience*, vol. 6, pp. 2317-2333, 2009.
[71] S. Barrau, P. Demont, C. Maraval, A. Bernes, and C. Lacabanne, "Glass Transition Temperature Depression at the Percolation Threshold in Carbon Nanotube-Epoxy Resin and Polypyrrole-Epoxy Resin Composites," *Macromolecular Rapid Communications*, vol. 26, no. 5, pp. 390-394, 2005.
[72] J. M. Brown et al., "Hierarchical morphology of carbon single-walled nanotubes during sonication in an aliphatic diamine," *Polymer*, vol. 46, no. 24, pp. 10854-10865, Nov. 2005.
[73] T. Wang et al., "Waterborne, Nanocomposite Pressure-Sensitive Adhesives with High Tack Energy, Optical Transparency, and Electrical Conductivity," *Advanced Materials*, vol. 18, no. 20, pp. 2730-2734, 2006.
[74] A. Nogales et al., "Low Percolation Threshold in Nanocomposites Based on Oxidized Single Wall Carbon Nanotubes and Poly(butylene terephthalate)," *Macromolecules*, vol. 37, no. 20, pp. 7669-7672, Oct. 2004.
[75] C. A. Mitchell and R. Krishnamoorti, "Dispersion of Single-Walled Carbon Nanotubes in Poly(ε-caprolactone)," *Macromolecules*, vol. 40, no. 5, pp. 1538-1545, Mar. 2007.
[76] A. Mierczynska, M. Mayne-L'Hermite, G. Boiteux, and J. K. Jeszka, "Electrical and mechanical properties of carbon nanotube/ultrahigh-molecular-weight polyethylene composites prepared by a filler prelocalization method," *Journal of Applied*

Polymer Science, vol. 105, no. 1, pp. 158-168, 2007.
[77] T. Chang, A. Kisliuk, S. Rhodes, W. Brittain, and A. Sokolov, "Conductivity and mechanical properties of well-dispersed single-wall carbon nanotube/polystyrene composite," *Polymer*, vol. 47, no. 22, pp. 7740-7746, Oct. 2006.
[78] O. Regev, P. ElKati, J. Loos, and C. Koning, "Preparation of Conductive Nanotube–Polymer Composites Using Latex Technology," *Advanced Materials*, vol. 16, no. 3, pp. 248-251, 2004.
[79] U. Dettlaff-Weglikowska et al., "Conducting and transparent SWNT/polymer composites," *physica status solidi (b)*, vol. 243, no. 13, pp. 3440-3444, 2006.
[80] R. H. Schmidt, I. A. Kinloch, A. N. Burgess, and A. H. Windle, "The Effect of Aggregation on the Electrical Conductivity of Spin-Coated Polymer/Carbon Nanotube Composite Films," *Langmuir*, vol. 23, no. 10, pp. 5707-5712, May. 2007.
[81] J. Z. Kovacs, B. S. Velagala, K. Schulte, and W. Bauhofer, "Two percolation thresholds in carbon nanotube epoxy composites," *Composites Science and Technology*, vol. 67, no. 5, pp. 922-928, Apr. 2007.
[82] J. Li, P. Ma, W. Chow, C. To, B. Tang, and J. Kim, "Correlations between Percolation Threshold, Dispersion State, and Aspect Ratio of Carbon Nanotubes," *Advanced Functional Materials*, vol. 17, no. 16, pp. 3207-3215, 2007.
[83] H. Chen et al., "Dispersion of carbon nanotubes and polymer nanocomposite fabrication using trifluoroacetic acid as a co-solvent," *Nanotechnology*, vol. 18, no. 41, p. 415606, 2007.
[84] R. Andrews, D. Jacques, M. Minot, and T. Rantell, "Fabrication of Carbon Multiwall Nanotube/Polymer Composites by Shear Mixing," *Macromolecular Materials and Engineering*, vol. 287, no. 6, p. 395, 2002.
[85] Y. Mamunya, A. Boudenne, N. Lebovka, L. Ibos, Y. Candau, and M. Lisunova, "Electrical and thermophysical behaviour of PVC-MWCNT nanocomposites," *Composites Science and Technology*, vol. 68, no. 9, pp. 1981-1988, Jul. 2008.
[86] M. Lisunova, Y. Mamunya, N. Lebovka, and A. Melezhyk, "Percolation behaviour of ultrahigh molecular weight polyethylene/multi-walled carbon nanotubes composites," *European Polymer Journal*, vol. 43, no. 3, pp. 949-958, Mar. 2007.
[87] B. E. Kilbride et al., "Experimental observation of scaling laws for alternating current and direct current conductivity in polymer-carbon nanotube composite thin films," *Journal of Applied Physics*, vol. 92, no. 7, p. 4024, 2002.
[88] M. B. Bryning, M. F. Islam, J. Kikkawa, and A. Yodh, "Very Low Conductivity Threshold in Bulk Isotropic Single-Walled Carbon Nanotube–Epoxy Composites - Bryning - 2005 - Advanced Materials - Wiley Online Library," *Advanced Materials*, vol. 17, no. 9, pp. 1186-1191, May. 2005.
[89] P. Spanos, M. Esteva, and J. Akin, "Determination of Elastic and Thermal Properties of Nanocomposites by Fiber Embedment in Finite Elements," presented at the NSTI Nanotechnology Conference, Houston,TX, 2009.